STORAGE OF SPATIOTEMPORAL INPUT SEQUENCES IN DENDRITES OF PYRAMIDAL NEURONS

Matej Macak

Thesis submitted for the degree of
Doctor of Philosophy in Neuroscience

University College London
2015

DECLARATION

I, Matej Macak confirm that the work presented in this thesis is my own. Where information has been derived from other sources, I confirm that this has been indicated in the thesis.

London, 14/09/2015

ABSTRACT

Plastic changes in neurons are widely considered to underpin the formation and maintenance of memory. The mechanisms of induction and expression of plasticity are, therefore, crucial to our understanding of the capacity of information storage that neurons possess. Using two-photon glutamate uncaging and whole-cell electrophysiological recordings, I demonstrate that dendrites of neurons are capable of preferentially storing specific spatiotemporal sequences, and describe the physiological properties of this new form of plasticity. Such plastic changes are dependent on Ca^{2+} influx through NMDA receptors, which is consistent with previous reports regarding induction of potentiation. Using two-photon Ca^{2+} imaging, I demonstrate that spatiotemporal plasticity is a result of a distinct homogeneous spatial increase in Ca^{2+} influx of different spatiotemporal sequences. Using the NEURON simulation environment, I used my experimental findings to perform simulations of synaptic plasticity rules. I found that homogeneous increases in synaptic strength across the dendrite can result in the spatiotemporal plasticity that I empirically observed. Moreover, I employed a genetic optimization algorithm and parallelized simulations to show that such changes are within physiological parameters observed in cortical neurons. My PhD therefore describes a novel form of plasticity, and proposes that dendrites are capable of more extensive information storage than was previously assumed.

ACKNOWLEDGEMENTS

I would first like to thank Michael Häusser and Tiago Branco for their support of my PhD for providing supervision and a very productive and stimulating scientific environment for my study.

I would also like to thank Arnd Roth, Beverley Clark, Christian Wilms, Christoph Schmidt-Hieber and Adam Packer for helping me with my experiments, analysis and for their help with experimental methods.

I would like to thank Charlotte Arlt and Sarah Rieubland for their constant support up to the submission stage in spite of them having to take care of their own academic work and PhD.

I would also like to thank Lea Goetz, Gabija Toleikyte, Yuya Kanemoto, Martine Groen, Matt Hoddinott, So Chun, Henry Dalgleish, James Cottam, Dara Sosulski, Mehmet Fisek, Lina Jeantin, Joanna Lau and Carmen Schiweck for providing an atmosphere of camaraderie, stimulating talks and for their constant tolerance of my choices of lunch places.

I would like to thank people who have been there for the last five years to provide constant reassurance, support and help. I am especially thankful to my mum Slávka and my brother Kubo who were there at every step or misstep of the way. I would also like to thank my grandparents Hela, Marka and Miki who were always ready with their cup of tea and advice whatever the topic.

Finally, I would like to thank to all my friends who were always ready to listen and take my mind off PhD matters when I needed it the most – Andy Williams, Vlad Hanzlík, Tim Jenner, Zuzka Gedeonová, Mať o Kurian, Juro Špilda, Peter Smittenaar, Rosie Shimell, Joe Johnson, Kubus Závodný, Markéta Šetinová, Maja Friedmannová and Hansel Ng.

TABLE OF CONTENTS

TABLE OF FIGURES

TABLE OF VIDEOS

TABLES

ABBREVIATIONS

ACSF – Artificial cerebrospinal fluid

AMPA - α-Amino-3-hydroxy-5-methyl-4-isoxazolepropionic acid

AP – Action potential

bAP – Backpropagating action potential

BAC (firing) – Backpropagation-activated Ca^{2+} spike

BDNF – Brain-derived neurotrophic factor

cAMP – Cyclic adenosine monophosphate

CNS – Central nervous system

EPSP – Excitatory post-synaptic potential

FRAP – Fluorescence-recovery after photo-bleaching

GIRK – G-protein activated K^+ currents

HCN – Hyperpolarization-activated Cyclic Nucleotide-gated

HVA – High-voltage activated Ca^{2+} channels (m – moderate conductance, l – low conductance)

LTD – Long-term depression

LTP – Long-term potentiation

LVA – Low-voltage activated Ca^{2+} channels

MVA – Medium-voltage activated Ca^{2+} channels

NMDA – N-methyl-D-aspartate

STDP – Spike-timing dependent plasticity

SEM – Standard error of the mean

t-LTP – timing-dependent long-term potentiation

t-LTD – timing-dependent long-term depression

VGCC – Voltage-gated Ca^{2+} channel

1 INTRODUCTION

The complexity and magnitude of information stored by neuronal dendrites is a fundamental question in neuroscience. Dendrites are the primary site of input in neurons and their ability to undergo plastic changes has been an active area of research for more than a century. Any review of dendritic plasticity needs to evaluate two, sometimes disparate, fields - dendritic information processing, and molecular mechanisms of plasticity. I will first evaluate historical and current research in the dendritic integration field. Second, I will consider the mechanisms of plasticity induction and maintenance. Finally, I will evaluate how plasticity of dendrites affects the integration of synaptic inputs. I will offer unanswered questions in the field and suggest new avenues for future research.

1.1 DENDRITIC INFORMATION PROCESSING

1.1.1 Historical perspective

Many major neuroscience texts pay tribute to the father of the discipline, Santiago Ramón y Cajal. Cajal, using light microscopy and the neuronal staining technique developed by Camillo Golgi in 1873, was able to draw neurons, their dendrites and axons in a remarkable detail for his time (Figure 1.1). Speculating purely on the basis of anatomical reconstructions, Cajal was able to make key insights as to the nature of information processing in neurons. Cajal was a proponent of the "cell" or "neuron" doctrine that was originally proposed by Theodor Schwann and Matthias Jakob Schleiden in the 19th century. Cajal argued that neurons are separate anatomical and processing units of the brain, a claim in which he famously disagreed with his colleague, Camillo Golgi, with whom he shared his Nobel Prize in 1906. Cajal proposed the direction of transmission that is currently known as the "law of dynamic polarization". He argued that information flows from the protoplasmic branches (or dendrites) to the nerve expansion (or axons). Cajal further conjectured

that memory or "cerebral gymnastics" could modify patterns of connections in the psychic cells (currently known as pyramidal cells) by means of morphological changes in axons and dendrites (Berlucchi & Buchtel, 2009).

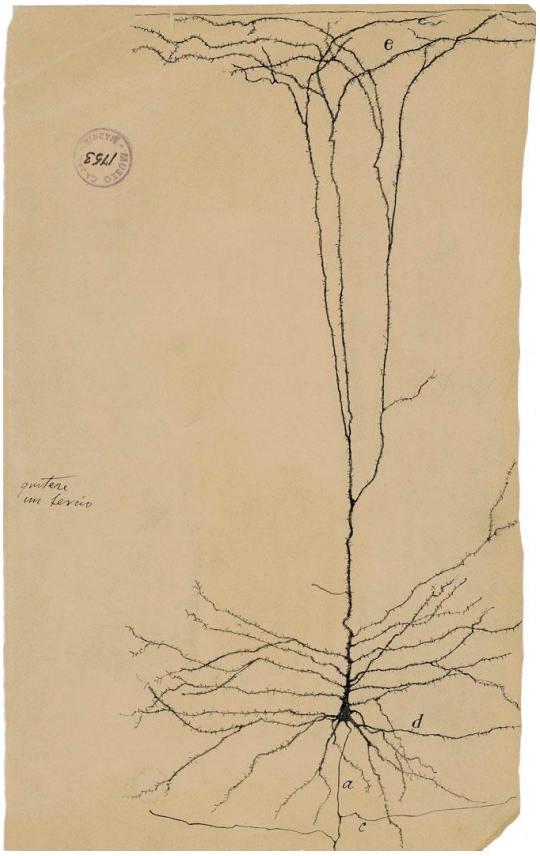

Figure 1.1 Ramón y Cajal's drawing of Layer 5 pyramidal cell in the cortex

Ramón y Cajal's drawing based on Golgi-stained Layer 5 pyramidal cell of cortex. (a) – axon, (d) – dendrite, (c) – collateral, (e) - spines. Note the prominent spines at both apical and basal part of the dendritic tree and aspiny axon and collaterals. Source: Museo Cajal Madrid, artattler.com.

1.1.2 Cable Theory and its application for synaptic integration

The theory of electric conduction in neurons and the cable theory that inspired it a similarly long history. The initial studies demonstrating electric nature of nerve conduction were performed by Galvani and Volta in the 18th century (Rall, 2011). Cable theory dates back to the mid-19th century and stemmed from the published correspondence of William Thomson (or Lord Kelvin) and

Professor Stokes (Thomson, 1854), which provided a mathematical formulation for the placement of submarine cable at the time. The empirical verification of cable theory in neurons depended on the development of equipment capable of fine electrical measurements. It was therefore not verified until 1946, when Hodgkin and Rushton (1946) used cable theory to accurately estimate values for membrane capacitance in 75 μm diameter axon from walking leg of lobster (1.3 μF cm^{-2}). Currently, the accepted value for membrane capacitance is considered to be 1 μF cm^{-2} or 0.65-0.7 μF cm^{-2} for the lipid moiety itself (Jack *et al.*, 1975; Shepherd, 2008*a*). Later studies by Hodgkin and Huxley (1952) opened doors for computational description of neuronal membrane properties. Hodgkin and Huxley chose squid giant axon as an appropriate model as the physical size of the cable allowed easy access for electrical recordings. Dendrites in the CNS of most mammalian species are much thinner and until recently, direct measurements of synaptic responses were not technically feasible. Since dendrites resemble leaky electrical cables, cable theory provided a useful approximation to obtain a mechanistic understanding of current flow along passive neurites.

Most early work that employed Cable Theory in dendritic integration was done under the assumption that dendrite is a passive cable with no active or non-linear conductances, such as voltage-gated sodium channels, present in the membrane. As a result of such theoretical work, several important insights emerged that were later on verified empirically. For example, dendrites can be described as "leaky cables" due to their relatively low specific membrane resistance. This "leak" results in voltage attenuation from the source of the current (i.e. synapse or synaptic event) to its readout (usually the soma).

Since dendrites taper with distance from soma, it follows that voltage attenuation is asymmetrical and favours propagation towards narrower parts of the dendrite or away from the soma (Rall & Rinzel, 1973; Rinzel & Rall, 1974). Whilst these equations hold analytically for a single-cable neuron under the steady-state condition, finding an analytical solution for a physiological neuron would be prohibitive due to numerous bifurcations, variations in diameter (Abbott *et al.*, 1991) and

presence of non-linear conductances. Therefore, compartmental models were developed which split the neuron and its dendritic tree into a multitude of segments. Within the segments spatial non-uniformity is neglected. Such multi-region boundary problem can then be solved as a system of ordinary differential equations (Rall, 1964). Compartmental models confirmed the uneven voltage propagation in various cell types such as CA1 pyramidal cells (Golding *et al.*, 2005), CA1 interneurons (Emri *et al.*, 2001), Purkinje cells (Roth & Häusser, 2001) or neocortical pyramidal cells (Stuart & Spruston, 1998). Locally, synaptic events would be larger in distal portions of dendrite due to increased input impedance due to tapering and due to end-effects. Nevertheless, the significant attenuation, greater than 100-fold in some cases (Stuart & Spruston, 1998; Williams & Stuart, 2002; Nevian *et al.*, 2007), results in smaller amplitude distal excitatory post-synaptic potential (EPSP) compared with proximal EPSPs in passive systems. Apart from amplitude attenuation, the filtering properties of dendrites result in slowing of the time-course of distal EPSPs with an increase in time-to-peak (Rall, 1964, 1967). This has been verified in experiments in layer 5 pyramidal cells (Sjöström & Häusser, 2006) and CA1 pyramidal cells (Magee & Cook, 2000).

Cable theory also provided predictions on the influence of clustered and distributed input on eliciting action potential at the soma. In a purely passive system, cable theory predicts that co-localized synaptic events will result in a local reduction of driving force as a result of a decrease in membrane resistance (Rall, 1964). Maximal (linear) summation can be achieved when synapses are separated sufficiently in spatial or temporal dimension. These predictions have been verified experimentally (Polsky *et al.*, 2004).

One important upshot of cable theory application to synaptic integration, was the realization of the complexity of information that is integrated at the level of dendrites. Even in purely passive systems, the location of synaptic events on the dendritic tree could be resolved from its amplitude and time-course. Furthermore, the degree of clustering of inputs, through local reduction in

driving force influences the likelihood of action potential induction at the soma. Cable theory predicted even more complex processing such as direction sensitivity to spatio-temporal inputs. Rall (1964) theoretically demonstrated that centripetal, temporally staggered input produces greater peak depolarization at the soma than is the case of the centrifugal input. Furthermore, the peak of centripetal input was predicted to occur at a later time following stimulation than the peak of centrifugal input. The amplitude and peak time differences occur because dendrites act as a delay line for incoming signals. This enables the resolving of spatiotemporal activation of individual inputs based on the time-course and amplitude of the recorded somatic voltage trace.

Further increase in complexity comes from the fact that both excitatory and inhibitory synapses dot the membrane of neurons. The primary inhibition that was described by Rall (1964) was shunting inhibition or a change of the overall conductance level with no effect on the membrane voltage. In his work, he realized that the location of the source of inhibition was important in the magnitude of the effect it exercises over somatic voltage. Rall (1964) discovered that a single inhibitory synapse centred on the incoming excitatory input or between somatic region and the site of the input ("on-path") is more effective than in the "off-path" condition. The more efficient shunting by "on-path" inhibition was verified in computational models (Koch *et al.*, 1983; Hao *et al.*, 2009). Rall (1964), himself, realized that his predictions hold in a passive, single-cable model with a single inhibitory synapse. More complex results are obtained when branching and active dendrites are considered. When non-linearities in dendrites are taken into account, "off-path" inhibition is more efficient at shunting dendritic spikes as a result of larger synaptic conductance in distal dendrites close to sealed ends and a smaller spatial attenuation for distal sites due to their distance from somatic sink (Gidon & Segev, 2012).

The theory based on passive cable properties provides a strong foundation or skeleton for understanding of the complexity of dendritic integration. Active properties of the membrane of the cell conferred by the variety of different channels and receptors cannot be ignored in a full

account of dendritic information processing. A large source of variance between different neuronal cell types, for example, comes from the types of channels expressed and their respective spatial profiles.

1.1.3 Active conductances in dendrites

Studies in alligator Purkinje cells first demonstrated that active conductances, typically associated with soma and axon are also present in the dendrites of cells (Llinás *et al.*, 1968; Llinás & Sugimori, 1980). The presence and role of active conductances in dendrites depends on, among others, the stage of development, cell-type, type of dendrite and its distance from the soma (Magee, 1998; Migliore & Shepherd, 2002; Shepherd, 2008*b*; Gazina *et al.*, 2010). The expression pattern of channels and receptors along the dendrite is a key influence on such properties as threshold for dendritic spike induction, action potential backpropagation or synaptic scaling.

1.1.3.1 Na^+ channels

The transient Na^+ current has the greatest importance in action potential generation and backpropagation. In the apical dendrites of CA1 pyramidal cells and nigral dopaminergic neurons (based on the full-amplitude bAP propagation), the Na^+ channel density is high and present relatively uniformly across the dendritic tree (Stuart & Sakmann, 1994; Magee & Johnston, 1995; Häusser *et al.*, 1995). However, in Purkinje cells and thalamocortical neurons, the density of voltage-gated Na^+ channels decreases rapidly with distance from the soma (Stuart & Häusser, 1994; Williams & Stuart, 2000*a*). The expression pattern of voltage-gated Na^+ channels also depends on the development, with expression of $Na_v1.1$, $Na_v1.2$, $Na_v1.3$ and $Na_v1.3$ channels peaking at around P15 in the mouse in cortex, cerebellum, thalamus and hippocampus (Gazina *et al.*, 2010).

1.1.3.2 K^+ channels

K^+ channels are possibly the most diverse population of voltage-gated conductances with over 100 different subunits being identified so far (Coetzee *et al.*, 1999). The most prominently studied in

the field of dendritic integration are the A-type, G-protein coupled inwardly-rectifying K^+ (GIRK) channels and K-type K^+ channels. A-type K^+ channels are responsible for repolarization of the cell-membrane following action potential. A-type K^+ channel expression seems to be more modulated with distance from the soma. In CA1 pyramidal cells and in rat mitral cells, the A-type K^+ channel expression increases with the distance (Hoffman *et al.*, 1997; Bischofberger & Jonas, 1997). In neocortical neurons, both A-type and K-type channels are relatively uniform across the dendritic tree (Korngreen & Sakmann, 2000; Bekkers, 2000). GIRK channels are present in most several cell types including CA3, CA1 pyramidal cells, neocortical pyramidal cells and substantia nigra cells in the brain (Takigawa & Alzheimer, 1999; Lüscher & Slesinger, 2010; Makara & Magee, 2013). In neocortical pyramidal cells, there is a notable increase in the expression of GIRK channels from soma to dendrites (Takigawa & Alzheimer, 1999).

1.1.3.3 Ca^{2+} channels

The distribution of voltage-gated calcium channels (VGCCs) in dendrites of cells is less-studied as compared to other channels. Magee and Johnston (1995) used dendrite-attached patches and discovered that high-voltage activated low conductance (HVAl) channels were restricted to proximal 50 μm of CA1 neurons, whilst high-voltage activated medium conductance channels (HVA_m) and low-voltage activated (LVA) were fairly constant across the dendritic tree. In neocortical cells, the spatial distribution of VGCCs is less well researched. To my knowledge, outside-out patches or dendrite-attached patch-clamp experiments from different parts of the dendritic tree to evaluate VGCC expression are yet to be done in neocortical pyramidal cells. Calcium imaging experiments studying backpropagation of action potentials suggest a relatively uniform distribution of VGCCs, consisting primarily of the L-, N- and R-type (Markram *et al.*, 1995). Using a pharmacological and numerical peeling procedure, Almog and Korngreen (2014) predict a decrease in conductance of HVA and medium-voltage activated (MVA) channels along the dendrite, but an increase in permeability of MVA channels between 400-600 μm from the

soma. This is consistent with reports of a calcium initiation hotspot in layer 5 cells which is activated when critical frequency of action potential is reached (Larkum *et al.*, 1999*a*). In Purkinje cells, HVA channels (P/Q-type) are the major source of Ca^{2+} ion entry (Usowicz *et al.*, 1992). Whilst detailed information about the conductance gradients of the channels is missing as well, calcium imaging experiments hint at a relatively uniform expression along the dendritic tree (Lev-Ram *et al.*, 1992).

1.1.3.4 I_h channels

(Hyperpolarization-activated cyclic nucleotide-gated) HCN channel based current (I_h) was first described in sinoatrial myocytes as a "funny" inward current that is hyperpolarization activated and enhanced upon the application of adrenaline ultimately resulting in an increased heart rate (Brown *et al.*, 1979). In the central nervous system (CNS), "funny" current is usually termed as a hyperpolarization activated non-specific cation current, or I_h, and in many cell types performs important functions in synaptic scaling and action potential backpropagation. In CA1 pyramidal cells, the current density increases more than sixfold from soma to distal (350 μm) dendrites (Magee, 1998). This gradient was found to normalize temporal summation in distal dendrites (Magee, 1999). The I_h gradient is also present in the apical dendrites of the layer 5 pyramidal cells. The exact nature of the gradient is contested – linear (Williams & Stuart, 2000*b*) or exponential increase after 400 μm (Berger *et al.*, 2001). In both of these studies, I_h, similarly to CA1 pyramidal cells, contributes to EPSP normalization. I_h also importantly affects the non-linear processing in dendrites, increasing the threshold for coincidence detection and induction of dendritic spikes (Berger *et al.*, 2003). HCN channels that underlie I_h current, were found to be importantly modulated by neuromodulators, especially adrenaline and dopamine presumably via cAMP pathway (Rosenkranz & Johnston, 2006; Wang *et al.*, 2007*a*).

1.1.3.5 Voltage-activated channel interactions in dendrites

At least two Na^+, six Ca^{2+} and seven distinct K^+ currents have been described so far in the literature (McCormick, 2008). This number of channel types is most likely an underrepresentation as many more are present on the membrane of the cell (Coetzee *et al.*, 1999; Kullmann, 2010). As a consequence of this channel expression, non-linear interactions between channel types occur, often resulting in cell-type specific dendritic integration as well as distinct action potential initiation and propagation profiles. Also commonly physiological models of neuronal behaviour usually employ only a small subset of available channels (Almog & Korngreen, 2014). Despite their relative simplicity, theoretical models have been very successful in predicting features of dendritic integration and action potential propagation in different cell types across the brain.

1.1.4 Propagation in active dendrites

Two aspects of sub-cellular neuronal behaviour received substantial attention in the past decades of neuroscience research. The first, is action potentials propagation through axons, which has been a well understood phenomenon since the research of Hodgkin and Huxley (1952). However, the converse propagation, back into the dendrite from the soma, was demonstrated fairly recently following the development of the patch-clamp method and its application to dendritic membranes (Stuart & Sakmann, 1994). The second aspect to receive attention was the role of the active properties of dendrites in the integration of synaptic inputs. For example, it was discovered that distal synapses can cooperate to produce dendritic spikes to overcome unfavourable voltage propagation (Llinás *et al.*, 1968; Schiller & Schiller, 2001; Major *et al.*, 2008; Branco & Häusser, 2011). As I will discuss in this introduction, both action potential backpropagation and non-linear properties of synaptic integration are important in the plasticity processes.

1.1.4.1 Action potential backpropagation in CNS neurons

The advent of dendritic patch clamp enabled the detailed study of the role of dendritic processing in neuronal function (Stuart *et al.*, 1993; Stuart & Sakmann, 1994; Stuart & Häusser, 1994). Whilst

antidromic action potential propagation had been observed previously in cerebellar Purkinje cell dendritic recordings with sharp microelectrodes (Llinás & Sugimori, 1980), the properties of action potential backpropagation were only fully elucidated with dendritic patch-clamp studies.

One of the early discoveries in the field was the realization that morphology (see Figure 1.2) is an important determinant of the extent of backpropagation into dendritic tree. More complex dendritic architecture is associated with a reduced degree of backpropagation into dendrites (Vetter *et al.*, 2001).

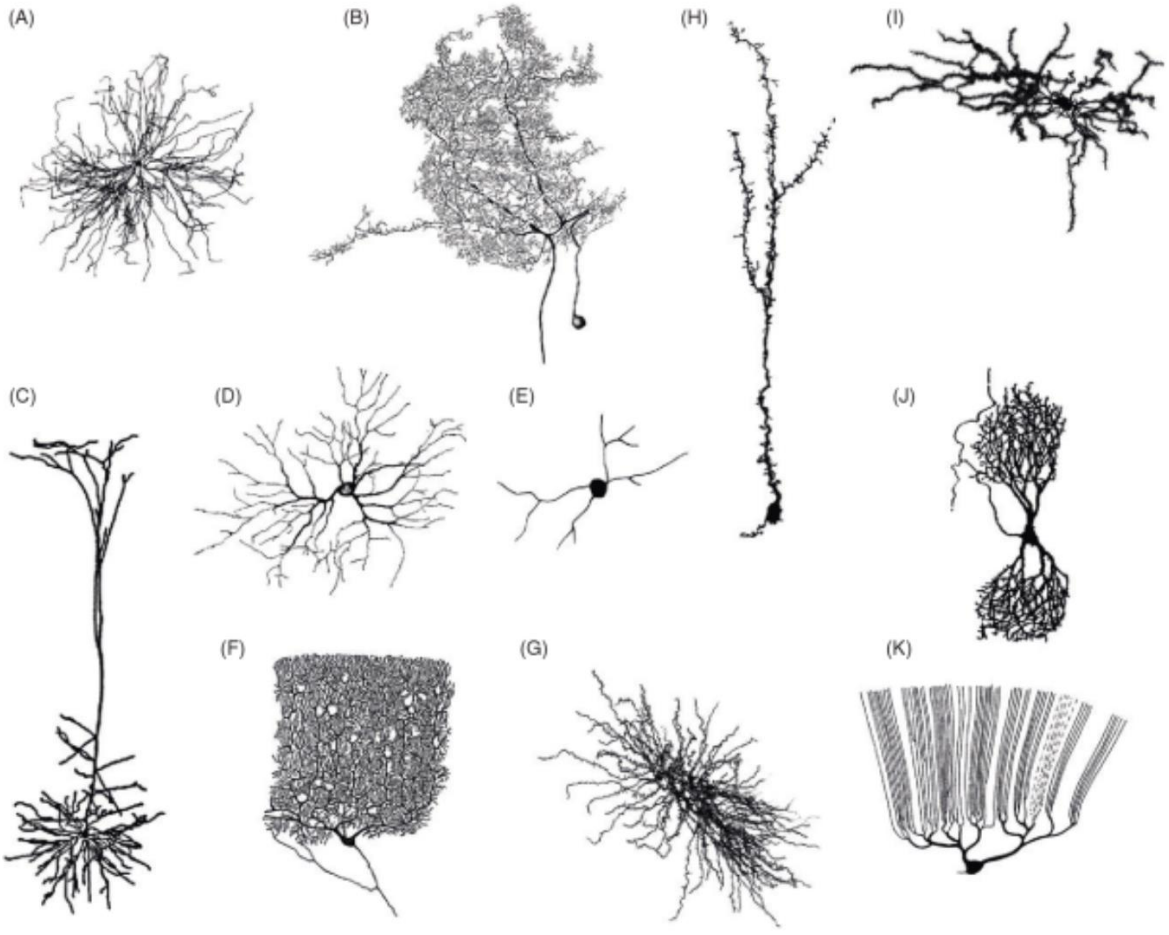

Figure 1.2 Diversity of dendritic morphologies in the brain.

Reconstructions shown are from: A) alpha motor-neuron of cat spinal cord, B) spiking interneuron from mesothoracic ganglion of locust, C) neocortical layer 5 pyramidal neuron of rat, D) retinal ganglion cell in cat, E) amacrine cell from retina of larval salamander, F) cerebellar Purkinje cell in

human, G) relay neuron in basoventral thalamus of rat, H) granule cell from olfactory bulb of mouse, I) spiny projection neuron from striatum of rat, J) nerve cell in nucleus of Burdach of human foetus, K) Purkinje cell of mormyrid fish. Sources: Spruston et al. (2012) and Mel (1994).

Consistently, the most limited action potential backpropagation is observed in the cerebellar Purkinje cells (Stuart & Häusser, 1994) which feature arguably the most complex dendritic architecture in the brain. The extensive arborisation of the tree and small steep decreasing gradient of Na^+ channel expression results in a steep voltage attenuation. ctive condunctances such as Na^+ channels open during backpropagation of action potential and thus boost spatial extent of back-propagating action potential (bAPs). In comparison, Layer 5 cells do express Na^+ channels in their apical dendrites (Stuart & Sakmann, 1994; Almog & Korngreen, 2014) and their dendrites are not as complex as those of Purkinje cells. As a result, single action potential backpropagation fails only at distal sites of layer 5 pyramidal neurons. Higher frequency inputs overcomes this distal attenuation by reaching a calcium initiation hotspot in the distal apical tuft (Larkum *et al.*, 1999*a*, 2009). In basal dendrites of layer 5 pyramidal neurons, backpropagation is aided by the presence of sodium channels, but nevertheless the bAPs are attenuated more than threefold at a distance of 150 μm from the soma (Nevian *et al.*, 2007). In the CA1, two populations of pyramidal cells were discovered with distinct differences of bAP attenuation, mostly due to the potassium and sodium channel expression in the membrane (Golding *et al.*, 2001). Finally, dopamine cells in substantia nigra and olfactory mitral cells show probably the most robust propagation with little attenuation in the distal dendrites (Häusser *et al.*, 1995; Bischofberger & Jonas, 1997). These results are due to the compact dendritic architecture of the cells and sodium channel expression throughout the arbor.

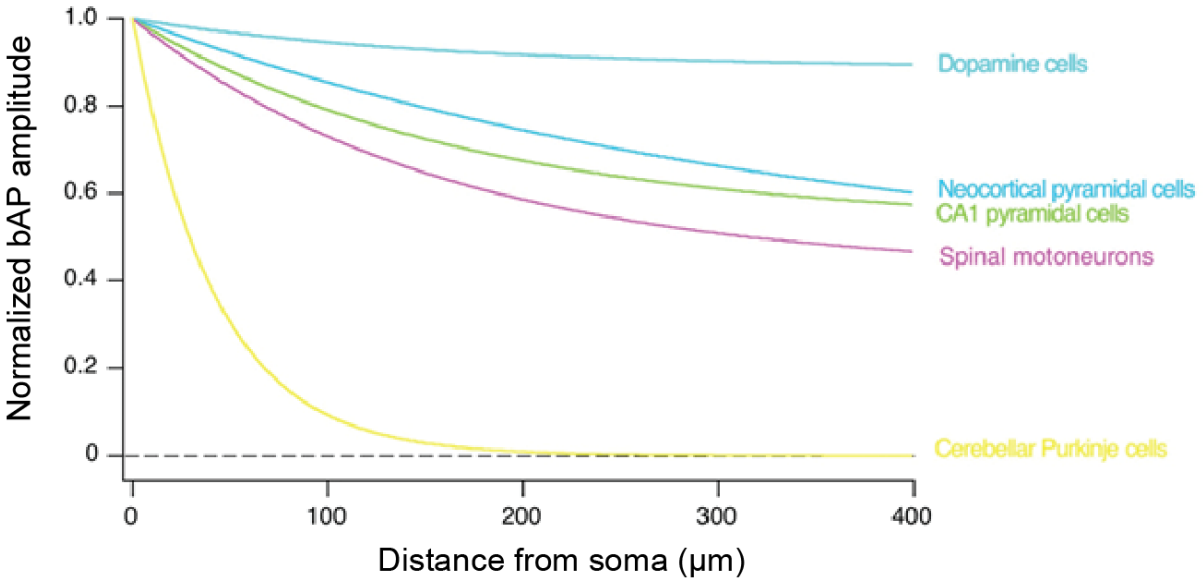

Figure 1.3 Backpropagation of action potentials in different cell types of the brain.

A schematic of the backpropagation efficacy as measured by distance from the soma in 5 representative neuronal morphologies coded by color. Source: Adapted from a figure by Stuart et al. (1997).

Multi-compartmental simulations confirmed that morphology and channel expression are key determinants (see Figure 1.3) of the extent of backpropagation (Vetter *et al.*, 2001; Roth & Häusser, 2001; Schaefer *et al.*, 2003). The morphology of dendritic arbors of neurons in the brain is very diverse, (Häusser *et al.*, 2000; Klausberger & Somogyi, 2008; DeFelipe *et al.*, 2013) often even within the same subtype of a cell – i.e. pyramidal or retinal ganglion cells (Dacey *et al.*, 2003; Spruston, 2008; Gee *et al.*, 2012). Dendritic morphology was also found to be critically important in determining the firing pattern of neurons (Mainen & Sejnowski, 1996; Graves *et al.*, 2012). In the model by Mainen and Sejnowski (1996), this was at least partly dependent on the presence of slow active channels in dendrites. In layer 5 pyramidal cells, bAPs coupled with dendritic depolarization results in burst firing of the cell that is called back-propagation activated Ca^{2+} (BAC)-firing (Larkum *et al.*, 1999*b*, 2001). The current injection needed to elicit firing is timing dependent with

a very similar time-course to that observed in spike-timing dependent plasticity protocols (Markram *et al.*, 1997; Bi & Poo, 1998; Sjöström *et al.*, 2001).

Whilst such studies were very influential because of their simple and powerful prediction on the extent of backpropagation, in physiological settings, the situation becomes much more complex. Backpropagation was found to influence and be influenced by the activation history of voltage-gated channels. Trains of action potentials can lead to inactivation of Na^+ channels and the reduction of bAP amplitude in CA1 cells (Spruston *et al.*, 1995). In contrast, depolarization of the dendrite enhances the backpropagation into the dendrite by increasing the likelihood of opening Na^+ and Ca^{2+} conductances (Stuart & Häusser, 2001). On the other hand, hyperpolarization of the dendrite or increasing the shunt level (for example by inhibition) decreases extent of back propagating action potential invasion (Tsubokawa & Ross, 1996; Larkum *et al.*, 2001; Schaefer *et al.*, 2003). In cat neocortical neurons *in vivo*, the high conductance state, due to a barrage of on-going synaptic activity, causes a significant (up to five-fold) drop in input resistance (Paré *et al.*, 1998; Destexhe *et al.*, 2003). Although input resistance in rat layer 2/3 cells *in vivo* is similar to that seen *in vitro* (Waters *et al.*, 2003), reductions in input resistance are expected to result in a decrement of backpropagation due to an increase in the leakiness of neuron. Finally, the physiological state of the neuron is profoundly affected by neuromodulation. In the substantia nigra, dopamine reduces backpropagation by tonic hyperpolarization as a result of increased availability of A-type K^+ channels (Gentet & Williams, 2007). Nevertheless, the role of neuromodulators like dopamine in the excitability of cells is controversial (Gulledge & Stuart, 2003) and the effects are often more complex than a simple hyperpolarization or depolarization of membrane (Seamans & Yang, 2004).

Whilst there are many state-dependent variables influencing the propagation of action potentials into dendrites, bAPs are also powerful modulators of neuronal integration processes. Coincident action potential (AP) and EPSPs result in supra-linear summation of synaptic input and Ca^{2+} entry into the dendrite (Stuart & Häusser, 2001; Nevian & Sakmann, 2004, 2006). Following bAP,

suprathreshold events at the dendrite are less likely to occur than before (Remy *et al.*, 2009). Such "resets" of dendritic activity are postulated to place a limit on the number of patterns that can be stored with dendritic spikes and/or how frequently they can be retrieved by the dendrite (Branco & Häusser, 2009).

The result of dendritic integration is not necessarily only passed to the soma but dendrites themselves may act as outputs. Multiple molecules have been shown to be released from dendrites ranging from typical neurotransmitters like glutamate and gamma-amino butyric acid (GABA) (Ludwig & Pittman, 2003) to neurotrophic factors like brain-derived neurotrophic factor (BDNF) (Kuczewski *et al.*, 2009). The release is Ca^{2+} dependent and relies on vesicle exocytosis machinery (Branco & Häusser, 2010). bAPs are involved in the release of BDNF (Kuczewski *et al.*, 2008) and are hypothesized to have a role in other cells like magnocellular hypothalamic cells, provided the bAP propagation does not fail (Ludwig & Pittman, 2003).

1.1.5 Synaptic integration and dendritic spikes

Apart from the propagation of action potentials, voltage-gated channels allow generation of supra-linear synaptic integration in the form of dendritic spikes. Neurons vary widely in the number of synapses that are present on the membranes with the estimated range being between 1,000 and 300,000. The primary focus of the dendritic integration field is to answer how inputs, when converted into graded synaptic potentials, result in the output of the neuron in form of action potentials.

1.1.5.1 The role of distance and synaptic scaling

I have already discussed that Cable Theory predictions followed by experimental verification postulated that all synapses are not equal in terms of their influence on action potential generation. Distance is a major factor, especially in cells with dense dendritic arbors such as Purkinje cells or layer 5 pyramidal cells, which determines the strong attenuation of distal synaptic inputs (Spruston *et al.*, 1994; Stuart & Spruston, 1998; Roth & Häusser, 2001; Nevian *et al.*, 2007). If distal synapses

are less efficient at inducing action potentials, it is tempting to question their importance for neuronal processing. One answer to this question is that some cells, such as CA1 pyramidal cells, show distance dependent scaling of synaptic responses (Magee & Cook, 2000). Synapses farther away from soma have an increased α-Amino-3-hydroxy-5-methyl-4-isoxazolepropionic acid (AMPA) conductance (Andrasfalvy & Magee, 2001) and tufts of these neurons have an increased N-methyl D-aspartate (NMDA)/AMPA ratio (Bittner *et al.*, 2012). The theory posits that the synaptic strength is "scaled" to equalize the voltage attenuation deficit of distal synapses. These findings gave rise to the theory of "synaptic democracy" (Häusser, 2001) which postulates that each of the synapses is equally heard at the soma. In its more stringent form, inputs are also expected to be distributed along the dendrites to ensure their independent and linear integration (Cash & Yuste, 1999; Yuste, 2011, 2013). The scaling argument is controversial, however. For instance, augmentation of synaptic strength was not observed in neocortical cells (Williams & Stuart, 2002). Furthermore, the increase in synaptic conductance as would be expected under *in vivo* conditions would result in a breakdown of such scaling-based synaptic democracy (London & Segev, 2001). These authors also noted that even if scaling could be obtained with a steeper gradient, small changes in the state of network statistics would quickly result in its disruption. It is possible that voltage attenuation is a feature rather than a "bug" of neuronal processing. Due to filtering properties of the dendrite, EPSP time course is slowed from more distal synapses. Although this results in lower likelihood of eliciting AP, it also prolongs the time course of integration enabling distal dendrites to be rate coding integrators. When active channels are also involved, dendritic morphology strengthens this effect. Due to high local input impedance of distal dendrites, fewer inputs are necessary to bring about a supra-linear NMDA and VGCC-mediated response and these inputs are integrated for longer time-scales in cortical neurons (Branco & Häusser, 2011). In the computational model of this study, it was observed that distal dendrites are surprisingly more efficient at driving AP output than proximal dendrites. This particular model does not depend on the inputs being located in close proximity. Nevertheless, it was argued in

other work that clustered synapses can amplify distal inputs by opening active conductances in the membrane and eliciting dendritic spikes (Larkum & Nevian, 2008; Kastellakis *et al.*, 2015).

1.1.5.2 Morphology of spines and electric compartmentalization

The extent to which synaptic inputs on a single dendrite are clustered and to which integration at soma relies on dendritic non-linearities is a subject of some controversy. As I mentioned above, one view argues that synapses summate mostly linearly (Yuste, 2011, 2013). The argument rests on two propositions both of which received some support in recent experimental literature. To ensure linear summation, enhancement of compartmentalization of individual inputs is desirable. If dendritic spines possessed high resistance necks, this would aid electrical compartmentalization on a single dendritic branch (Segev & Rall, 1998). Because spines are small, inaccessible structures for direct observations, past studies of spine compartmentalization as a function of neck morphology were indirect and their estimates vary (Grunditz *et al.*, 2008; Harnett *et al.*, 2012; Tønnesen *et al.*, 2014). In a study on CA1 pyramidal neurons, spine neck resistance was estimated by calibrating voltage-gated Ca^{2+} signal resulting from propagation of voltage from dendritic injection into the spine (Harnett *et al.*, 2012). Using this method, Harnett and colleagues (2012) were able to estimate that spine neck resistance is around 500 MΩ, high enough to allow for the compartmentalization required by the linear integration theory. However, it is known that spine morphology of both heads and necks can be very variable and malleable to plasticity processes (Majewska *et al.*, 2000; Noguchi *et al.*, 2005; Grunditz *et al.*, 2008; Araya *et al.*, 2014). Experiments using FRAP measurements result in a fairly wide range & of spine neck resistance with reported values ranging from 55 MΩ (Tønnesen *et al.*, 2014) to 1.2 GΩ (Grunditz *et al.*, 2008). Both of these studies report a significant variance (interquartile range from 1 MΩ to 1 GΩ) as would be expected given the variability in spine head and neck morphologies. Despite the diversity, it is reasonable to expect thin-necked spines to have high resistances required for passive electrical compartmentalization of signals. However, many spine-heads are studded with active

conductances primarily of NMDA and VGCCs type (Zito *et al.*, 2009). In active case, high spine neck resistance would result in non-linear response to synaptic input which would favour cooperativity between spines on a single dendrite (Harnett *et al.*, 2012). Similar to my argument in synaptic democracy discussion, spines are very variable structures and their degree of electrical compartmentalization will be a function of their morphology, the input impedance of the parent branch and their expression of conductances - especially of the active kind.

1.1.5.3 Distribution of synaptic inputs on a dendrite

It is currently controversial whether synapses on dendrites in neurons are distributed randomly or whether similar inputs are clustered in space. A requirement for linear integration is the relatively uniform distribution of synapses along the dendritic tree. On the other hand, clustered input would favour the involvement of active conductances (if present) and the generation of dendritic spikes. The uniform distribution requirement for linear integration is important to minimize the shunting due to an increase in conductance as a result of active synapses on the dendrite. Such arrangement of synapses known as Peters' rule is expected if the connectivity of neural circuits is determined purely by the overlap of dendrites and axons. Several *in vivo* studies in the neocortex following auditory, visual or whisker stimulation suggested that synapses can be tuned to random input features (Jia *et al.*, 2010; Chen *et al.*, 2011*a*; Varga *et al.*, 2011). Despite these studies, computational models suggest that clustered representation leads to enhanced information storage in dendrites (Poirazi & Mel, 2001; Kastellakis *et al.*, 2015). Several recent studies demonstrated clustering of inputs both *in vivo* and *in vitro*. Druckmann (2014) observed that connectivity between CA3-CA1 neurons is more clustered than would be observed by chance which can be seen both in neurons and dendrites. In CA1 pyramidal cells of organotypic slices, Kleindienst (2011) showed that clusters of active synapses are seen following bursts of synaptic activation. These clusters depend on neuronal activity and NMDA receptors. In layer 5 neurons of the mouse motor cortex, practicing a novel forelimb task lead to the formation of spine clusters that are more persistent

than non-clustered counterparts (Fu *et al.*, 2012). A different motor learning task also leads to clustering on different dendrites and such clustering is enhanced by sleep post-training (Yang *et al.*, 2014). In layer 2/3 neurons in somatosensory cortex *in vivo*, neighbouring spines display an increased concentration of GluA1 receptor in comparison to animals with their whiskers trimmed (Makino & Malinow, 2011). Clustering can also be seen in other animal models. In barn owls that were prism reared during their development, the presynaptic contacts are selectively sculpted. The prism-adapted side showed a reduced inter-contact distance (i.e. enhanced clustering) compared to non-adapted side or controls (McBride *et al.*, 2008). Finally, in the monkey prefrontal cortex, a preference for spatial clusters of spines was found that to be branch specific. Branches with higher degrees of clustering were found to be richer in mushroom and stubby synapses suggesting active plasticity processes (Yadav *et al.*, 2012). As I will describe below, many plasticity processes are biochemically constrained and are thus primarily local in their nature. As a result, they tend to favour generation of clustered formation or stabilization of spines on the dendrite.

1.1.5.4 Dendritic spikes

In a clustered representation, dendritic spikes are seen to perform an important role in neuronal processing (Branco & Häusser, 2010; Antic *et al.*, 2010; Major *et al.*, 2013). Dendritic spikes can be further subdivided into three major classes based on the type of non-linear conductance that underpins them – sodium spikes (Losonczy & Magee, 2006), Ca^{2+} spikes (Llinás & Sugimori, 1980; Amitai *et al.*, 1993) and NMDA spikes (Schiller *et al.*, 2000). The roles that dendritic spikes play in neuronal processing are versatile. It is well established that non-linear units enhance the computational capacity of neurons (Poirazi & Mel, 2001; Poirazi *et al.*, 2003; Häusser & Mel, 2003). In a detailed biophysical model, it was shown that a point neuron is much worse than a 2-layer neuron with sigmoidal units at predicting the firing rate of a distributed set of excitatory synapses (Poirazi *et al.*, 2003). Dendritic nonlinearities with slower time-courses (such as NMDA-receptor dependent spikes) may be particularly effective at compensating for filtering properties of

dendrites. Distal dendrites, with their higher input impedance, are more likely to elicit dendritic spike (Branco *et al.*, 2010). Such dendritic spike are then likely to propagate to soma where they were found to induce spiking more reliably than proximal synapses (Branco & Häusser, 2011). As mentioned above, dendritic spikes coupled with bAPs push layer 5 cells in the cortex into burst firing mode (Larkum *et al.*, 2001).

As dendritic spikes provide a prolonged depolarization, often with a Ca^{2+} component, it is likely that they play a major role in eliciting long-term potentiation in dendrites. In CA1 cells, dendritic spikes were found sufficient to induce LTP (Golding *et al.*, 2002). In the same neurons, single burst dependent on VGCC and NMDARs were found to elicit LTP (Remy & Spruston, 2007). In contrast, in layer 5 pyramidal neurons, single dendritic spikes can induce LTD (Holthoff *et al.*, 2004). Whilst some authors found greater difficulty in linking NMDA spikes to induction of plasticity (Gordon *et al.*, 2006), recently it was found in an *in vivo* study that sensory stimulation elicits NMDA spikes which in turn cause long-term plasticity in layer 2/3 cortical neurons (Gambino *et al.*, 2014). The likelihood of a single branch eliciting a dendritic spike can be enhanced by down-regulation of A-type K^+ channels in what has been termed branch-strength potentiation (Losonczy *et al.*, 2008) and this effect is observed preferentially in animals housed in enriched environments (Makara *et al.*, 2009). Such branch strength potentiation "protects" against the effects of inhibition further enhancing the coupling between dendrites and the soma (Müller *et al.*, 2012).

As described above, dendrites are capable of releasing neurotransmitters of their own. As this process is Ca^{2+} dependent, it is quite likely that dendritic spikes play a role in eliciting release (Branco & Häusser, 2010). In mitral tufted cells, subthreshold depolarizations were shown to induce local release of glutamate that was dependent on group I metabotropic glutamate receptors (mGluRs) (Castro & Urban, 2009). An A17 amacrine cell in the retina is specific in having a varicose like structure of dendrite leading to an effective compartmentalization of electrical

signals (Grimes *et al.*, 2010). As a result, hundreds of compartments in the dendrites send and receive signals in parallel. Whilst parallel computation on this scale is most likely specific to that particular cell, many cells are known to release neurotransmitters from the dendrite (Ludwig & Pittman, 2003). Given the highly localized nature of Ca^{2+} following dendritic spikes, it is tantalizing to expect dendrites to perform complex local computations.

Finally, up until recently, the role of dendritic spikes in sensory processing and behaviour was largely unknown. NMDA spikes occur spontaneously or as a result of whisker or hindlimb stimulation in layer 2/3 neurons (Palmer *et al.*, 2014; Gambino *et al.*, 2014). Blocking NMDARs decreases the sensory evoked output from neurons (Palmer *et al.*, 2014) and in layer 2/3 and 4 neurons preferentially decreases response to a tuned angular input following visual or whisker stimulation (Lavzin *et al.*, 2012; Smith *et al.*, 2013). Direct dendritic recordings from layer 2/3 neurons combined with simultaneous Ca^{2+} imaging confirmed that visually evoked NMDA spikes were local (Smith *et al.*, 2013). Computer model based on the data further confirmed that favorable conditions for eliciting NMDA spikes are when inputs are spatially clustered (Palmer *et al.*, 2014).

1.1.5.5 Models of integration

In the simplest model of dendritic integration, the "point neuron", all inputs are propagated to the soma where an action potential is generated when somatic voltage crosses threshold (see Figure 1.4A). This view was primarily represented in the traditional neural network models where soma is the only (nonlinear) filter of inputs in neuron (McCulloch & Pitts, 1943). In this view, dendrites are considered to be nothing more than passive propagators of signals. However, local integration of signals by dendrites and local computation, for example by dendritic spikes, was shown to enhance the information capacity of neurons (Poirazi *et al.*, 2003). This theory argues that the integration in dendrites is independent from other dendritic subunits or from the soma (see Figure 1.4B). More complex integration models were proposed for some neurons with complex dendritic morphology. For example, apical tufts of deep neocortical pyramidal cells are postulated to have

several compartmental zones which has been sometimes represented in a three- or multi-layer structure of integration (Häusser & Mel, 2003; Larkum *et al.*, 2009). A further missing component in single and multi-layer models of dendritic integration is the assumption of signal flow from dendrites to soma. As I mentioned above, dendrites are capable of releasing neurotransmitters (Ludwig & Pittman, 2003) on their own and their integration properties are fundamentally affected by backpropagating action potentials (Branco & Häusser, 2009; Remy *et al.*, 2009) or the coupling from other dendrites (Remme *et al.*, 2010). These "near-instantaneous" models of dendritic integration also fail to account for the individual histories of the computational subunits. A more accurate representation of the dendritic integration contains, for each computational subunit, a temporally-sensitive component corresponding to the summed influences from other areas of the neuronal tree (see Figure 1.4C). Such model is required to adequately address the recent findings showing spatiotemporal input sensitivity of dendrites.

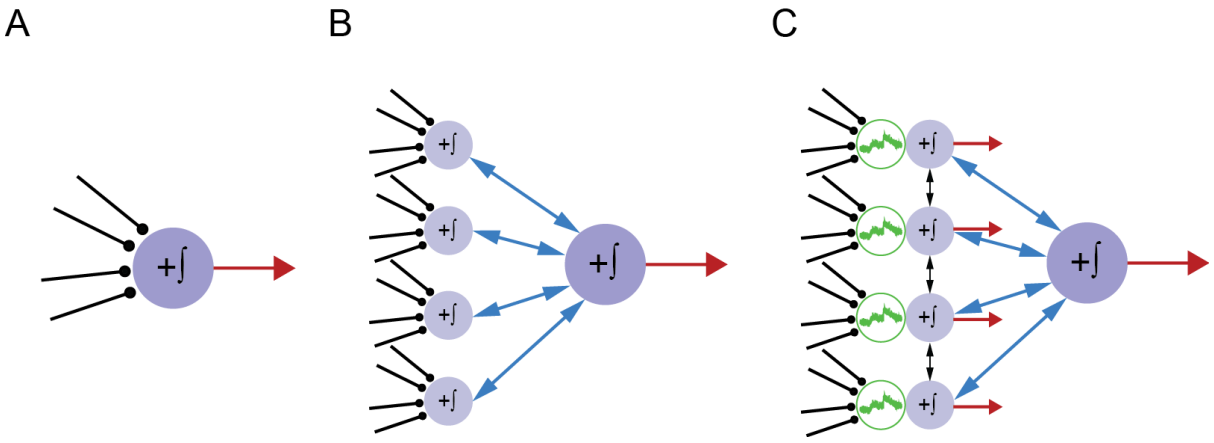

Figure 1.4 A schematic of different models of dendritic integration.

A) In the 'point neuron' representation all dendritic inputs are integrated at the soma, with an output (red arrow) generated when somatic voltage crosses threshold. B) In the two-layer network representation (Poirazi *et al.*, 2003), synaptic inputs are integrated locally in dendritic subunits each of which sums the local inputs and applies a thresholding non-linearity (i.e. a dendritic spike) to generate final output (red arrow). C) Inputs are first integrated in a pattern-dependent manner

(Branco *et al.*, 2010) (green circle) following which a thresholded non-linearity is applied and passed to the soma where an output is generated. Alternatively or concurrently, dendritic release of neuromodulators and neurotransmitters allows local output to be generated. Finally, there is a bidirectional communication between individual subunits and the soma. Figure modified from Branco and Häusser (2010).

1.1.5.6 Spatiotemporal integration in dendrites

In his original works on passive properties of signal propagation, Rall (1964) suggested that dendrites are capable of resolving different spatiotemporal inputs. Such capacity would be useful as it was demonstrated in several studies that sensory systems are capable of resolving neural stimuli that would be too fast for rate codes (Thorpe *et al.*, 2001). In sensory systems, spike timing was shown to correspond to features of stimuli (Meister *et al.*, 1995; deCharms & Merzenich, 1996; Johansson & Birznieks, 2004). In principle, sensitivity to spatiotemporal sequences would greatly enhance the computational capacity of neurons. Recently, Branco and colleagues (2010) confirmed that dendrites are capable of resolving patterned sequences of uncaged glutamate (see Figure 1.5). This is a result of the impedance gradient of dendrites that results in an unequal activation of NMDAR conductance when different spatiotemporal patterns are presented to the dendrite. Centripetal activation of inputs results in a greater recruitment of NMDAR conductance and concurrently a greater likelihood for inducting action potentials (see Figure 1.5I,J) than centrifugal due to high input impedance in the distal regions of the dendrite. This effect is substantially diminished with the application of NMDAR blockers.

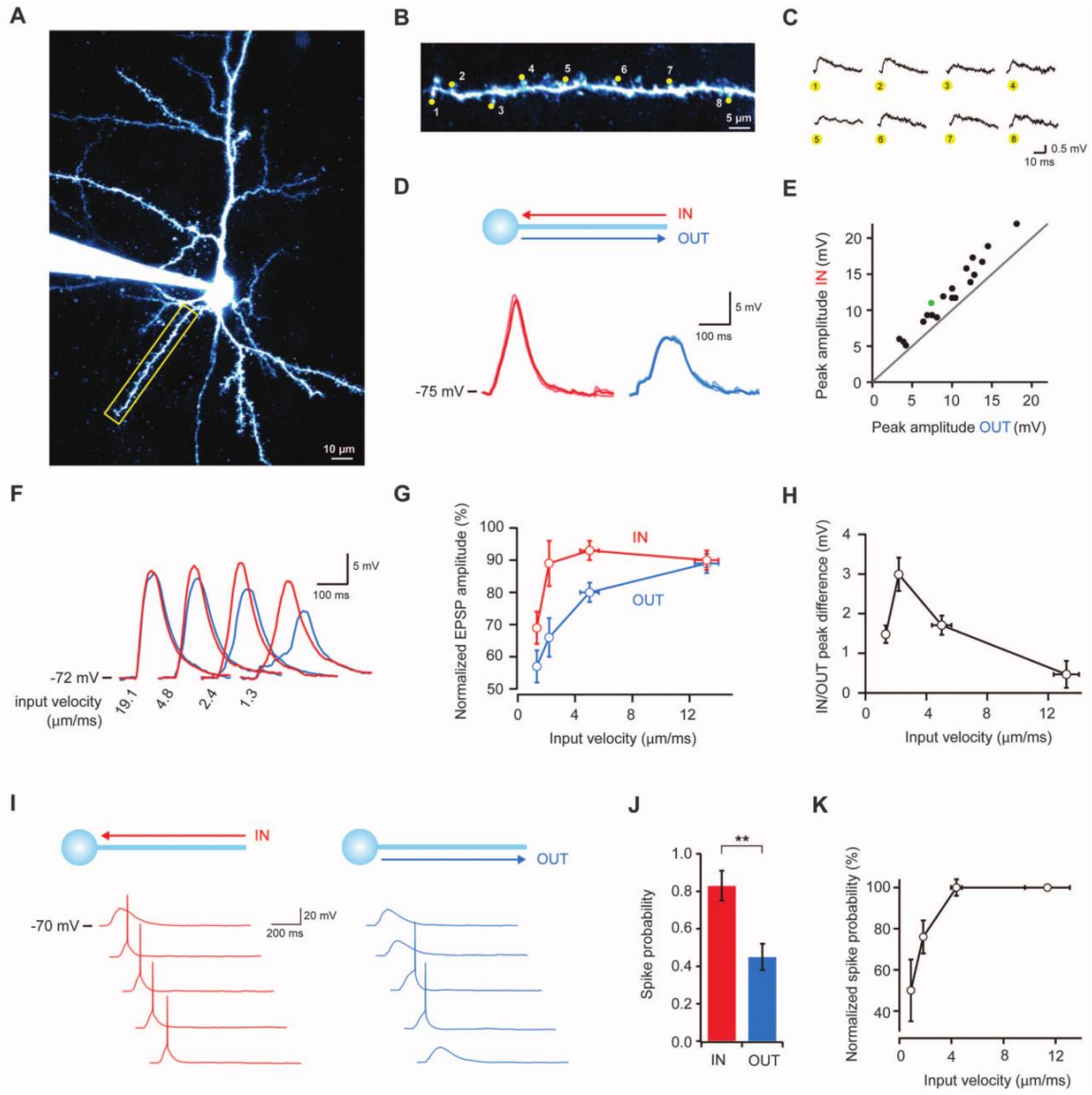

Figure 1.5 Dendrites are sensitive to the direction and velocity of synaptic input patterns.

A) Layer 2/3 pyramidal cell filled with Alexa 594 dye; yellow box indicates the selected dendrite. B) Uncaging spots (yellow) along the selected dendrite. C) Average individual uncaging responses at the soma. D) Somatic responses to IN (red) and OUT (blue) directions at 2.3 µm/ms (averages denoted by bold lines). E) Plot comparing peak amplitudes for IN and OUT sequences at the optimal velocity for direction selectivity [green circle example shown in D)]. F) Direction-selective responses at different velocities. G) Relation between peak voltage and input velocity (values normalized to the maximum response in the IN direction for each cell, N=15). Error bars indicate SEM. H) Relation between direction selectivity and input velocity (N=15). I) Direction selectivity

of spike probability; population data shown in J) (**p = 0.0013, N=7). K) Relation between spike probability and velocity (N=7, average of both directions). Source: Branco et al. (2010).

Ca^{2+} influx through NMDA receptors is tightly linked to the induction of plasticity. Since different spatiotemporal sequences show unequal recruitment of NMDA spikes, it is an open question whether they can result in an unequal induction of plasticity. This thesis is primarily concerned with answering this question.

1.2 PLASTICITY IN NEURONS AND DENDRITES

1.2.1 Historical perspective

Whilst Donald Hebb (1949) is often considered the father of the plasticity field due to his work *Organization of Behaviour*, the term and concept of plasticity has a much longer history, one that Hebb readily acknowledged in his correspondence (Berlucchi & Buchtel, 2009). The term plasticity was probably coined by Ramón y Cajal in a paper in Spanish following from his Croonian Lecture (Cajal, 1894; DeFelipe, 2006). Nevertheless, the concept of neuronal changes as a result of learning was postulated since William James (1890) in his *Principles of psychology*. The Italian neuropsychiatrist Eugenio Tanzi (1893), inspired by Cajal's Neuron Doctrine, hypothesized that the connections between neurons, which were termed synapses 4 years later, constituted a barrier for the transmission of signals. As a result, Tanzi (1893), in what was later termed "synaptic resistance theory", argued that the reduction in the efficacy of such barrier was lowered as a result of repetitive activity between neurons. Donald Hebb's work was instrumental because of his operationalization of the general principles of plasticity described above. Hebb's neurophysiological postulate states that cells that are simultaneously and persistently coactive result in a metabolic process in which (at least) one of the cells efficiency is increased (Hebb, 1949; Sjöström *et al.*, 2008). This rule was later popularized by Carla Shatz (1992) as "neurons that fire

together wire together". In 1964, Kandel and Tauc (1964) showed that pairing a subthreshold EPSP in one pathway of abdominal ganglion cells with spike train in the second pathway sometimes results in facilitation of the EPSP for up to 20 minutes.

The experimental confirmation of Donald Hebb's theory was provided by the famous experiments by Tim Bliss and Terje Lømo (1973). They discovered that repetitive stimulation of the perforant path in the anaesthetized rabbit leads to an increase of the amplitude of EPSP and the reduction of the latency of population spike. Such enhancement of responses was termed long-lasting or long-term potentiation. It became quickly apparent that if the only mechanism for the induction of plasticity were potentiation, the circuit would quickly tend towards runaway excitation. In their theoretical work that was later termed BCM model, Bienenstock, Cooper and Munro (1982) argued that low-frequency activity of presynaptic neurons should result in depression of the synaptic strength and that the converse should occur with high frequency activity, consistent with Bliss and Lømo (1973) results. The depression aspect was later confirmed by Dudek and Bear (1992) who discovered that prolonged low-frequency stimulation of the Schaffer collaterals resulted in the reduction of the EPSP amplitude. Several other forms of long-term modifications have since been described to account for the runaway excitation or depression problem. A prolonged reduction of firing rate (by means of Na^+ blocker Tetrodotoxin (TTX) or AMPA receptor blocker 6-cyano-7-nitroquinoxaline-2,3-dione (CNQX)) leads to the up regulation of synaptic glutamate receptors, whilst increase in excitation (by means of $GABA_A$ blockade via bicuculline) leads to the converse (Turrigiano *et al.*, 1998). This firing rate adaptation was later termed homeostatic synaptic plasticity (Turrigiano & Nelson, 2004; Turrigiano, 2011).

1.2.2 Spike-timing dependent plasticity

In 1996, several theoretical models argued for the role of action potential timing relative to the input in the induction of plasticity (Abbott & Blum, 1996; Gerstner *et al.*, 1996). Non-linear summation of EPSPs and bAPs was found in hippocampal cells (Markram *et al.*, 1995; Magee &

Johnston, 1997). Markram er al. (1997) were the first to show in neocortical cells that synapses are potentiated if the EPSP precedes the AP by few milliseconds, whilst depression is observed if the timing is reversed. Bi and Poo (1998) then quantified the timing requirements in the induction of timing-dependent long-term potentiation (t-LTP) or timing-dependent long-term depression (t-LTD) in hippocampal CA1 cells.

Since the initial studies, spike-timing dependent plasticity has become an important field of the neuroscience on its own, informing multitude of theoretical models of plasticity (Clopath & Gerstner, 2010; Gerstner, 2010; Markram *et al.*, 2011), experimental studies (Sjöström *et al.*, 2008; Caporale & Dan, 2008; Markram *et al.*, 2012) and critiques (Lisman & Spruston, 2005, 2010). Spike-timing dependent plasticity has been described in a number of cell types (see Figure 1.6) – pyramidal cells of the cortex (Markram *et al.*, 1997; Feldman, 2000; Sjöström *et al.*, 2001), CA1 hippocampal cells (Bi & Poo, 1998), GABAergic cells in the ventral tegmental area (VTA) (Kodangattil *et al.*, 2013), fusiform cells of the dorsal cochlear nucleus (Tzounopoulos *et al.*, 2004), and medium spiny neurons in the striatum (Fino *et al.*, 2005; Pawlak & Kerr, 2008).

In cortical cells, the mode of t-LTD and t-LTP induction differs. The locus of t-LTD is located on the pre-synapse and is dependent on CB1 (Sjöström *et al.*, 2003) and pre-synaptic NMDA receptors (Rodríguez-Moreno & Paulsen, 2008; Rodríguez-Moreno *et al.*, 2010). In fact, a purely presynaptic patterned activation (burst of three spikes followed by a spike) is sufficient for LTD induction in what is called the pattern-dependent LTD (Rodríguez-Moreno *et al.*, 2013). On the other hand, t-LTP is dependent on the post-synaptic receptors (Sjöström *et al.*, 2003, 2008).

There are several roles that are hypothesized for spike-timing dependent plasticity in neural circuits. Computationally, spike-timing dependent plasticity (STDP) learning rules are expected to reduce the latency with which the presynaptic cell drives the postsynaptic cell (Song *et al.*, 2000). Due to its spike-timing sensitivity, STDP is postulated to be involved in temporal coding learning (Gerstner *et al.*, 1996). Furthermore, STDP was shown in a computational model to underlie

receptive field development and remapping after injury (Song & Abbott, 2001). Such changes in receptive field remapping were observed in visual cortex (Schuett *et al.*, 2001; Meliza & Dan, 2006; Pawlak *et al.*, 2013), somatosensory (Celikel *et al.*, 2004; Jacob *et al.*, 2007; Gambino & Holtmaat, 2012) and in auditory cortex after STDP-like pairing of tones with nucleus basalis stimulation (Froemke *et al.*, 2007, 2012).

The basic STDP learning rule appears to be conserved across several animal species (see Figure 1.6C) and it was demonstrated in developing retinotectal synapses of *Xenopus* tadpoles (Zhang *et al.*, 1998), Kenyon cells of locusts (Cassenaer & Laurent, 2012), visual cortex of cats (Frégnac *et al.*, 1988), corticospinal synapses of macaques (Nishimura *et al.*, 2013) and in M1 cortex of humans following transcranial magnetic stimulation (Müller-Dahlhaus *et al.*, 2010).

STDP learning rules gained popularity due to their relative simplicity, biological plausibility and relative stability (Paulsen & Sejnowski, 2000; Song *et al.*, 2000; van Rossum *et al.*, 2000) compared to other models such as Hebbian plasticity, which suffers from the runaway excitation. Nevertheless, STDP remains mostly a phenomenological model of learning and the biochemical mechanism for the observed bidirectional plasticity remains to be elucidated.

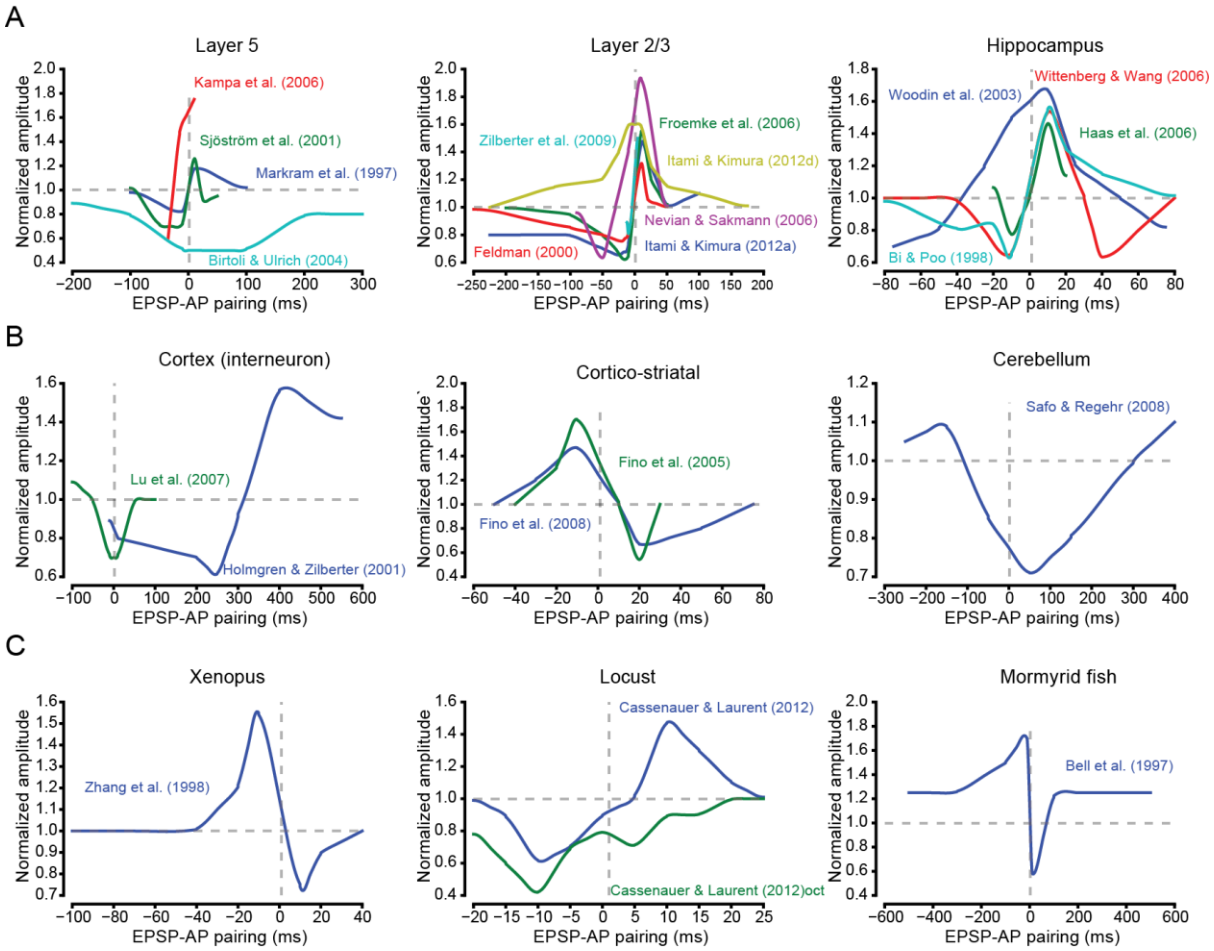

Figure 1.6 Spike-timing dependent plasticity is cell-type dependent

Schematic of observed spike-timing dependent plasticity curves in the literature. A) Principal cells of the cortex and hippocampus show largely Hebbian STDP. Suffixes: (a) – adult, (d) – development. B) Anti-Hebbian STDP in cortical interneurons, cortico-striatal cells and cerebellum. C) Hebbian and anti-Hebbian STDP in non-mammalian species. Suffix: (oct) – octopamine application.

1.2.3 Plasticity induction

LTP is a catch-all term for a substantial number of different potentiation mechanisms that have been observed in a variety of cell-types. The mechanisms of induction, such as the type of receptors required, the site of modification (i.e. pre- or post-synaptic membrane) and the nature of modification (i.e. upregulation of synaptic receptors, or change in intrinsic conductances) can vary considerably (Malinow & Malenka, 2002; Sjöström *et al.*, 2008). As a result of this "embarrassment of riches" of LTP-types (Malenka & Bear, 2004), I will restrict the discussion to primarily NMDA-dependent LTP in hippocampal cells and pyramidal cells of cortex.

1.2.3.1 Role of calcium in plasticity induction

In its canonical form, LTP is dependent on Ca^{2+} entry through NMDA receptors (Collingridge *et al.*, 1983; Bliss & Collingridge, 1993). Buffering of Ca^{2+} using a slow ethylene glycol-bis(β-aminoethyl ether)-N,N,N',N'-tetraacetic acid (EGTA) or fast 1,2-bis(o-aminophenoxy)ethane-N,N,N',N'-tetraacetic acid (BAPTA) buffer results in a block of plasticity induction (Lynch *et al.*, 1983; Nevian & Sakmann, 2006; Lee *et al.*, 2009). Whilst it is clear that Ca^{2+} elevation is important for both LTP and LTD, it is not clear what spatial or temporal profile of Ca^{2+} increase is required for the differential induction.

One of the most popular is the so-called Ca^{2+} control hypothesis (Lisman, 1989; Lee *et al.*, 2000) in which the magnitude of Ca^{2+} influx activates either kinases or phosphatases to phosphorylate or dephosphorylate AMPA receptors and thus determine the sign of plasticity. Large increases in Ca^{2+} are expected to lead to potentiation primarily by the recruitment of Ca^{2+}/calmodulin-dependent protein kinase II (CaMKII) (Lisman *et al.*, 2002). This Ca^{2+} influx is sensed by the calmodulin domain of CaMKII and is autophosphorylated at the T286 site which results in its persistent activity (Lisman *et al.*, 2012). Following such an event, CaMKII is upregulated and translocates specifically to the potentiated spines during LTP (Lee *et al.*, 2009), where it phosphorylates AMPA receptor and increases its conductance (Barria *et al.*, 1997), binds to NR2B

subunit of NMDA receptor (Barria & Malinow, 2005) and binds to F-actin and α-actinin (Hell, 2014). CaMKII interaction with actin and actin-binding proteins is consistent with the role of actin in structural plasticity (Dillon & Goda, 2005*a*; Cingolani & Goda, 2008). Furthermore, the growth and maintenance of spines observed *in vivo* during learning is dependent on the phosphorylation at the T286 site (Wilbrecht *et al.*, 2010) and the level of CaMKII activity is predictive to whether synapses will persist after monocular deprivation (Mower *et al.*, 2011). The sensor for moderate or small increases of Ca^{2+} , which are required for the induction of NMDAR dependent form of LTD, is presumed to be protein phosphatases as this was demonstrated demonstrated for both CA1 and cortical cells (Lisman, 1989; Mulkey & Malenka, 1992; Kirkwood & Bear, 1994).

Despite these simple rules, both LTP and LTD come in many forms with induction parameters differing based on the type of synapse (i.e. CA1, mossy fiber), receptor type responsible (i.e. NMDAR, mGluR) or the type of biochemical cascade (Malenka & Bear, 2004). For example in the case of t-LTD in the cortex, the mechanism is more complex due to the role of pre-synapse and astrocyte network in depression of synaptic efficacy (Sjöström *et al.*, 2003; Bender *et al.*, 2006; Min & Nevian, 2012). Support for Ca^{2+} control hypothesis has come from rate-based induction protocols in cortex and in cerebellar granule cells (Ismailov *et al.*, 2004; Gall *et al.*, 2005). EPSP-AP pairings were found to result in EPSP enhancement in electrophysiological recordings, in simulations and in supralinear rise of Ca^{2+} (Stuart & Häusser, 2001; Nevian & Sakmann, 2006; Kampa *et al.*, 2006; Kampa & Stuart, 2006). Nevertheless, t-LTD induction protocols were found to have indistinguishable peak Ca^{2+} influx from protocols that resulted in t-LTP (Nevian & Sakmann, 2006).

There are several methodological problems that frustrate the study of the profile of Ca^{2+} in plasticity induction. Firstly, Ca^{2+} dyes are Ca^{2+} buffers, and, as has been shown above, Ca^{2+} buffers prevent the induction of plasticity. As a result, few studies have attempted to measure plasticity magnitude at the same time as measuring Ca^{2+} influx. Secondly, physiological Ca^{2+} buffers tend to

be immobile as compared to synthetic dyes or genetically encoded calcium indicators (Higley & Sabatini, 2008). Thus, if the Ca^{2+} role in plasticity induction happens in a micro- or nano-domain (Berridge, 2006), our current dyes may not able to capture this. Finally, the dye's affinity for Ca^{2+} needs to be taken into account. The difference in Ca^{2+} influx between a small amplitude EPSP and high-frequency AP-EPSP pairing can span several orders of magnitude. High affinity dyes saturate at high levels of Ca^{2+} entry, thus underestimating the Ca^{2+} influx, whereas low affinity dye may not detect the small events. Whilst Ca^{2+} entry is clearly necessary for plasticity induction, the relationship between Ca^{2+} profile and magnitude or sign of plasticity is unknown. Nevertheless, several electrophysiological, biochemical and morphological processes have been shown to account for plastic changes that I will briefly discuss below.

1.2.3.2 Changes in synaptic receptor content

One of the first identified mechanisms of the expression of canonical LTP was via the change in AMPA receptor conductance at the synapse. Following an LTP induction protocol, it was shown that AMPA-receptor conductance was increased (Benke *et al.*, 1998). One already discussed means of increasing conductance is via phosphorylation of AMPA receptors, which was demonstrated to happen via PKA (Banke *et al.*, 2000) or CaMKII (Barria *et al.*, 1997), resulting in an increased channel opening of the AMPA receptor (Kristensen *et al.*, 2011; Derkach, 2011). Another source of conductance increase is through the trafficking of AMPA receptors to the synapse (Malinow & Malenka, 2002; Bredt & Nicoll, 2003). Such trafficking into membrane is dependent on the interaction between the AMPA receptor GluA1 subunit C-tail with the PDZ domain proteins (Shi *et al.*, 1999, 2001; Hayashi *et al.*, 2000). The delivery of AMPA receptors can happen through exocytosis (Park *et al.*, 2004; Kopec *et al.*, 2006) or lateral diffusion from extrasynaptic sites (Ehlers *et al.*, 2007; Makino & Malinow, 2009), the importance of each of these modes is currently an area of active research. Despite the importance of C-tail interaction with PDZ in traditional LTP induction protocols (Shi *et al.*, 2001; Kessels & Malinow, 2009), it was recently found that any

receptor subunit, even artificially expressed kainate receptors, is capable of LTP induction (Granger *et al.*, 2013). Apart from kainate receptors, NMDAR-dependent currents were found to be potentiated following LTP induction protocol (Watt *et al.*, 2004). The full review of the plasticity of synaptic receptors is beyond the scope of this introduction, however, the results from these studies suggest that several synaptic conductances can be modified in parallel following induction stimulus.

1.2.3.3 Structural plasticity

Spines on which most of the synapses are located are motile and can increase in size following LTP stimuli (Matsuzaki *et al.*, 2004). Furthermore, new spines may emerge following LTP induction (Engert & Bonhoeffer, 1999; Kwon & Sabatini, 2011). Despite their size, spines are very complicated structures both structurally and biochemically (Hering & Sheng, 2001; Dillon & Goda, 2005*b*; Cingolani & Goda, 2008; Bramham, 2008; Rochefort & Konnerth, 2012). Similarly, multiple good reviews have been written on the topic of structural plasticity of spines in cortex and hippocampus (Matus, 2000; Segal, 2005; Alvarez & Sabatini, 2007; Holtmaat & Svoboda, 2009; Kasai *et al.*, 2010; Bourne & Harris, 2011; Colgan & Yasuda, 2014). In this introduction, I will restrict my discussion to the interaction between electrophysiological and structural correlates of potentiation.

Observing morphological changes of spines as a proxy for LTP is mostly useful in *in vivo* settings where direct electrophysiological recordings are difficult or impossible due to the time required for recording. Experience-dependent changes were reliably found to induce spine turnover, growth and maintenance or persistence of spines for different tasks or deprivation protocols, in different animal models and in several regions of the brain (Trachtenberg *et al.*, 2002; Holtmaat *et al.*, 2005; Hofer *et al.*, 2009; Xu *et al.*, 2009; Yang *et al.*, 2009; Roberts *et al.*, 2010; Wilbrecht *et al.*, 2010). Increase in the spine head size is associated with an increase in AMPA receptor content (Matsuzaki *et al.*, 2004; Zito *et al.*, 2009). Other structural modifications are possible such as

widening or increasing the length of the spine neck and thus modulating the level of spine-dendrite compartmentalization (Grunditz *et al.*, 2008; Tønnesen *et al.*, 2014; Araya *et al.*, 2014). Nevertheless, whilst structural plasticity is often correlated with its functional counterpart, morphological changes do not necessarily imply electrophysiological changes. One proposed reason for this discrepancy is that the post-synaptic density (PSD) region where synaptic receptors are located and which is close to the area of vesicle fusion is relatively small (Cingolani & Goda, 2008). An increase in spine volume head therefore would not lead to functional plasticity if it is not followed by changes in the receptor content of the PSD. Similarly, if the presynaptically released glutamate fails to saturate receptors in their basal state, increasing spine size and receptor content would not necessarily lead to an enhancement of synaptic strength. At present, it is unclear whether reported dissociation between functional and structural changes at the synapse (Sdrulla & Linden, 2007; Wang *et al.*, 2007*b*) is due to insufficient receptor content, the size of PSD or the amount of released glutamate.

1.2.3.4 Intrinsic excitability plasticity

Despite the changes in synaptic conductances described above, plasticity can also lead to changes in intrinsic excitability of a cell. These can be either local or global changes of excitability. LTP induction protocols have been found to enhance overall excitability of cells in cerebellar granule cells (Aizenman & Linden, 2000), visual cortical cells (Cudmore & Turrigiano, 2004) and in *Xenopus* tadpole optic tectum (Aizenman *et al.*, 2003). These changes were found to be dependent on Ca^{2+} influx or were dependent on Ca^{2+} permeable receptors. In fact, changes in global intrinsic excitability are common across different species and have been described for a range of vertebrate and invertebrate animal models (Zhang & Linden, 2003). The nature of the excitability changes can vary considerably as well, such as by modifying Na^{+} (Ganguly *et al.*, 2000) , K^{+} (Sourdet *et al.*, 2003), VGCC (Su *et al.*, 2002) or HCN based currents (Fan *et al.*, 2005).

1.2.4 Plasticity in dendrites

Apart from the mode of plasticity expression being variable, dendrites also exert an important influence on its induction. I will discuss two aspects that received substantial attention here – the location of the synapses and the degree of clustering's influence on the magnitude and sign of plasticity observed.

1.2.4.1 Location and plasticity induction

As I described above, propagation of voltage signals such as EPSPs and bAPs are spatially regulated in dendrites. Therefore, it has been proposed that the STDP rule should be influenced by the location of synapses to be potentiated or depressed (Sourdet & Debanne, 1999). Proximal dendrites, where APs back-propagate efficiently, express typical STDP. Nevertheless, the magnitude of potentiation shows a distance-dependent gradient, even switching into depression at distant synapses (Froemke *et al.*, 2005; Sjöström & Häusser, 2006; Letzkus *et al.*, 2006; Gordon *et al.*, 2006). Such distance-dependent LTD can be rescued by either enhancing cooperativity between inputs via strong extracellular stimulation or by boosting backpropagation of action potential via dendritic current injection (Sjöström & Häusser, 2006). This depolarization dependency of potentiation was also found for the proximal dendrites, presumably depending on the voltage-dependence of the Mg^{2+} unblocking from NMDA receptors (Kampa *et al.*, 2004). Alternatively exogenously applied BDNF was found to also rescue distal failure of potentiation (Gordon *et al.*, 2006). Whilst some studies did not observe this switch into depression at positive EPSP-AP intervals (Froemke *et al.*, 2005), the preference for depression at distal synapses is consistent. This is presumably due to the more compact dendritic tree of layer 2/3 cells (Froemke *et al.*, 2005) compared to layer 5 cells where bAP propagation does not reach to the farthest extents of the apical tree (Häusser *et al.*, 2000). Such location dependence of potentiation rules is expected to enhance the computational capacity of neurons (Froemke *et al.*, 2010).

1.2.4.2 Spatial extent of plasticity

One fundamental aspect of plasticity predicted by Donald Hebb is the synapse specificity of potentiation. In his view, only synapses that are repeatedly involved in driving postsynaptic cell firing should undergo potentiation. However, we now know that there is a breakdown of synapse specificity at short distances. Harvey and Svoboda (2007) discovered that a subthreshold pairing protocol induces structural potentiation if a nearby spine (> 10 μm) undergoes LTP pairing. Surprisingly, the small guanosine triphosphate Ras spreads approximately the same distance following an uncaging LTP pairing protocol (Harvey *et al.*, 2008). An influential theory of plasticity, the synaptic tagging hypothesis, postulates that potentiation protocols set a "tag" at a synapse which then attracts a group of translated plasticity-related proteins, resulting in a late-phase LTP (Frey & Morris, 1997, 1998). Although the initial hypothesis stated that the translation occurred at the soma, it is more likely that local translation plays an important role in the maintenance of plasticity in dendrites (Kang & Schuman, 1996; Sutton & Schuman, 2006), and this has been recognized in the updated version of the theory (Redondo & Morris, 2011). According to Clustered Plasticity Hypothesis, local protein translation and the synaptic tagging hypothesis should naturally lead to the dendritic branch becoming an integrative unit of plasticity induction (Govindarajan *et al.*, 2006), a theory which was indirectly supported in a structural plasticity study in a culture (Govindarajan *et al.*, 2011). The support for clustering of synapses in plasticity was also found *in vivo* (Makino & Malinow, 2011; Gambino *et al.*, 2014). Surprisingly, the hypothesis that plasticity results in clustering is much less controversial than the presence of clustered synaptic inputs in the basal state (see above), despite the fact that the results predicted are the same.

1.2.4.3 Spatiotemporal plasticity

What other integration modalities are dendrites capable of? We know that dendrites are sensitive to distinct spatiotemporal patterns (Branco *et al.*, 2010) and that the timing of afferent input in CA1 cells can influence the sign of plasticity (Kwag & Paulsen, 2009).

Nevertheless, it is uncertain whether neurons can learn to decode such patterns. Neurons can respond to stimuli that are timed only milliseconds apart (VanRullen *et al.*, 2005; Gollisch & Meister, 2008; Gütig, 2014). Learning to respond to a particular spike input pattern has been the subject of numerous computational studies. Utilizing reinforcement learning to change the release probability of synapse depending on their recent actions, a neural network of integrate-and-fire neurons learned to accurately perform as a XOR function for four input patterns (Seung, 2003). These so-called "hedonistic synapses" perform stochastic gradient descent learning that is, however, typically slower than direct gradient approaches (Gütig, 2014). Utilizing a direct gradient descent approach, Gütig and Sompolinsky (2006) derived the tempotron-learning rule which minimizes the distance between maximal postsynaptic voltage and the neuron's firing threshold.

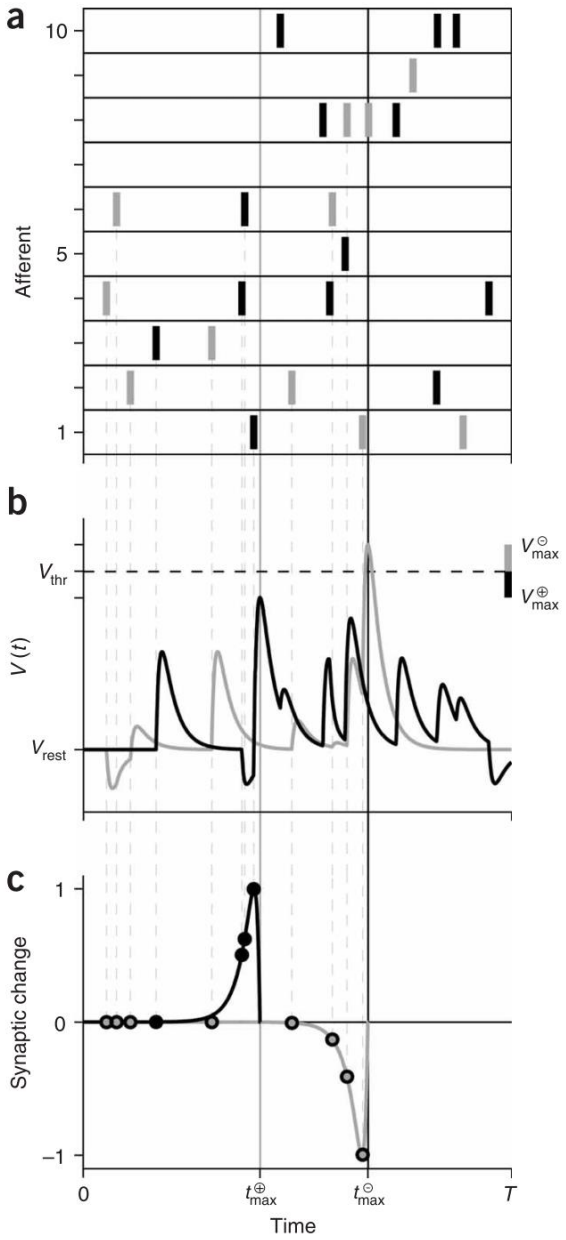

Figure 1.7 The tempotron learning rule.

A) Spike times (thick vertical lines) of ten afferents in two schematic input patterns $\oplus$ (black) and $\ominus$ (gray). B) Resulting postsynaptic voltage traces $V(t)$. Maximal voltages are reached at $t_{max}^{\oplus}$ and $t_{max}^{\ominus}$ (thin solid vertical lines), respectively. Because $V(t_{max}^{\oplus}) < V_{thr} < V(t_{max}^{\ominus})$ with V_{thr} (dashed horizontal line) denoting the spike threshold, both patterns generate an error. Inputs arriving after a threshold crossing (gray trace) are shunted. Black and gray thick vertical lines indicate the cost terms $V_{max} - V_{thr}$ and $V_{thr} - V_{max}$ associated with the $\oplus$ and $\ominus$ patterns

respectively. C) Resulting synaptic changes (in units of maximal change, λ) depend on presynaptic spike times (circles) relative to the corresponding voltage maximum. Thin dashed vertical lines in (a-c) mark presynaptic spike times. Source: Gütig and Sompolinsky (2006).

Compared to other decoders, the tempotron-learning model was shown to be able to quickly classify various complex visual features and be robust to spike-time jitter (Gütig *et al.*, 2013). Surprisingly, the number of patterns that a single neuron can store was a multiple (up to 3x under some conditions) of the number of synapses. Nevertheless, the tempotron model is based on a simplified model of integrate-and-fire neuron. As a result, inputs do not have a spatial component that is present in a morphologically realistic neuron. Despite their simplicity, such models are can encode precise spike-timing inputs and have practical utility in categorization tasks. It is currently unclear whether realistic neurons are capable of learning to encode arbitrary spatiotemporal inputs. The existence of spatiotemporal plasticity is currently an unknown tantalizing frontier of neuroscience.

1.3 AIM OF THE THESIS

The main aim of the thesis is to explore the capability of cortical neurons to potentiate specific spatiotemporal patterns of activity, and investigate the underlying mechanisms for such pattern storage. To analyse such enhancement of spatiotemporal read-out, glutamate uncaging is a useful method. Uncaging of MNI-glutamate was previously used in plasticity experiments (Matsuzaki *et al.*, 2004) and spatiotemporal activation of synapses (Branco *et al.*, 2010). The method allow precise control of synaptic activation on a micrometer scale (Harvey & Svoboda, 2007; Harvey *et al.*, 2008) with sub-millisecond temporal precision. As a result, glutamate uncaging is a natural candidate for such experiments to be carried out. However, currently most widely used compound, MNI-glutamate was also found to block inhibition (Maier *et al.*, 2005) which plays a significant role in the induction of plasticity. RuBi-glutamate was previously found to reduce the degree of inhibition, however, the reduction was partial (Fino *et al.*, 2009). To my knowledge, no uncaging compound

exists at the moment that would prevent GABA blockage. However, it is currently unclear what the appropriate physiological conditions are during the induction of plasticity. UP states in cortex which are associated with greater excitatory drive and thus expected increase in plasticity occurrence can result from a decrease in tonic inhibitory drive. Consistently with this view, many experimental setups use blockers of GABA(A) receptors to enhance the likelihood of induction of plasticity (Magee & Johnston, 1997).

The role of inhibition is well established in plasticity literature. Generally, a decrease in inhibition is associated with an increased likelihood of induction of plasticity (Buonomano & Merzenich, 1998). There are two known modes of inhibition in the cortex. Phasic is transient, recruited at a millisecond scale often following excitatory stimulus. Under basal state, this form of inhibition can be seen in spontaneously occurring miniature post-synaptic currents (mIPSCs). Tonic inhibition is longer acting, initially discovered by the decrease of holding current required to clamp cells at a given membrane potential (Kaneda *et al.*, 1995). It is likely that both of these modes of inhibition are recruited in the modulation of plasticity although their relative roles are yet to be elucidated. Phasic inhibition could serve as a gating mechanisms for the induction of plasticity, preventing the development of the plasticity during induction. On the other hand, tonic inhibition could serve to set the "tone" or the level of plastic changes in the cortex. This would be consistent with the important role of inhibition in setting up critical periods in cortex. Tonic inhibition was found to be important before maturation of synapse formation takes place (Farrant & Nusser, 2005). Furthermore, maturation of inhibition was linked with the end of critical period and reduction of the intracortical inhibition was found to re-activate critical period for ocular dominance plasticity (Sale *et al.*, 2007; Harauzov *et al.*, 2010). As a result, inhibition is expected.

In Chapter 1, I will explore potentiation induction using two-photon glutamate uncaging. I will describe the induction of spatiotemporal dependent plasticity in basal dendrites of layer 5 neurons in the rat from the electrophysiological standpoint.

In Chapter 2, I will employ pharmacology to explore the requirements for induction of potentiation. I will also explore the kinetics of Ca^{2+} using two-photon calcium imaging to further characterize the properties of spatiotemporal plasticity.

In Chapter 3, using compartmental modelling and a genetic optimization algorithm, I will isolate the key parameters for potentiation. I will show that the potentiation of distinct spatiotemporal sequences is possible with physiological constraints partly derived from my calcium imaging experiments.

Finally, I will discuss what these findings suggest for future research on the topic of spatiotemporal plasticity, and the implications for neural circuit function.

2 METHODS

2.1 ELECTROPHYSIOLOGY

2.1.1 Slicing and experimental solutions

All experiments were performed in acute parasagittal slices (300 μm) containing both visual and somatosensory cortices prepared from P14-21 Sprague-Dawley rats in accordance with national and institutional guidelines. Rats were anaesthetized with isoflurane, decapitated and the brain quickly removed and placed in ice-cold artificial cerebrospinal fluid (ACSF) (in mM: NaCl 125, KCl 2.5, glucose 25, NaH_2PO_4 1.25, $NaHCO_3$ 26, $MgCl_2$ 1, $CaCl_2$ 2 (pH 7.3 when bubbled with 95% O_2 and 5% CO_2)). Slices were cut on a Leica Vibratome (Leica VT1200S). Slices were transferred to ACSF at 36 °C for approximately 10-30 minutes and allowed to cool to room temperature for another 30 minutes. Slices were disposed of after 6 hours post-slicing. Recordings were done at 32-35 °C. When required, 50 μM D-APV was added to the regular ACSF solution and to the uncaging solution (see below) to block NMDA receptors. During experiments, slices were placed in an experimental chamber and were constantly perfused with carbonated ACSF.

2.1.2 Whole-cell recordings

Somatic whole-cell recordings were obtained from layer 5 pyramidal cells of somatosensory cortex with a Multiclamp 700B amplifier (Molecular devices) and data was acquired at 50 kHz using custom-written software in MATLAB interfacing with a National Instruments board. Patch pipettes had a resistance of 4-7 MΩ and were filled with internal solution containing (in mM): K-Gluconate 125, KCl 20, HEPES 10, MgATP 4, NaGTP 0.3, Na-Phosphocreatine 10 (pH 7.2-7.4 adjusted with KOH to fit). 20 μM Alexa-594 was added to the solution for visualization purposes and 100 μM of Fluo-5F for calcium imaging. The series resistance of recordings was less than 30 MΩ.

2.2 TWO-PHOTON IMAGING AND UNCAGING

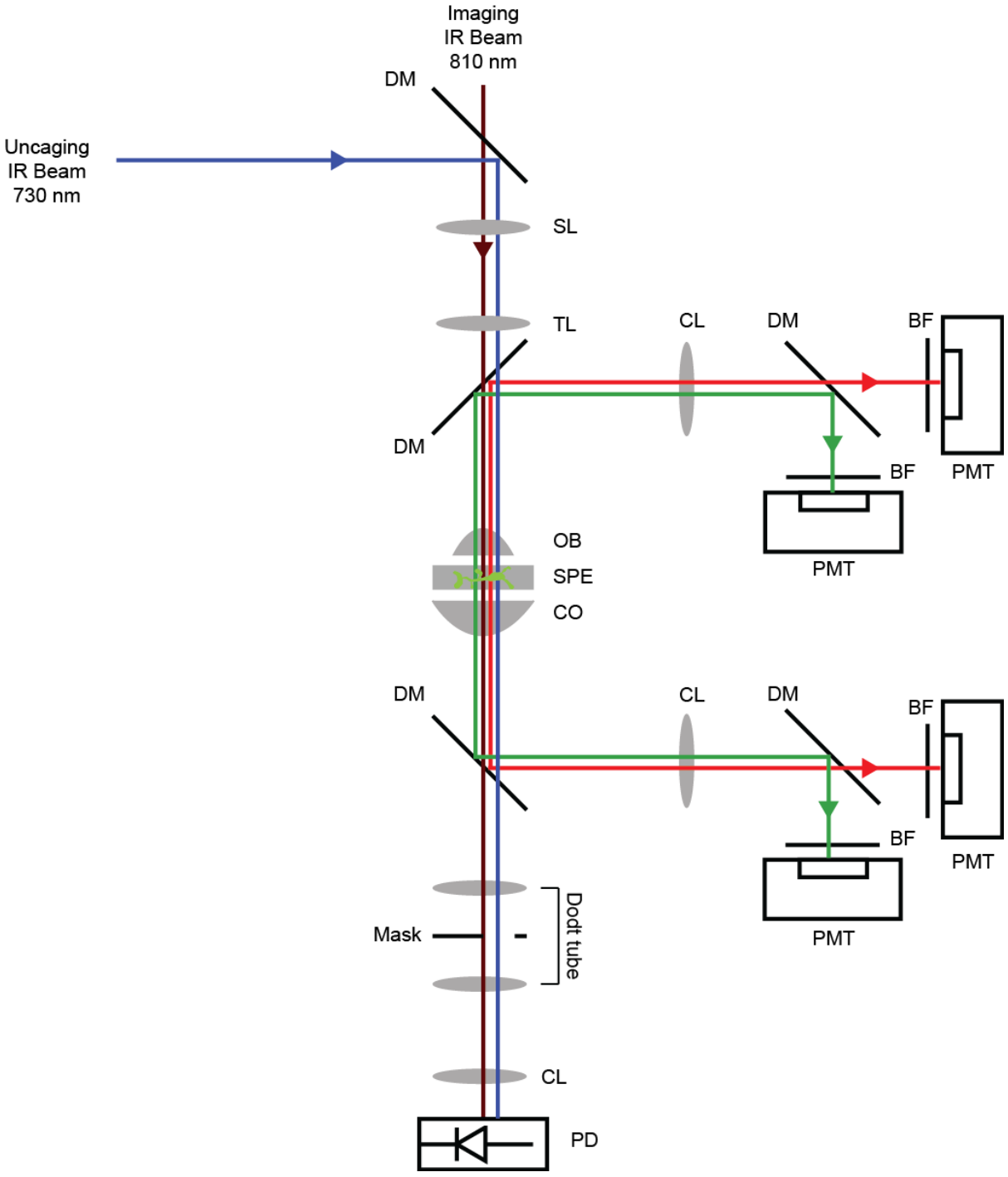

Figure 2.1 Schematic of the two-photon uncaging and imaging setup used in experiments.

Specimen (SPE) or MNI-glutamate is excited with Ti:sapphire laser at a wavelength 810 nm (imaging laser) and 730 nm respectively. The 730 nm and 810 nm pass a separate set of scan lens (SL) and tube lens (TL) and are filtered using dichroic mirror (DM) to minimize crosstalk. Epi-

and trans-flourescence are collected using objective (OB) and condenser (CO) respectively. Fluorescence photons are reflected by dichroic mirrors into detection systems composed of collection lenses (CL) that image the respective back apertures onto photomultiplier tube detectors (PMT). Dichroic mirrors and bandpass filters (BF) separate the signals from red and green fluorophores. Furthermore, the laser light passing through the sample is collected through a Dodt tube and is detected by photodiode (PD) to enable gradient contrast microscopy. The figure is inspired by a similar schematic in Yasuda et al. (2004) and adjusted to correspond to my 2-photon uncaging and imaging setup.

2.2.1 MNI-glutamate uncaging and calcium imaging

Simultaneous two-photon imaging and uncaging was performed using a dual-galvanometer based scanning system (see Figure 2.1) using two Ti:sapphire pulsed lasers with one tuned to 810 nm for calcium and cell morphology imaging, and another tuned to 730 nm for photolysis of the caged MNI-L-glutamate (24 mM, Tocris). MNI-L-glutamate was dissolved in (in mM): NaCl 125, KCl 2.5, HEPES 10, $CaCl_2$ 2, $MgCl_2$ 2, glucose 25. The uncaging solution was delivered with a glass pipette with a large opening using Picospritzer III (Parker Instrumentation). Uncaging exposure time was 500 μs. Recordings were rejected from analysis when they developed signs of excitotoxicity (see Figure 2.2) Calcium imaging was performed by selecting arbitrary trajectories defined by the dendritic trajectory at 500 Hz. All data were acquired using custom written software in MATLAB.

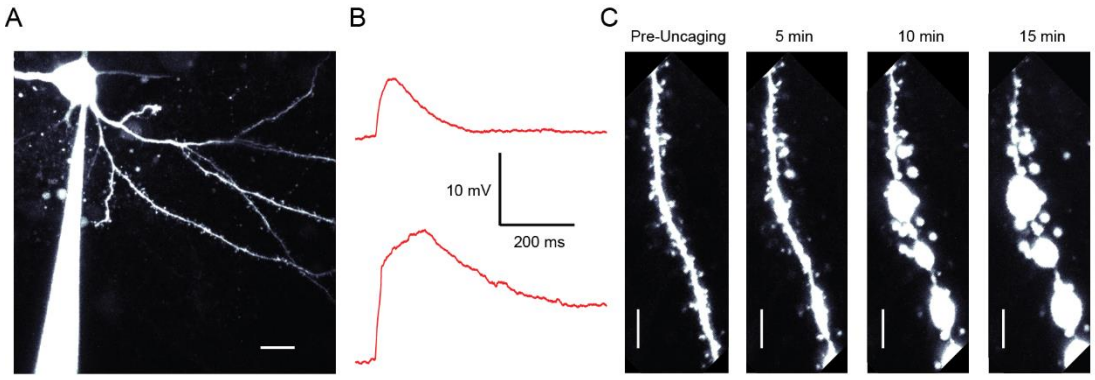

Figure 2.2 Uncaging induced photodamage in dendrites.

A) A sample Layer 5 pyramidal cell from which recording was made (Scale bar: 20 μm). B) Sample whole-cell recordings following compound uncaging stimulus. Top: Standard recording non-indicative of photodamage. Bottom: Failure to re-polarize is indicative of photodamage. C) Time-lapse example of photodamage to dendrite following over-stimulation (Scale bar: 10 μm).

To minimize the influence of drift on the quality of recordings, a baseline image was collected at the beginning of the recording. Subsequently, images of dendrite were sampled at regular intervals (~5 minutes) and offset in position of the dendrite was corrected manually to correspond with the baseline image.

2.3 LONG-TERM PLASTICITY INDUCTION PROTOCOLS

2.3.1 Uncaging-based LTP induction protocol

A giga-ohm seal was obtained from a neuron after which a whole-cell recording was established. 4-24 synapses were selected on a dendrite manually based on the position of putative spines. Unless noted otherwise, a baseline measurement was obtained by stimulation of all synapses at a variable inter-spine interval (in a range of 0.6-8 ms) for 6 minutes at a rate of 1 compound stimulation per minute. A negative current pulse (-25 pA) was injected after the EPSP to measure R_N. The cell was rejected from analysis if the mean of the first half of baseline measurement deviated by more than 10% from the second half. Following baseline measurements, LTP was induced by pairing spike trains with EPSPs consisting of five spikes at a desired frequency (20-100 Hz). The pairing was performed 15 times at 0.1 Hz. Paired spikes were induced using 3 ms current injection (1-1.8 nA) and followed the onset of compound stimulation (EPSP) by a variable time interval (30-130 ms). After the induction, the responses were monitored for as long as possible. The degree of potentiation was measured as the average response following induction until the end of recording divided by the initial response obtained during baseline recording. Recordings where the puffing

pipette delivering MNI was visibly blocked were removed from analysis. Recordings were not included in the analysis if they were shorter than 15 minutes post-induction. Unless otherwise noted, recordings were also excluded from the analysis if the input resistance changed by more than 30% compared to baseline measurement.

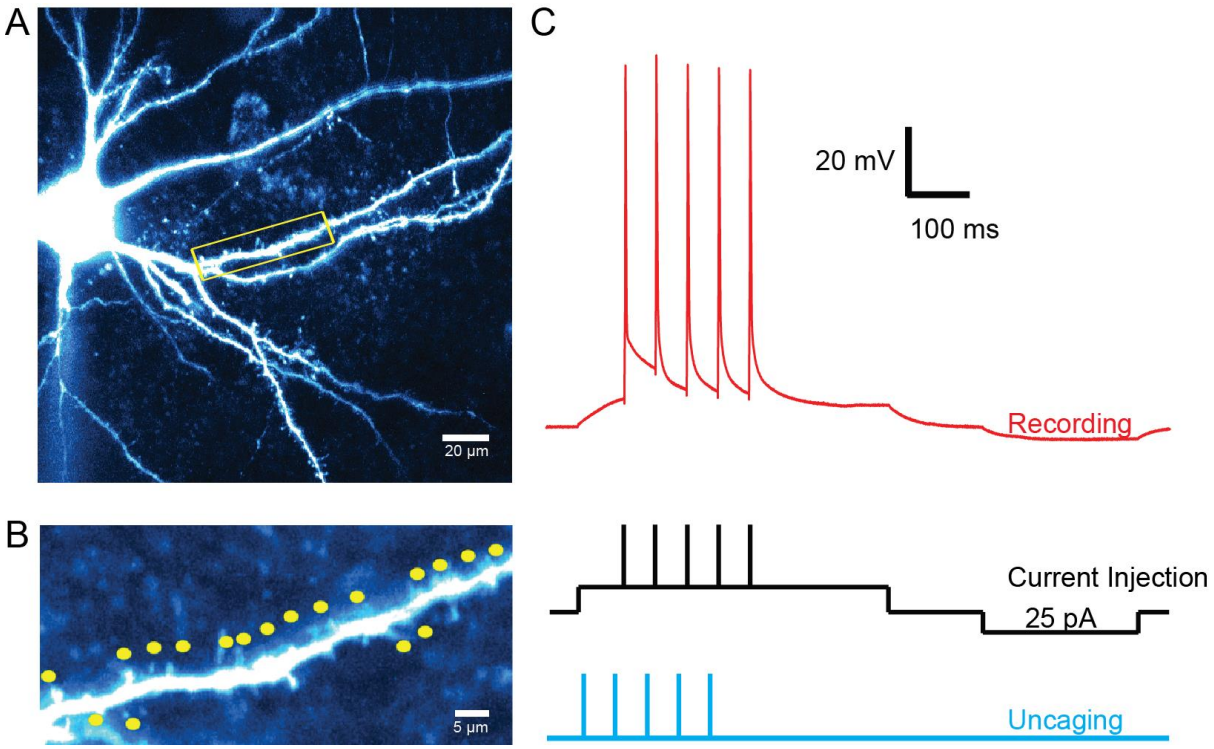

Figure 2.3 Methodology for uncaging-based induction of plasticity.

A) Layer 5 pyramidal neuron filled with Alexa 594 dye; yellow box indicates selected basal dendrite for uncaging. B) Uncaging spots (yellow) along the selected dendrite. C) Uncaging pulses with spike trains with current injection to elicit action potentials at variable Δt. Sample recording during induction is shown on the top.

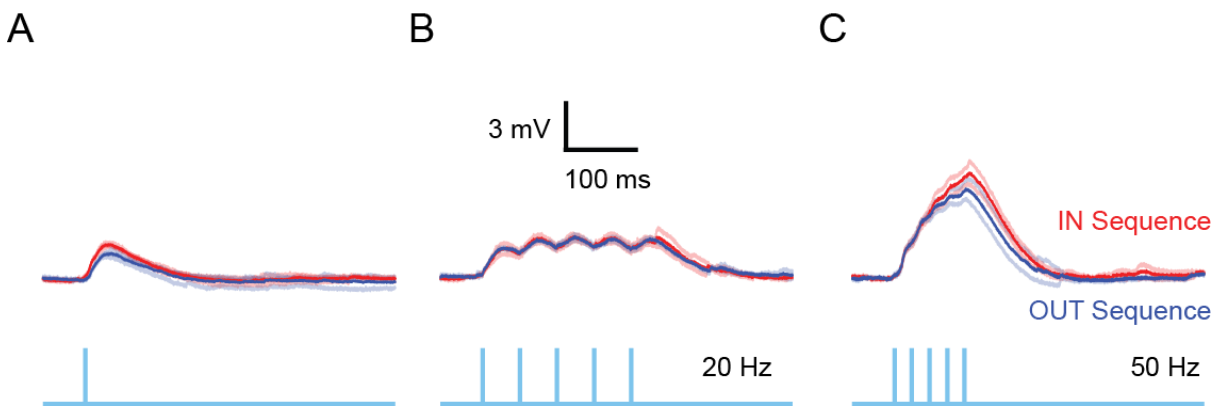

Figure 2.4 Sample compound EPSPs during induction protocol in absence of current injection.

Example compound EPSPs during induction protocol. Example baseline EPSP generated with (A) a single sequential uncaging pattern (IN or OUT), (B) 20 Hz train of uncaging pattern and (C) 50 Hz train of uncaging pattern.

2.3.2 Sequence-dependent induction

In the sequence-dependent induction plasticity protocol, the compound stimulation consisted of two interleaved ordered sequences of synaptic activation – centripetal for the IN sequence and centrifugal for the OUT sequence as described previously (Branco *et al.*, 2010). During the induction protocol, only a single sequence was paired with spikes IN/OUT. The degree of sequence dependent potentiation was then measured as the average response to the particular ordered sequence of activation (IN/OUT) divided by its respective baseline. As the degree of postsynaptic membrane depolarization determines the magnitude of LTP induction and also enhances induction at distal synapses (Sjöström & Häusser, 2006), a 25 pA depolarizing pulse was injected during the spike-sequence pairing protocol.

2.4 CALCIUM IMAGING ANALYSIS

As described above, induction of plasticity required a burst of compound uncaging stimuli paired with action potential induction at the soma. As a result, artefacts resulting from uncaging laser

stimulation contaminated the traces resulting from calcium imaging. I developed an algorithm to identify and minimize the contamination described in (Chapter 4). I first calculated mean of all traces in a given recording and performed principal component analysis on the result. The principal components are ordered by explained variance. I tested whether principal components contained information about the underlying artefact. I then performed dimensionality reduction taking the first 10 principal components, unrolled the resulting matrix and selected values which were above an arbitrary threshold value (1 standard deviation above the mean) restricted within the time-frame in which uncaging was occurring. The values fulfilling this criterion were eliminated from the original matrix containing calcium imaging data and the missing values were linearly interpolated. Example imaging traces were filtered using 1st order Savitzky-Golay filter or two-dimensional Gaussian blurring (in the case of spatial Ca^{2+} profile plot).

2.4.1.1 Elimination of the uncaging-induced artefact

To remove the uncaging-induced artefact, Ca^{2+} imaging was performed as described above and a subsequent masked trial was recorded. In the masked trial, imaging was performed in the absence of current injection and MNI-glutamate. I then generated an average image from the masked trials (Figure 2.5B) and performed principal component analysis (Figure 2.5C). Principal component analysis allows identification of the largest sources of variance in the image. Unrolling the top 10 principal components and selecting the outliers identified the image location of the underlying uncaging artefact (Figure 2.5D). I eliminated pixels that corresponded to the outliers and linearly interpolated to obtain the corrected trace (Figure 2.5E).

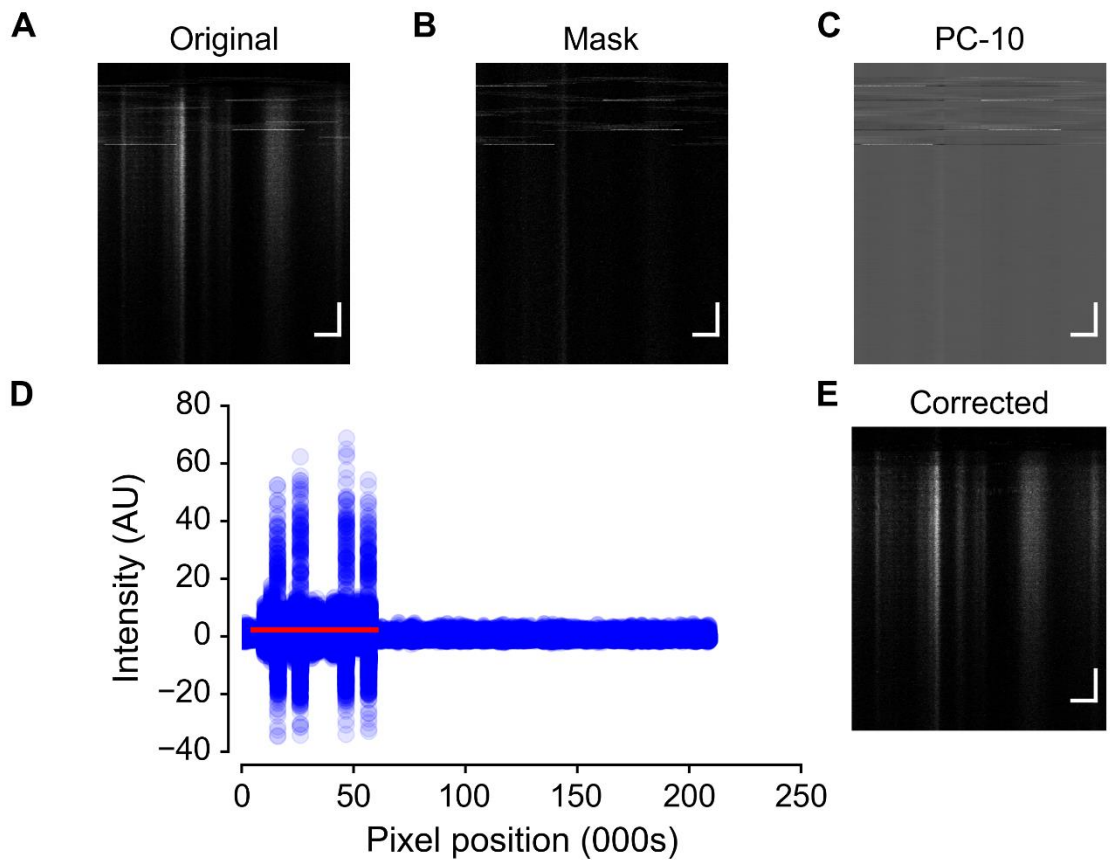

Figure 2.5 Principal Component Analysis method for elimination of uncaging artefact.

A) Original line-scan analysis with uncaging artefact. B) Calcium imaging performed in the absence of MNI-glutamate or action potential induction at the soma (mask) is used to extract principal components of the underlying artefact. C) The dimensionality reduction of the mask input based on the first ten principal components from the Principal Component Analysis. D) Elimination of unrolled pixels that correspond in time to the uncaging artefact and are at least one standard deviation above the mean (red line corresponds to threshold of acceptance). E) Adjusted image following PCA-based correction. Scale bar: x-axis: 5 μm, y-axis: 100 ms.

2.5 COMPARTMENTAL MODELLING

2.5.1 Model cell parameters and NEURON environment

Simulations were performed in the NEURON simulation environment using a detailed 3D reconstruction of layer 2/3 cell from a previous study (Branco *et al.*, 2010). Passive parameters were $C_m = 1\ \mu F/cm^2$, $R_m = 10\ 000\ \Omega \cdot cm^2$, $R_i = 150\ \Omega \cdot cm$. As previously described, this yields a somatic input resistance of $110\ M\Omega$. In basal and apical oblique dendrites, C_m was doubled to account for the presence of dendritic spines. AMPA receptor-mediated conductances were modelled as a sum of two exponential functions ($\tau_{rise} = 0.1\ ms, \tau_{decay} = 1\ ms$). NMDA receptor mediated conductances were modelled using a 10-state kinetic model (Kampa *et al.*, 2004) with unbinding and desensitization rates adjusted to physiological temperatures (Cais *et al.*, 2008), opening and closing rates from Lester and Jahr (1992) and Mg^{2+} unbinding rates to produce a time constant of ~10 ms (Vargas-Caballero & Robinson, 2003). Maximal peak conductances for both AMPA and NMDA were varied depending on the simulation experiment in the range of 0-1.5 nS and 0-24 nS respectively. All simulations were performed at a resting membrane potential of -75 mV unless otherwise stated.

2.5.2 Genetic algorithm and simulation

It was previously shown that genetic optimization can be useful in constraining the vast parameter space commonly encountered in when using the NEURON simulation environment (Keren *et al.*, 2005; Almog & Korngreen, 2014). A genetic algorithm is an optimization algorithm that is loosely based on the mechanisms of Darwinian evolution. The use of random point mutations and crossover operations result in breeding better models, or solutions, compared to the original starting population. I started with 100 vectors drawn from a uniform random distribution, each vector describing a parameter set. The population was sorted according to a fit score defined by a cost function (see below). To prevent genetic drift, the best individual was preserved unchanged

for the next round of optimization. The modification of the rest of the individuals was done, first, by introducing a random point mutation to vectors (with probability of mutation equal to 0.1 per parameter). The mutated parameter was exchanged for a random one drawn from a uniform distribution. The point mutation was followed by a crossover operation in which 0.2 vectors randomly swapped one parameter. The iterations were run until a termination criterion was met or if 2,000 generations were reached. Depending on the computational complexity of the task, the optimization protocol was run for a defined number of iterations usually lasting up to 4 days on a LINUX cluster utilizing 32 cores or on a personal computer utilizing up to 4 cores.

2.5.2.1 Cost function

Previously, it was shown that asymmetric cost functions can be efficient in optimization problems (Silva *et al.*, 2010). The asymmetric cost function was a reasonable approach as the algorithm was required to discover parameters that would reproduce results of the sequence induction plasticity. As a result, simulations that lead to greater sequence potentiation than empirically tested were penalized less than simulations that resulted in a smaller sequence potentiation or in a sequence depression.

The default asymmetric cost function used in genetic algorithm optimization parameters was set as follows:

$$cost = \begin{cases} \sum_{P}^{\{IN,OUT\}} \left(\frac{P_{max}}{NP_{max}}\right)^2, & \left(\frac{P_{max}}{NP_{max}}\right) < 0 \\ \sum_{P}^{\{IN,OUT\}} \left(\frac{P_{max}}{NP_{max}}\right), & \left(\frac{P_{max}}{NP_{max}}\right) \geq 0 \end{cases}$$

Where P_{max} and NP_{max} correspond to the maximal amplitudes of simulated EPSPs of preferred and non-preferred spatiotemporal sequence of activation of modelled synapses. P corresponds to the preferred type of the spatiotemporal sequence (i.e. IN or OUT).

2.6 DATA ANALYSIS

The data was captured by a custom software written in MatLab as described previously (Branco *et al.*, 2010). The recorded data was then converted using NumPy and SciPy libraries of Python. The statistical analysis was performed by using the statistical libraries contained in SciPy and scikit-learn libraries of Python. The plotting was performed using Matplotlib library and further visualisation improvements were performed in Adobe Illustrator.

2.6.1 Statistical analysis

Statistical significance in comparisons of different groups was tested using Student's paired or independent groups t-test or the non-parametric equivalents depending on the number of data available and the likelihood of normality assumption violation. In comparisons of multiple groups one-way or repeated measures ANOVA or its non-parametric equivalent Friedmann χ^2 was used. Statistical significance was defined as $p < 0.05$. Data are presented as mean ± SEM unless otherwise noted.

3 INDUCTION OF SPATIOTEMPORAL PLASTICITY IN BASAL DENDRITES OF LAYER 5 PYRAMIDAL NEURONS

3.1 INTRODUCTION

Several theories consider dendrites as the local units of computation and plasticity (Govindarajan *et al.*, 2006; Branco & Häusser, 2010). Recently, *in vivo* studies have suggested that a single dendritic branch can act as a separate unit for plasticity and that such plasticity was generally dependent on NMDA receptors (Makino & Malinow, 2011; Yang *et al.*, 2014; Gambino *et al.*, 2014; Cichon & Gan, 2015). NMDA receptors are also required to enhance spatiotemporal sensitivity in dendrites (Branco *et al.*, 2010). Since modulation of NMDA receptors is tightly linked to plasticity in cortical cells and different spatiotemporal patterns result in differential NMDAR recruitment, it is natural to enquire whether plasticity can also be spatiotemporally modulated. Such plasticity, if found, would have profound implications for the complexity of information that single dendrites are capable of storing.

Induction of plasticity is location-dependent and may fail or result in depression if dendrites experience insufficient depolarization (Sjöström & Häusser, 2006; Letzkus *et al.*, 2006). Furthermore, induction also depends on the frequency of action potentials (Sjöström *et al.*, 2001). To elicit spatiotemporal plasticity, an uncaging-based protocol is required. However, most literature to date of uncaging-induced plasticity used spine morphology as a proxy for underlying electrophysiological changes. Nevertheless, previous work in hippocampal CA1 cells showed that pairing uncaging stimulation of a dendritic branch with application of the cholinergic agonist carbachol or theta-pairing protocol (2-3 bAPs) resulted in an enhancement of branch strength that was dependent on the intrinsic excitability changes via the downregulation of A-type K^+ currents (Losonczy *et al.*, 2008).

3.1.1 Aims of the chapter

I was, therefore, interested whether similar branch potentiation to that observed in CA1 cells (Losonczy *et al.*, 2008) can be induced in Layer 5 cells of pyramidal neurons. Upon induction of potentiation, I looked at the properties of potentiation and how they relate to the potentiation observed in other cell types and induction protocols. Furthermore, upon confirming properties of this potentiation, I looked at whether pairing specific spatiotemporal uncaging patterns influences the outcome of induction.

3.2 RESULTS

3.2.1 Uncaging-induced whole-branch potentiation

3.2.1.1 Induction of branch potentiation

I used two-photon MNI-glutamate uncaging at multiple-synapses to evoke gluEPSPs recorded at the soma in the whole-cell patch clamp configuration. Glutamate uncaging is an appropriate method due to its highly specific nature of synapse activation (see Figure 3.1).

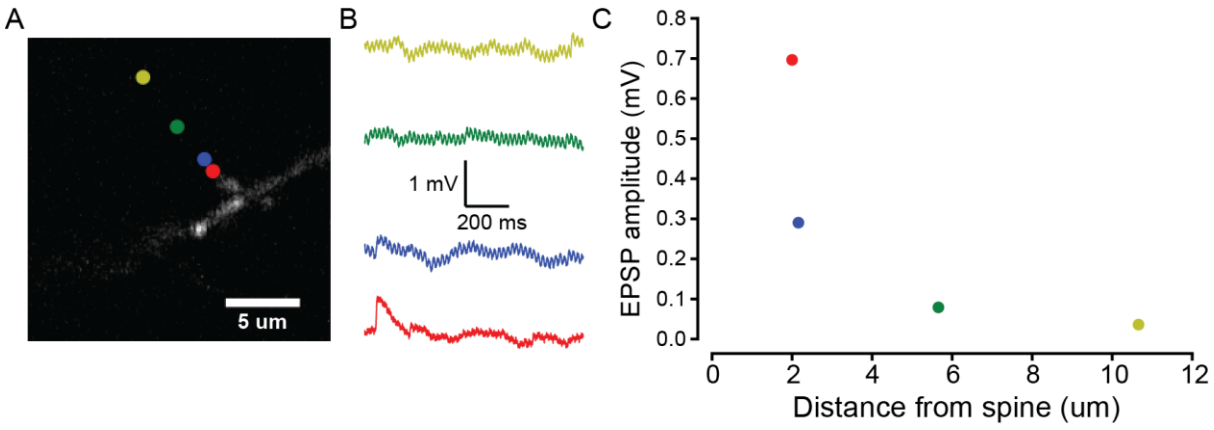

Figure 3.1 MNI-uncaging activates single synapses with high spatial precision.

A) Example colour coded uncaging sites that were stimulated with the same power laser-light. B) Example whole-cell patch clamp recordings from soma at different spatial distances from the

stimulated spine. C) EPSP amplitude is dependent on the distance from the spine receiving uncaging stimulus.

The mean compound EPSP recorded during the baseline measurements was 4.6 ± 1.1 mV (N = 32). As glutamate uncaging is known to potentially affect the integrity of the dendrite, care had to be taken to avoid damage of the dendrite due to photodamage (see Figure 2.2) which was previously found to be sufficient to perturb current flow in the dendrite (Hirase *et al.*, 2002). As a result, each baseline measurement was recorded at 1 minute intervals instead of customary 0.1 Hz used in traditional electrophysiological studies. The mechanisms of uncaging-induced plasticity in dendrites of layer 5 neurons has not yet been explored extensively by previous studies. Modes by which plasticity is induced can be variable such as changes in receptor content (Malinow & Malenka, 2002; Watt *et al.*, 2004) or local intrinsic excitability (Frick *et al.*, 2004; Losonczy *et al.*, 2008). It is therefore important that the initial investigation of the plasticity does not rule out either of these, such as by rejection of cells whose input resistance changed significantly from baseline after induction which is a common requirement (Sjöström *et al.*, 2001). I initially tested AP bursts at two frequencies 20 and 50 Hz. To enhance backpropagation in the lower frequency condition, we applied a subthreshold current injection (25 pA). At these frequencies, it would be predicted that, irrespective of timing conditions, LTP would predominate (Sjöström *et al.*, 2001). I observed LTP at both frequency pairings (see Figure 3.2, LTP 20 Hz: N=37, 1-sample $t = 3.4$, $p < 0.01$, LTP 50 Hz: N=22, 1-sample $t=2.5$, $t <0.05$). Although the 50 Hz condition was not significantly different from the 20 Hz condition (independent t-test $t=-1.7$, $p > 0.05$), the absolute magnitude of potentiation from baseline was comparable to the potentiation observed in other studies (Sjöström *et al.*, 2001). Another likely reason for smaller difference was the presence of depolarizing pulse that was injected to prevent distance-dependent LTD (Sjöström & Häusser, 2006).

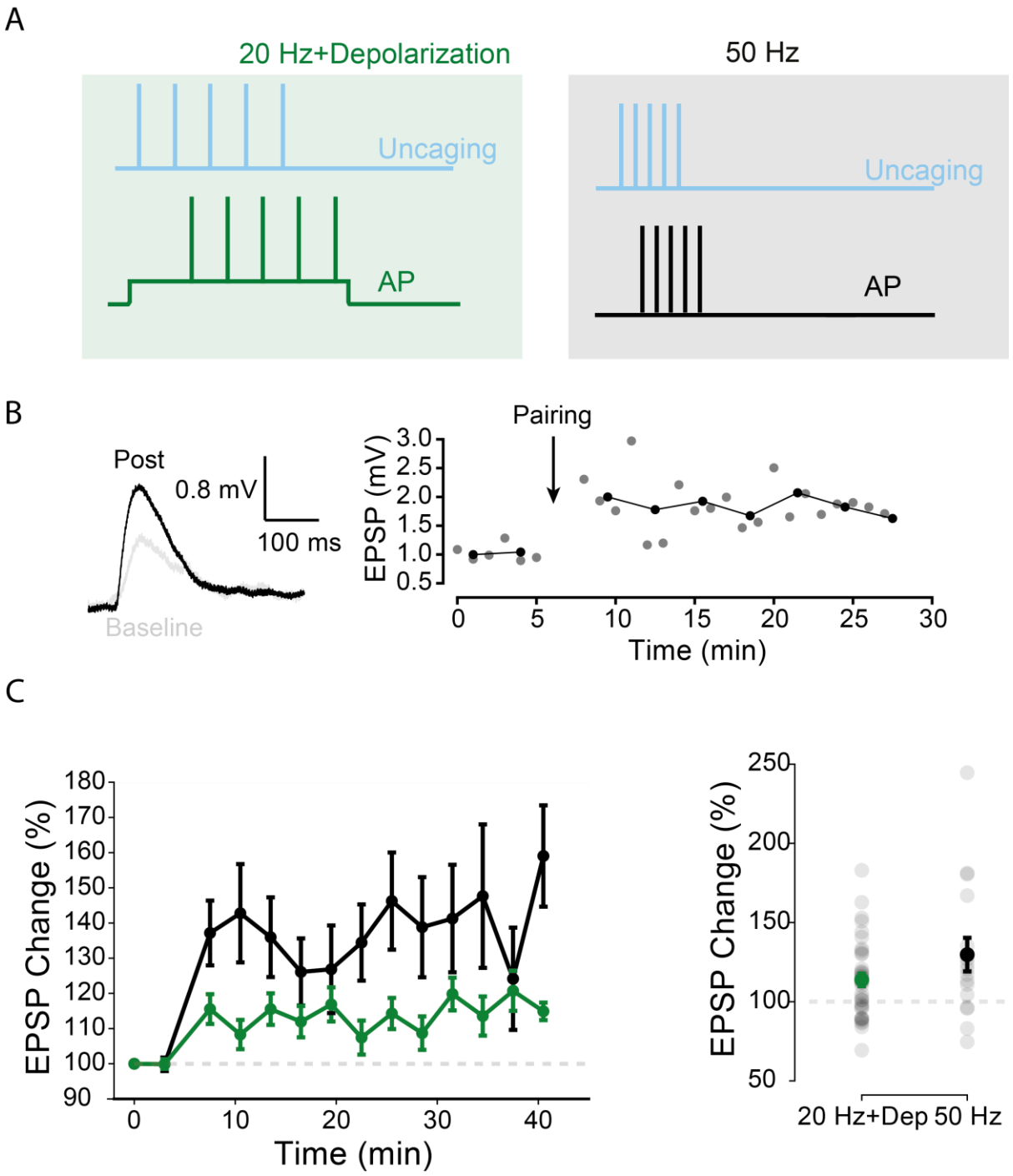

Figure 3.2 Uncaging-induced long-term potentiation in basal dendrites of Layer 5 pyramidal neurons.

A) Schematic of two LTP induction patterns. (Left) Multi-site uncaging was paired with action potentials elicited at the soma at variable intervals at 20 Hz coupled with subthreshold depolarization (40 pA, 500 ms). (Right) Multi-site uncaging was paired with action potentials

elicited at variable intervals at 50 Hz in absence of subthreshold depolarization. B) (Left) An example multi-site uncaging compound EPSP recording during the baseline and post-induction periods (20 Hz protocol). (Right) Example time-course in a cell showing significant potentiation of peak EPSP amplitude post-induction. C) Branch dendritic potentiation at two different EPSP-AP pairing frequencies 50 Hz and 20 Hz with subthreshold depolarization. Both frequency pairings result in significant potentiation that is not significantly different. (Right) A recording that developed putative non-linear integration following 50 Hz pairing is marked in red. The presence of this outlier did not affect results of the statistical tests.

I was further interested in whether there is a difference between dendritic compartments in the magnitude of potentiation induction. I performed whole-branch induction protocol on apical oblique and apical trunk branches (apical condition) and on basal branches (basal condition) using the 50 Hz pairing protocol described above. There was no difference in magnitude of induction between apical and basal branches (Mann-Whitney U: 240.0, $p > 0.05$). Nevertheless, only basal branches were significantly different from baseline (see Figure 3.3, Basal: N=16, Wilcoxon 19.0, $p < 0.05$, Apical: N=5, Wilcoxon 4.0, $p > 0.5$). This is presumably due to the existence of outliers in the apical condition and relatively low number of trials. More apical trials are required to evaluate the difference between apical and basal branches and their relative propensity for plasticity induction.

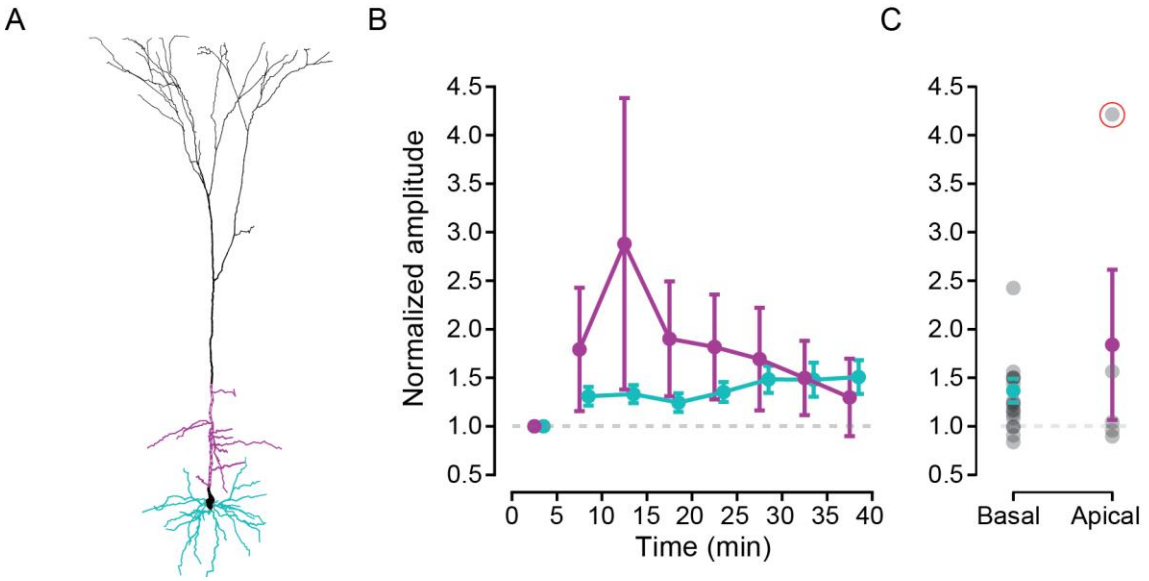

Figure 3.3 Comparison of uncaging-induced LTP between apical and basal dendrites.

A) Schematic layer 5 neuronal morphology colour-coded based on the dendritic site – (magenta) apical trunk and oblique dendrites, (cyan) basal dendrites. B) and C) In both apical and basal dendrites the 50 Hz induction protocol was associated with an enhanced EPSP amplitude post-pairing. C) Selected data point in red shows switch to supra-linear integration of synaptic inputs post-pairing. The presence of the outlier did not significantly affect the results of the statistical tests.

The uncaging-induced plasticity therefore exhibited similar properties to the electrophysiological plasticity reported previously using traditional protocols (for further confirmation regarding pharmacology and Ca^{2+} dependence, see Chapter 2).

3.2.2 Spatiotemporal potentiation induction

Next, I examined whether specific spatiotemporal sequences of inputs can be preferentially potentiated. 8-20 synapses were selected on basal dendrites of layer 5 pyramidal cells. A stable baseline for the two tested sequences (IN and OUT) was first recorded, with IN being consecutive activation of synapses from distal to proximal and OUT being the converse (both at a time delay of ~2 ms between synapses). In baseline simulations, I found that the IN sequence was

significantly larger than the OUT sequence (Figure 3.4, Paired t-test: 2.8, $p<0.01$) which is consistent with previous findings (Branco *et al.*, 2010). In total, 22 out of 32 recordings showed greater magnitude of IN sequence EPSPs as compared to OUT with the rest predominated by OUT sequence. Following baseline recordings, spatiotemporal potentiation was induced by repeated pairing of one sequence - IN for the IN-pairing, OUT for the OUT pairing. Afterwards, the potentiation was tested in comparison to the baseline level of each individual sequence type (IN/OUT). I found that spatiotemporal potentiation induction results in a preferential potentiation of the sequence being paired with action potentials (OUT pairing: N = 17, Wilcoxon ranked-sum test: 30, $p<0.05$, IN pairing: Wilcoxon ranked-sum test: 30, N = 15, $p<0.05$). Following the IN-pairing protocol, the IN sequence showed greater potentiation compared to the OUT sequence and I found converse following the OUT-pairing protocol (Figure 3.4, IN vs. OUT EPSP change: Paired t-test: 3.3, $p < 0.01$, OUT vs IN EPSP change: Paired t-test: 2.4, $p < 0.05$, IN-pairing vs. OUT-pairing potentiation change independent t-test: 4.0, $p < 0.001$). I also compared magnitude of potentiation of IN-IN and OUT-OUT sequences from IN-pairing and OUT-pairing protocols. IN and OUT sequences were larger in IN- and OUT-pairing protocols respectively but this did not reach statistical significance (IN-IN pairing: N=15,17, Independent t-test: 1.34, $p>0.05$; OUT-OUT pairing: N=15,17, Independent t-test: 1.34, $p>0.05$). Finally, the magnitude of potentiation was correlated with the degree of spatiotemporal potentiation, calculated as the difference between paired and non-paired sequence potentiation (Figure 3.5, N=31, $R^2 = 0.19$, $p < 0.05$).

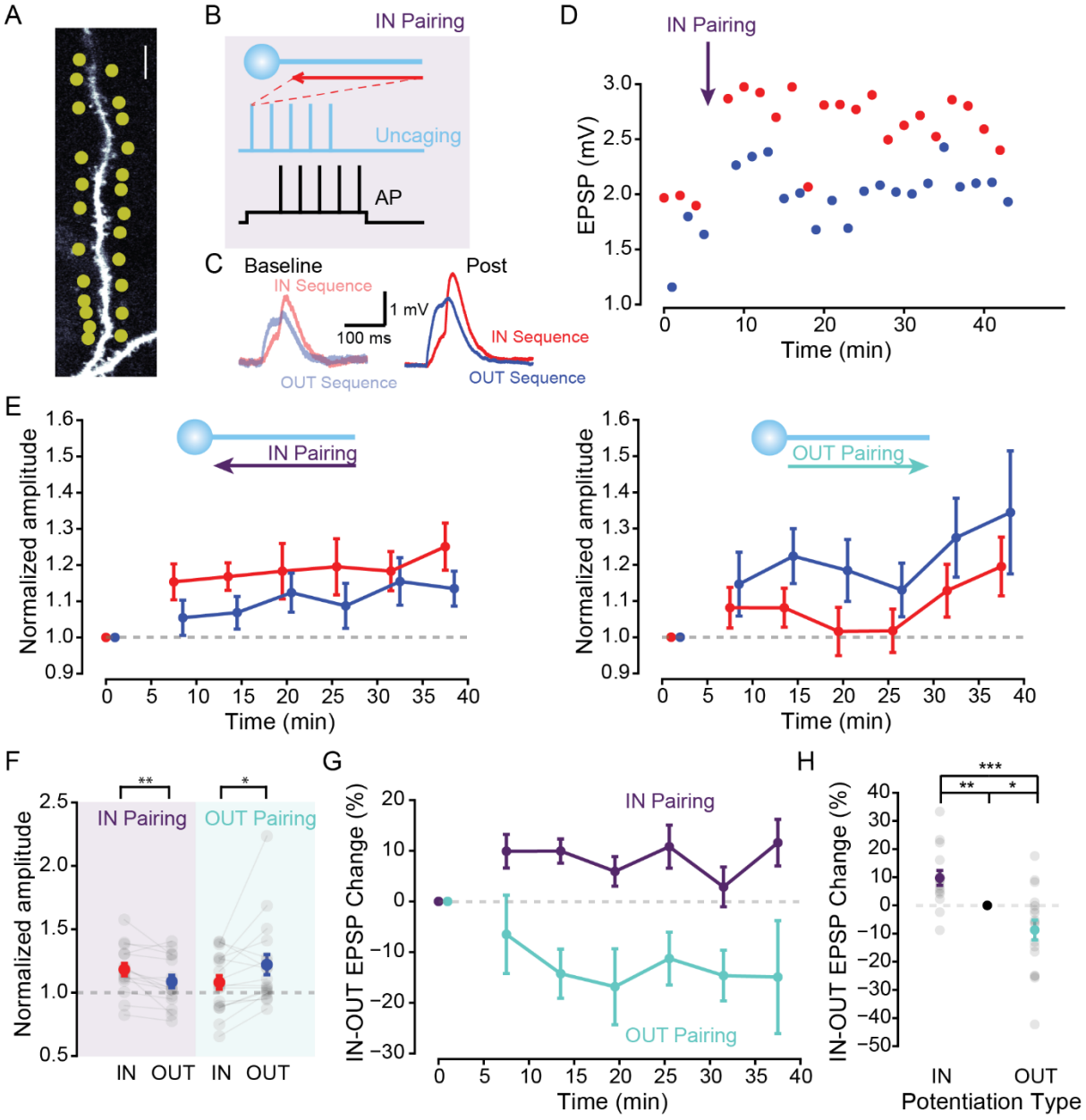

Figure 3.4 Potentiation of sequences in Layer 5 pyramidal neurons.

A) Sample selection of uncaging points on a dendrite. B) Schematic of induction protocol. Uncaging pulses of a single sequence (IN or OUT) were paired (15x) with action potentials at variable Δt. C) Example EPSP recording of the layer 5 pyramidal dendrite before and after IN pairing. D) Example cell showing preferential plasticity of the IN sequence following IN pairing during induction. E) The spatiotemporal pattern of synapse activation during induction results in a preferential potentiation of that pattern. IN pairing results in the preferential potentiation of the

IN sequence (N = 15), OUT pairing results in the preferential potentiation of the OUT sequence (N = 16). F) The magnitude of potentiation of IN sequence is preferentially potentiated after IN-pairing (purple shaded region) whilst the magnitude of potentiation of the OUT sequence is preferentially potentiated after OUT-pairing (turquoise region). G) and H) Spatiotemporal plasticity induction results in a significant difference between IN-potentiation and OUT-potentiation that favours the paired sequence. (*p<0.05, **p<0.01, ***p<0.001, scale bar = 10 μm).

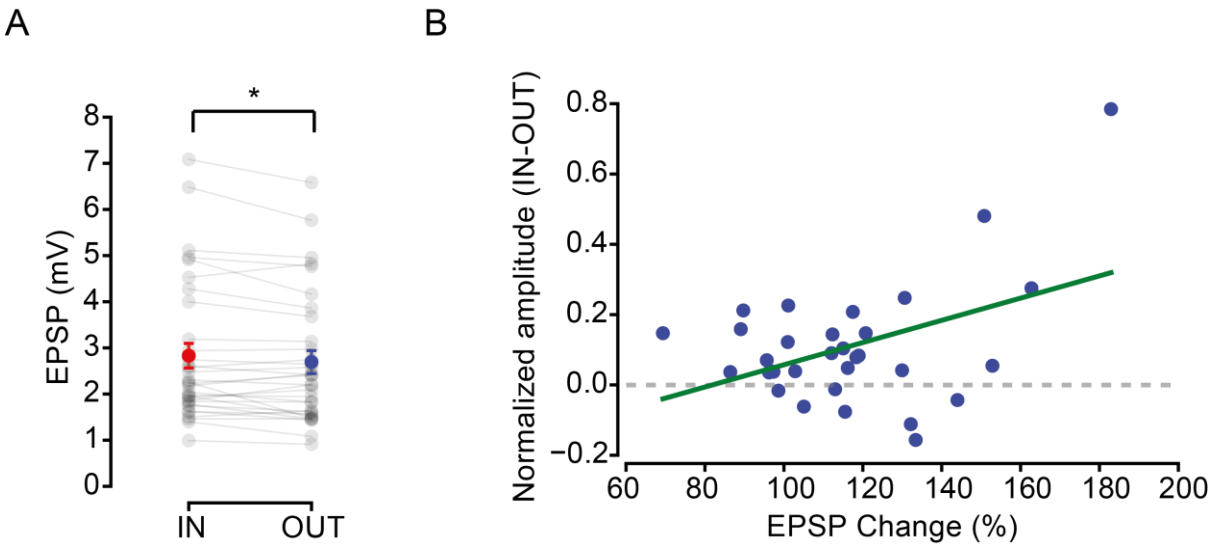

Figure 3.5 Magnitude of potentiation is correlated with the degree of spatiotemporal plasticity

A) In baseline condition, peak IN sequence is of greater magnitude than OUT sequence (N=31, *p<0.05). B) The magnitude of spatiotemporal potentiation calculated as the difference in potentiation of paired and non-paired sequence is correlated with the magnitude of overall potentiation. The linear regression of EPSP change to normalized amplitude is shown in green (N=31, $p < 0.05$).

3.2.2.1 EPSP amplitude and spatiotemporal potentiation

I then investigated other properties of the spatiotemporal plasticity. It was previously discovered that the initial size of EPSP determines the magnitude of plasticity observed, events below 2.4 mV were found incapable of inducing LTP (Sjöström *et al.*, 2001) . In my experiments, I did not observe such dependence on the magnitude of potentiation (Figure 3.6A, N=31, R^2 squared = 0.0003, $p > 0.05$). There was a trend towards lower potentiation with higher amplitude EPSPs but this did not prove significant (Figure 3.6B, N=31, R^2 squared = 0.03, $p > 0.05$). Also there was no difference in the magnitude of spatiotemporal plasticity evaluated as a difference between the respective potentiation of IN and OUT sequences that would depend on the magnitude of baseline EPSP.

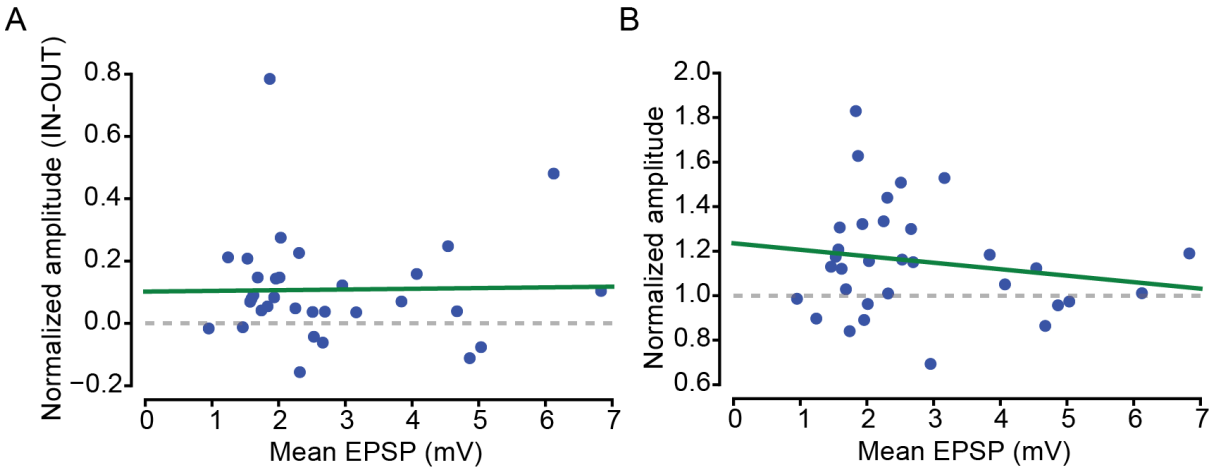

Figure 3.6 Baseline EPSP size does not significantly affect uncaging-induced LTP or spatiotemporal LTP.

A) Mean EPSP peak size in baseline condition is not correlated with the difference between preferred and non-preferred pairing sequence. The linear line of best fit is shown in green (ns). B) Mean EPSP peak size is not correlated with the magnitude of potentiation post-pairing. The linear regression fit is shown in green (ns).

3.2.2.2 *Action-potential timing and spatiotemporal potentiation*

In traditional STDP-induction protocols, the timing of action potentials relative to EPSP determines the sign of plasticity. However, only frequencies at 20 Hz and below were found capable of inducing LTD (Sjöström *et al.*, 2001). In my experiments, I observed only a weak, non-significant relationship between the timing of the action potentials and the onset of uncaging-induced EPSPs (Figure 3.7B, N=31, $R^2 = 0.04$, $p > 0.05$). The time-window of integration for LTP was also slightly wider than previously reported (Feldman, 2012). There was also no relationship between the EPSP-AP timing and the magnitude of spatiotemporal plasticity induction (Figure 3.7C, N=31, $R^2 = 0.01$, $p > 0.05$).

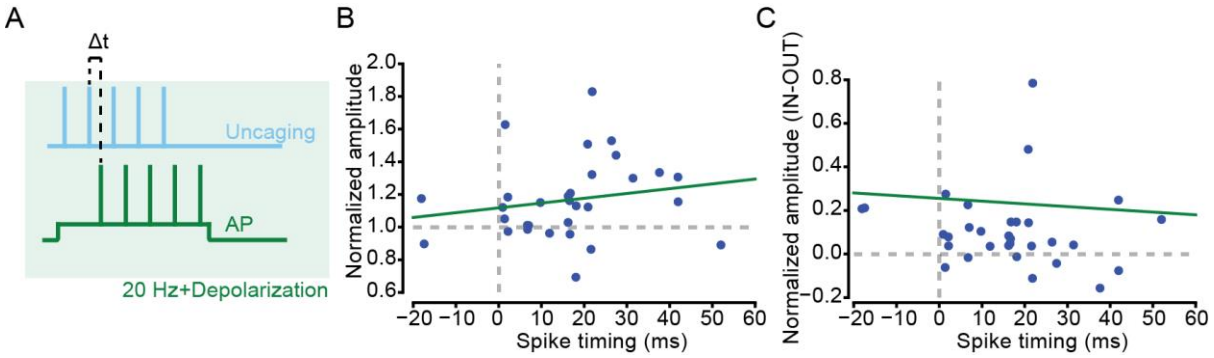

Figure 3.7 AP-EPSP timing does not significantly affect the magnitude or sign of uncaging-induced plasticity.

A) Schematic of the timing of uncaging at the defined set of synapses coupled with action potentials. B) Mean EPSP change from baseline was not correlated with the EPSP-AP timing. B) and C) The linear regression fit is shown in green (ns). C) Difference between preferred and non-preferred sequence is not correlated with spike timing.

3.2.2.3 *Role of clustering in spatiotemporal plasticity*

Previous reports indicated that the degree of synaptic clustering influences induction of plasticity in cortical cells (Harvey & Svoboda, 2007). I used inter-spine distance as a measure of clustering on the dendrite. The range of inter-spine distances in my experiments was 1.7-8.7 μm with a mean

of 3.7±0.3 μm. Whilst there was a trend of preferential enhancement of paired sequence with increased inter-spine distance, this did not reach significance (Figure 3.8B, N=31, R^2=0.09, p > 0.05). Similarly, there was no linear relationship between the magnitude of potentiation and inter-spine distance at these ranges of clustering (Figure 3.8C, N=31, R^2=0.04, p>0.05).

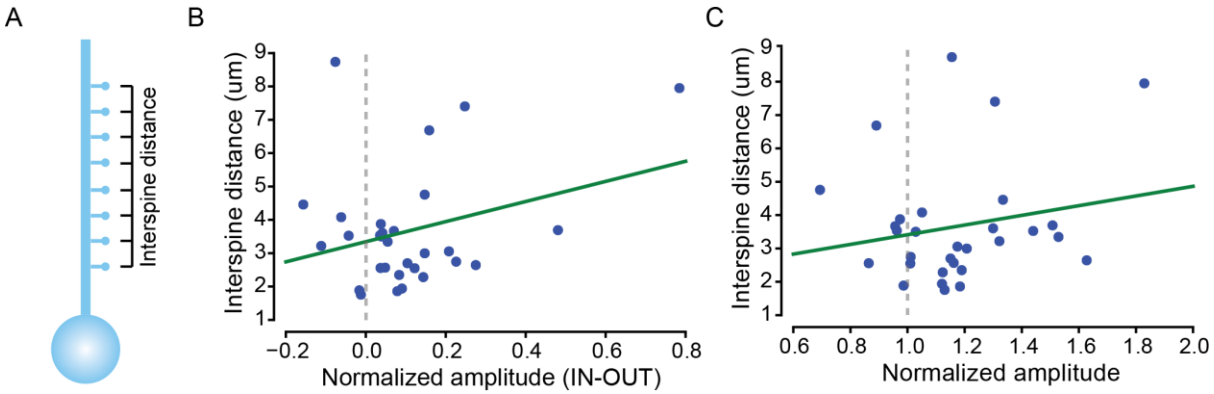

Figure 3.8 Clustering of spines does not significantly affect spatiotemporal plasticity

A) Inter-spine distance was calculated as a direct line along the dendrite between the neighbouring spines (schematic). B) Difference of preferred and non-preferred pairing protocols is not correlated with inter-spine distance. B) and C) The linear regression fit is shown in green (ns). C) The magnitude of EPSP change is not correlated with inter-spine distance.

3.2.2.4 Role of distance in spatiotemporal plasticity

I injected subthreshold depolarizing current (see Methods) to normalize the relative magnitude of plasticity induction. As a result, if there is a role of distance in plasticity induction, it is expected to be diminished in my data. Consistent with this view, there was no linear relationship between distance and magnitude of EPSP change following induction (Figure 3.9B, N=31, R^2 = 0.04, p > 0.05). Also, I did not observe a linear relationship between the magnitude of spatiotemporal plasticity and the distance of the dendrite from the soma (Figure 3.9C, N=31, R^2 = 0.08, p > 0.05).

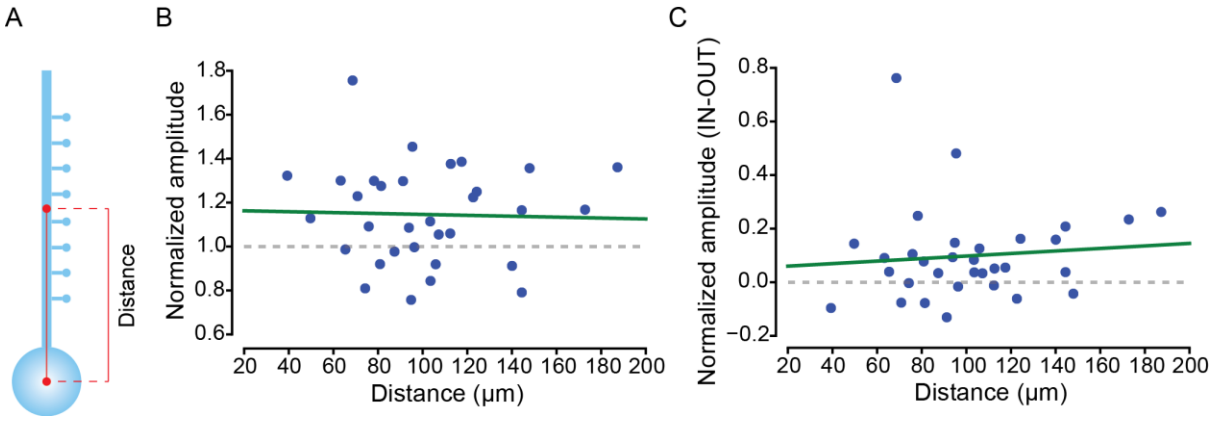

Figure 3.9 Distance from the soma does not significantly affect the induction of spatiotemporal plasticity.

A) Distance was calculated from the mid-point of the dendrite on which uncaging was performed to the center of soma (schematic). B) Increasing distance from the soma does not decrease the magnitude of EPSP change. B) and C) The linear regression fit is shown in green (ns). C) The magnitude of difference between preferred and non-preferred pairing is not dependent on the distance.

3.2.2.5 Induction of branch potentiation can result in spike-like supra-linear events

The clustered enhancement of synaptic strengths is expected to increase the likelihood of dendritic spike occurrence. I expected such enhancement to manifest as a potentiation over-and-above that normally observed in other induction paradigms. In one recording, I observed an increase that was approximately 8-fold from baseline (see Figure 3.10). This recording was labelled as an outlier and statistical analysis was verified on a set in which the outlier was excluded. Nevertheless, it is an interesting example of single-branch clustered potentiation. This finding is also consistent with the previous report *in vivo* of enhanced dendritic spike likelihood following whisker sensory-evoked LTP (Gambino *et al.*, 2014).

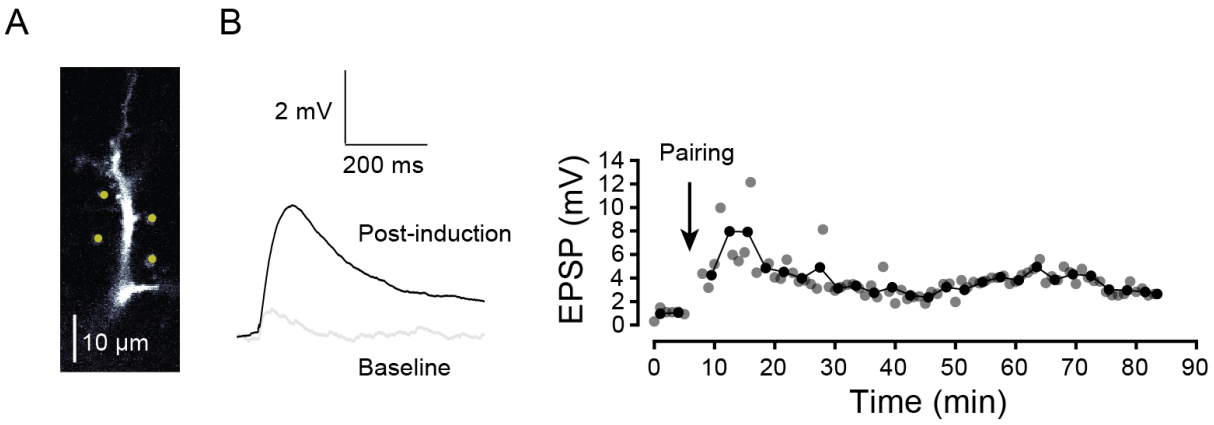

Figure 3.10 Putative supra-linear enhancement of EPSP post-induction

A) Selected dendrite for uncaging and branch plasticity induction. Uncaging spots are shown in yellow. B) (Left) Example averaged EPSP following uncaging with a 2 ms interspine interval. The baseline condition is shown in light grey, post-induction EPSP trace is shown in black. (Right) Example recording that resulted in putative supra-linear integration after pairing.

3.3 Discussion

In this chapter, I discuss a novel form of plasticity that is sensitive to the spatiotemporal pattern of induction. Pairing either a centrifugal or a centripetal spatiotemporal sequence with action potentials results in a specific potentiation of that particular sequence. This novel form of plasticity is expected to considerably improve the information storage available to the cell.

I also verified that plasticity on a dendritic branch can be elicited by pairing action potentials with EPSPs in layer 5 pyramidal neurons of the rat cortex. Consistently with previous studies, higher frequency pairing resulted in a greater magnitude potentiation. I also performed a direct comparison between the relative magnitudes of long-term potentiation between apical and basal dendrites of layer 5 pyramidal neurons. I did not observe significant differences between the basal dendrites and dendrites of apical trunk. It is possible that tuft dendrites, which are often considered a separate integrative unit of layer 5 dendritic tree (Larkum *et al.*, 2009), exhibit differential plasticity. For example, the distance dependence of potentiation is well-recognized (Sjöström &

Häusser, 2006) as is the existence of calcium spike initiation zone in the tuft (Larkum *et al.*, 1999*a*) which may support the induction of plasticity.

Previous studies have demonstrated the sensitivity of EPSP readout to spatiotemporal input sequences (Branco *et al.*, 2010) and the ability of synapses to encode temporal information at synapses in hippocampus (Kwag & Paulsen, 2009). My work provides an important extension to these studies. To my knowledge, the experiments presented in this chapter are the first demonstration of the ability of dendrites to encode spatiotemporal sequences. I observed a relationship between the spatiotemporal pattern of uncaging stimulation and the plasticity read-out in the post-induction phase. Pairing a specific spatiotemporal sequence with action potentials resulted in a preferential potentiation of that sequence. In cortex, such spatiotemporal plasticity mechanisms could be important in many feature binding tasks where millisecond precision was shown to be required (Johansson & Birznieks, 2004; VanRullen *et al.*, 2005). Spatiotemporal plasticity could also underpin the reverberation of visually evoked cortical activity observed in rat visual cortex following the repeated presentation of a given visual stimulus (Han *et al.*, 2008) and could play a significant role in circuit refinement. Whilst this study was primarily focused on the layer 5 pyramidal cells, it is tempting to conclude that such a plasticity mechanism could play a major part in refining other circuits of the brain encoding spatiotemporal information. Spatiotemporal sequence discrimination was shown to be a robust general feature of neurons which possess NMDA receptors such as dentate gyrus granule cells, CA1 pyramidal cells and substantia nigra dopamine neurons (Branco *et al.*, 2010). Moreover, previous studies showed that dendrites of CA1 pyramidal cells can show robust plasticity (Losonczy *et al.*, 2008; Govindarajan *et al.*, 2011) that is modified by the regulation of A-type K^+ current. In Chapter 5, I will describe how even uniform modulation of recruited synaptic conductance at the dendrite (such as by changes in A-type K^+ channels) can result in spatiotemporal plasticity.

Following the establishment of the spatiotemporal plasticity rule, I proceeded to evaluate the parameters involved in induction. Interestingly, timing of action potentials relative to EPSPs did not importantly determine the magnitude or sign of plasticity. One potential explanation for this is the subthreshold depolarization which was previously shown to enhance the likelihood of plasticity induction (Kelso *et al.*, 1986; Sjöström & Häusser, 2006). Also, the frequencies at which pairings were made were usually quite high, and this is generally not permissive for the induction of LTD (Sjöström *et al.*, 2001). Furthermore, previous studies did not have control over dendrites on which stimulated synapses were located. When synapses are distributed along multiple dendrites, plasticity induction mechanics change (Govindarajan *et al.*, 2011). Finally, several recent *in vivo* studies have shown that action potential firing is not necessary for plasticity induction (Gambino *et al.*, 2014; Cichon & Gan, 2015).

A key further step in the evaluation of spatiotemporal plasticity is to verify what changes are observed at the level of individual synapses. The advantage of the uncaging method is that it allows precise spatial control of stimulation. Nevertheless, the increased likelihood of phototoxicity of the spines makes such experiments challenging. Another possibility is employing calcium imaging in dendrites. Calcium imaging allows fine spatial resolution and further insights into the local hotspots of Ca^{2+} influx as well as time-course of the induction.

A further reason to evaluate single synapse input is because it is currently controversial whether uncaging method produces physiologically valid stimulation of individual synapses (both stimulated and not). Uncaging method can potentially activate extrasynaptic sites. Both AMPA and NMDA extrasynaptic receptors were found to be important in the induction of plasticity (Lau & Zukin, 2007). Lateral diffusion of synaptic receptors becomes restrained following the release of glutamate (Ehlers *et al.*, 2007). Whilst the relative role of extrasynaptic diffusion in the induction of plasticity is currently controversial (Choquet & Triller, 2013), the recent findings in organotypic slices of CA1 show that diffusion is clearly an important component in maintaining and enhancing

synaptic strength (Makino & Malinow, 2009). Furthermore, previous reports have shown changes in the likelihood of plasticity induction for spines that were spatially close to the induction site (Harvey & Svoboda, 2007). The spread of Ras is a likely candidate for mechanisms of induction (Harvey *et al.*, 2008). As a result, it is important to evaluate the spatial spread of glutamate following uncaging stimulus. In my work, I have used the same approach that was described in previous work by Branco et al. (2010) where mean reported amplitude for a single synaptic site was 0.58 mV. In my work, I have generally employed even lower stimulation amplitudes (~0.3 mV) to limit photodamage which would result in even lower unitary gluEPSP amplitude. These values correspond well to empirically observed mEPSPs in the literature for basal dendrites of cortical neurons (Nevian *et al.*, 2007).

Another avenue for further research into spatiotemporal plasticity is the role of specific AMPA and NMDA subunits in enabling it. Previous research has confirmed the diversity of both AMPA and NMDA subunits (Cull-Candy *et al.*, 2001; Malinow & Malenka, 2002; Shepherd & Huganir, 2007). The subunits contained in NMDA receptors importantly determine their physiology. For example, deactivation kinetics of NMDA receptors following 1 ms pulse of glutamate vary widely from time constants of 100 ms in GluN2A containing receptors to 4s of GluN2D receptors. Banerjee and colleagues (2009) discovered that the type of NMDA subunit importantly modulates the sign of plasticity in layer 2/3 – layer 4 synapses. Specifically, GluN2C/D subunit containing NMDA receptors were required for the induction of t-LTD and this form of plasticity was only present early in development. However, GluN2A was found to be required for the induction of t-LTP instead. The relative composition of NMDA subunits and deactivation kinetics is expected to have an important effect on spatiotemporal plasticity as well. The longer deactivation kinetics of GluN2D receptors could prolong the time-window of integration required for induction of plasticity. Faster deactivation kinetics, could be responsible for a finer temporal discrimination in the induction. In some aspects, AMPA receptors are even more diverse than NMDA receptors. Depending on the presence of GluA1 subunit, AMPA receptors gain or lose their Ca^{2+} permeability

(Cull-Candy *et al.*, 2006). Given the requirement of Ca^{2+} to induce plasticity (Lynch *et al.*, 1983), GluA1 containing receptors could be an important modulator of the spatiotemporal plasticity as well. Furthemore AMPA receptors are powerfully influenced by transmembrane AMPA receptor regulatory proteins (TARPs) by affecting insertion into the membrane and modulation functional properties of the receptor (Nicoll *et al.*, 2006; Milstein & Nicoll, 2008; Jackson & Nicoll, 2011). The precise distribution and types of synaptic and extrasynaptic receptors in basal dendrites of layer 5 neurons is currently unknown. Both AMPA and NMDA receptor modulation was found to importantly affect induction of plasticity (Benke *et al.*, 1998; Malinow & Malenka, 2002; Watt *et al.*, 2004). Spatiotemporal plasticity is, likewise, expected to be affected by the complex interaction of synaptic proteins with the regulatory elements at the synapse by for example deactivation kinetics, Ca^{2+} permeability and insertion to or removal from synapse. Further research and computational studies are required to tease out the precise role of synaptic receptor types in influencing spatiotemporal plasticity.

A further question is the role of NMDA spikes in eliciting plasticity in general and spatiotemporal plasrticity in particular. It has been previously demonstrated that NMDA plateau potentials are sufficient for induction of plasticity and that this induction occurs *in vivo* conditions (Gambino *et al.*, 2014). Substantial evidence exists for recruitment of NMDA-dependent non-linear processing *in vitro* and *in vivo* (Schiller *et al.*, 2000; Schiller & Schiller, 2001; Lavzin *et al.*, 2012). To what extent a thresholding event (a spike) is necessary for recruitment of NMDA receptors is currently an open and active area of research. In this thesis, I presented examples of individual recordings that tentatively display such thresholding behaviour (see Figure 3.4). Further research is required to verify whether this is indeed an all-or-none instance or a more gradual recruitment of NMDA conductance that underlies these non-linear events.

In this chapter, I described a novel form of spatiotemporal plasticity. Previous computational studies suggested that the existence of such plasticity would enhance the computational capacity

of neurons (Gütig & Sompolinsky, 2006; Gütig, 2014). In these computational studies, the number of patterns stored was discovered to be a multiple (2-3x) of the number of synapses on the dendritic tree. Due to the methodological limitations of the uncaging method and whole cell patch-clamp technique, it is not feasible to attempt a multiple spatiotemporal pattern storage experiment. The Tempotron model is a strong example of the utility of the spatiotemporal learning (Gütig *et al.*, 2013), however physiological neurons exhibit certain properties that are not shared with tempotrons. The trained tempotron is allowed to only fire a single spike per input pattern and it is assumed that learned input patterns are isolated from other inputs (Florian, 2008). The tempotron model also requires monitoring of the time when postsynaptic potential was maximal. This is especially problematic when neuron incorrectly spikes to an input pattern as at the time membrane potential is reset, compromising the ability to monitor postsynaptic potentials (Florian, 2008). Finally, tempotron uses a gradient descent learning rule which, whilst efficient, is not a physiologically valid representation of how neurons adjust their synaptic weights.

My findings build upon a vast theoretical background on the role of dendrites in neuronal computation (Poirazi & Mel, 2001; Poirazi *et al.*, 2003; Häusser & Mel, 2003). These studies importantly adjusted our view on the theoretical computational capacity enhancement in neurons with active dendrites. Spatiotemporal plasticity further enhances the number of possible patterns that can be stored in the dendrite. The number of patterns that a single dendrite can store is an important next step for both empirical and theoretical work. The complexity of the problem is potentially daunting as the approach needs to account for the spatial extent over which patterns are stored (i.e. single dendrite or the whole tree) and the degree of interaction between the spatial units of pattern storage.

To my knowledge, this study describes, for the first time, the storage of specific spatiotemporal patterns under physiological conditions. Spatiotemporal plasticity is a promising candidate for

storage and refinement of neural circuits and likely greatly enhances the complexity of information that the dendrite is capable of representing.

4 PHARMACOLOGY AND CALCIUM DYNAMICS OF SPATIOTEMPORAL PLASTICITY

4.1 INTRODUCTION

Following the discovery of spatiotemporal plasticity in the basal dendrites of layer 5 pyramidal cells, I was interested in describing the underlying mechanisms. Practically all forms of plasticity in cells depend on Ca^{2+} influx. The canonical form of LTP was shown to depend on the entry through the NMDA receptors (Bliss & Collingridge, 1993). Chelating Ca^{2+} using BAPTA or EGTA was shown to abolish plasticity in several plasticity induction protocols and cell types (Lynch *et al.*, 1983; Hansel *et al.*, 1996; Cho *et al.*, 2001; Nevian & Sakmann, 2006; Lee *et al.*, 2009). By using photolysis of Ca^{2+} loaded into CA1 cells, Malenka and colleagues (1988) demonstrated that an increase in intracellular calcium is sufficient for LTP induction. The standard theory of the relationship between Ca^{2+} and plasticity was proposed by Lisman (1989) - moderate levels of intracellular Ca^{2+} increases result in LTD, whereas large increases in Ca^{2+} result in LTP. This theory has received fair amount of support from studies using Ca^{2+} chelators (Hansel *et al.*, 1996; Cho *et al.*, 2001), glutamate and calcium uncaging (Neveu & Zucker, 1996; Tanaka *et al.*, 2007; Cormier *et al.*, 2013). In the field of STDP, the relationship between Ca^{2+} influx and plasticity is more controversial. Some studies failed to see a (moderate) increase in intracellular Ca^{2+} in protocols that commonly elicit t-LTD – in fact, a small decrease was observed (Koester & Sakmann, 1998). In other studies, t-LTD and t-LTP protocols resulted in a supra-linear influx into dendrite (Nevian & Sakmann, 2006). The magnitude of Ca^{2+} influx was not informative of the sign of the resulting plasticity as both t-LTP and t-LTD elicited similar increases in intracellular Ca^{2+}. Despite some lingering controversies, it is evident that Ca^{2+} plays a major role in the induction of LTP and LTD. The literature on the role of Ca^{2+} in plasticity induction is primarily centred on Ca^{2+} increases in single spines. Previous studies confirmed that concurrent stimulation of neighbouring spines

increases the likelihood of (structural) plasticity induction (Harvey & Svoboda, 2007) whilst localizing the concurrently stimulated spine on a neighbouring dendrite decreases it (Govindarajan *et al.*, 2011). One possibility is that the dendritic increase in Ca^{2+} results in setting a plasticity "tag" that enhances the likelihood of plasticity induction (Frey & Morris, 1997; Govindarajan et al., 2006). The biochemical identity of the plasticity tag is currently unclear, nevertheless it is likely that different spatial Ca^{2+} profile influences the threshold for setting of the plasticity tag for neighbouring spines. At the current time, there is little experimental data to draw predictions from in terms of what the spatial profile of spatiotemporal plasticity might be. Different Ca^{2+} increases were observed in the dendrites of cortical cells following distinct spatiotemporal patterns of synapse activation (Branco *et al.*, 2010). Centripetal activation of synapses resulted in an NMDA-dependent enhancement of responses compared to centrifugal activation in cortical cells.

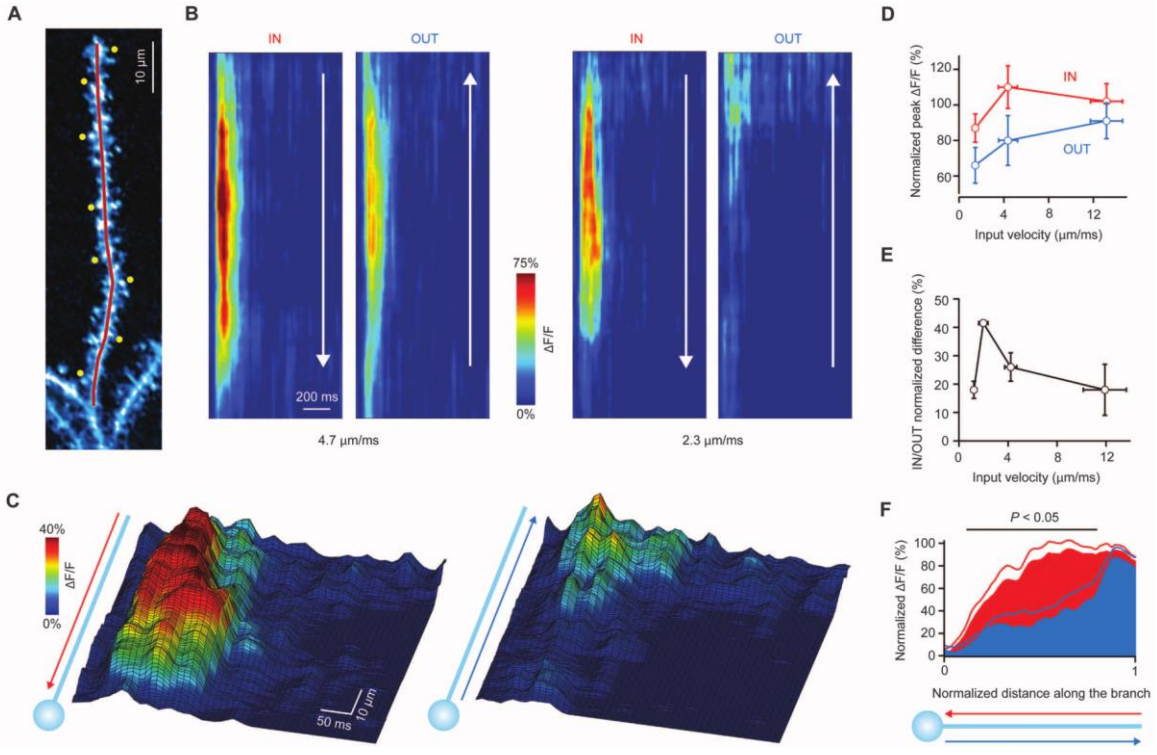

Figure 4.1 Dendritic calcium influx is direction and velocity sensitive.

A) Basal dendrite of layer 2/3 pyramidal neuron. Uncaging locations indicated in yellow: linescan profile used for Ca^{2+} imaging in red. B) Spatiotemporal profile of Ca^{2+} signals triggered by IN and

OUT input patterns at two different input velocities. C) Three-dimensional plot of the data in (B) (2.3 μm/ms). (D) Relation between Ca^{2+} signals and input velocity (ΔF/F values where F is fluorescence normalized to the mean ΔF/F of all velocities in the IN direction of each cell). Error bars indicate SEM. E) Relation between direction selectivity of Ca^{2+} signals and input velocity. F) Average spatial profile of the integrated Ca^{2+} transient across the dendrite (n=5 cells) (lines indicate SEM; bar indicates region of statistical significance). Source: Branco et al. (2010).

Nevertheless, these increases corresponded to a single uncaging stimulation of selected synapses that is unlike the high frequency pairing of uncaging stimulation and action potentials present in my protocol. During such high frequency pairing protocol, recruitment of voltage-gated calcium channels is expected to affect the spatial profile of Ca^{2+} increases. I suggest three possible hypotheses for the spatial profile of Ca^{2+} influx (Figure 4.2) that might underpin the induction of spatiotemporal plasticity. The faster unblocking of NMDA receptors in the IN-pairing protocol (see Figure 4.2A - top) could result in a uniform increase in the Ca^{2+} influx when compared to the OUT-pairing protocol. Alternatively, preferential spatial profile could be observed in locations where different sequences are expected to have a maximal Ca^{2+} profile – IN-pairing protocol in the proximal part of the dendrite and OUT-pairing protocol in the distal part (Figure 4.2 – middle). Finally, the baseline synapse strength could be the primary determinant of the observed Ca^{2+} influx, giving rise to a complex spatial rule that depends on the relative distribution of synaptic weights (Figure 4.2 – bottom).

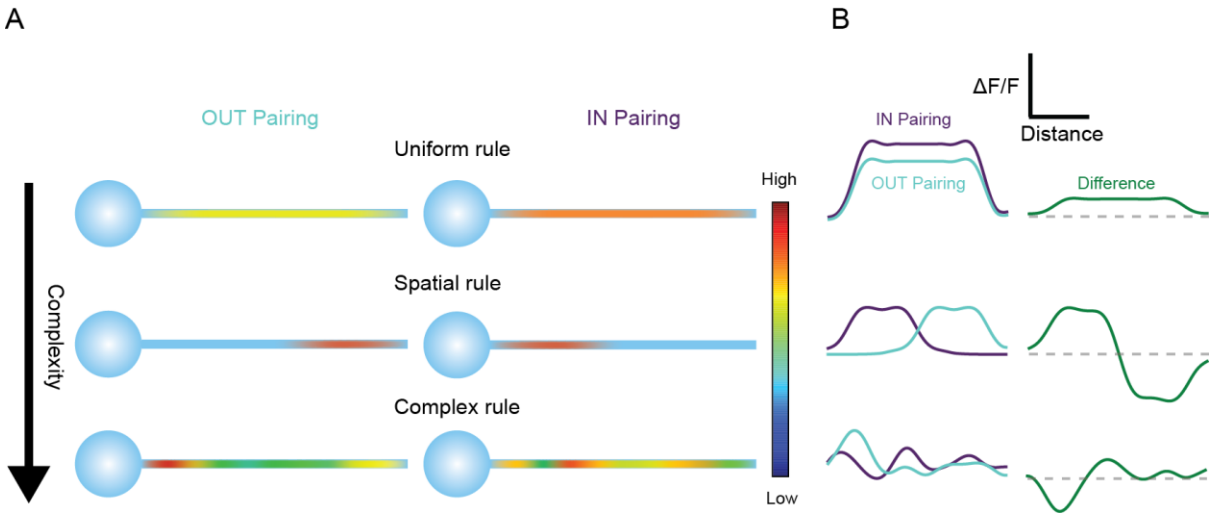

Figure 4.2 Schematic of potential dendritic Ca^{2+} profiles underpinning spatiotemporal plasticity

A) Schematic of hypothesized dendritic Ca^{2+} profiles underlying the induction of spatiotemporal plasticity. The averaged potential spatial profile of the Ca^{2+} influx is shown in B). (Top) The schematic shows a uniform preferential Ca^{2+} influx in the IN-induction protocol compared to the OUT induction protocol with no variation in the spatial profile. (Middle) A differential increase in Ca^{2+} for IN and OUT-induction protocols favouring proximal and distal locations respectively. (Bottom) A complex spatial profile of IN and OUT-induction protocols showing arbitrary localized increases in Ca^{2+}.

4.1.1 Aims of the chapter

In this chapter, I will look at the Ca^{2+} profile (see Figure 4.2) during the induction of spatiotemporal plasticity described in Chapter 3. I will then study the properties of supralinearity and cooperativity of different stimulation protocols in the dendrites of layer 5 pyramidal neurons. Finally, I will look at the pharmacology underlying the induction of spatiotemporal plasticity, specifically the role of NMDA receptors in the induction.

4.2 RESULTS

4.2.1 Imaging of Ca^{2+} influx following spatiotemporal-plasticity induction protocol

4.2.1.1 Calcium imaging protocol

As Ca^{2+} influx is a determinant of whether potentiation is induced, my goal was to test whether distinct sequences can result in a differential spatial Ca^{2+} profile that underpins the observed spatiotemporal plasticity observed in Chapter 3. However, Ca^{2+} indicators act as Ca^{2+} buffers, which have been previously shown to prevent the induction of plasticity. As a result, it is difficult to demonstrate the induction of plasticity in the presence of Ca^{2+} dyes. Therefore in this chapter, I describe the Ca^{2+} profile during the induction protocol and not the spatiotemporal plasticity described in the previous chapter.

The induction of plasticity at high frequencies is expected to lead to strong membrane voltage changes and result in a significant Ca^{2+} influx through various voltage-dependent sources such as voltage-gated calcium channels and NMDA receptors. As a result, high affinity indicators such as OGB-1 will show saturation, and thus, I selected Fluo-5F, which has moderate affinity (K_d = 2.3 μM) for supra-linear increases in Ca^{2+}. To compare IN-potentiation and OUT-potentiation protocols, I selected uncaging points as previously described and interleaved pairing of IN- and OUT-sequences with action potentials for multiple trials (see Figure 4.3). This consistently resulted in a strong, supralinear Ca^{2+} influx into dendrite (see below).

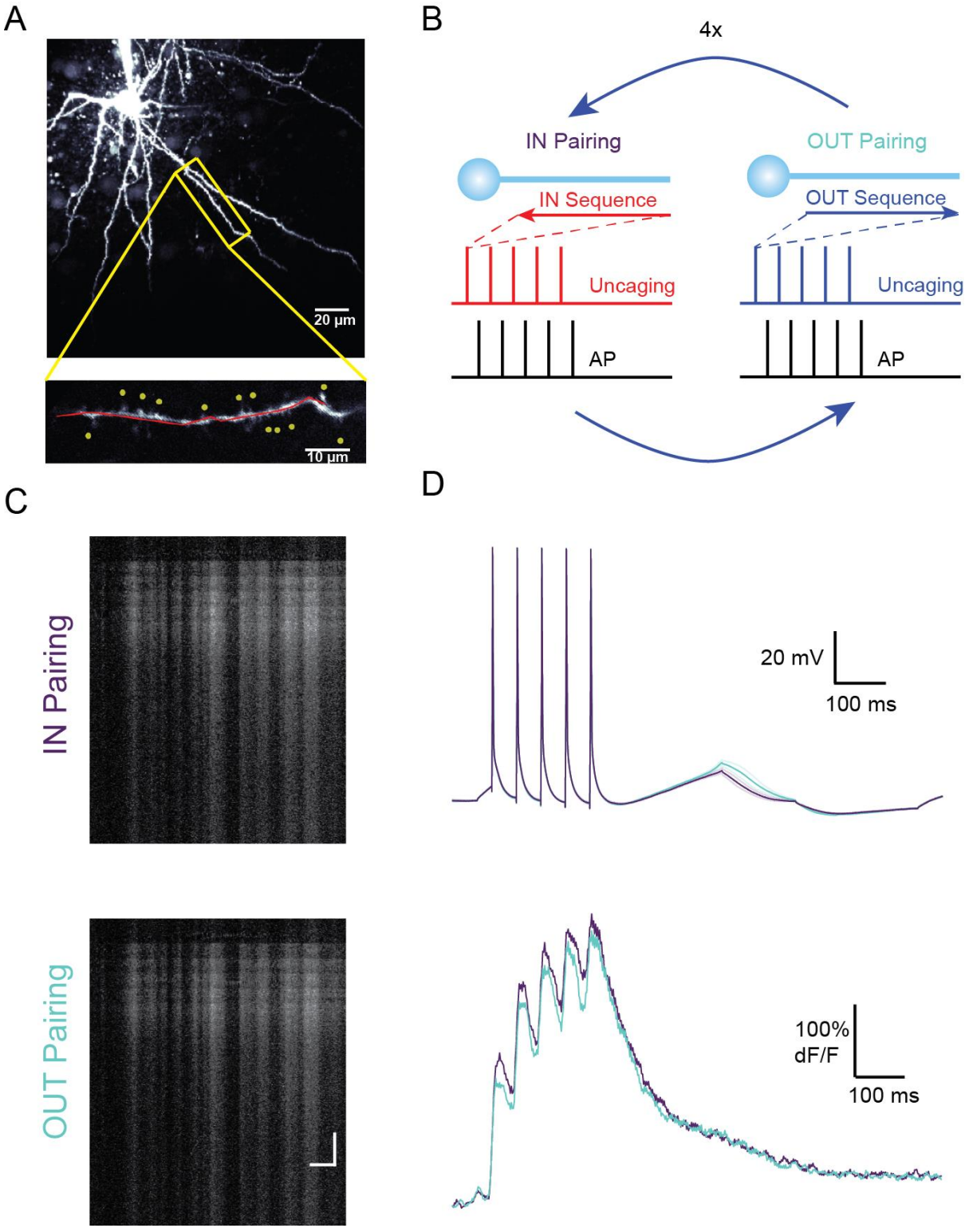

Figure 4.3 Schematic of a method used for imaging the profile of Ca^{2+} influx during induction.

A) Top – Example cell recorded in a whole-cell patch-clamp configuration filled with Alexa-594 dye. Bottom – uncaging locations indicated in yellow and the defined profile of line-scan shown in red. B) Schematic of interleaved induction protocol used. IN-pairing and OUT-pairing were interleaved during calcium imaging. C) Example Ca^{2+} imaging of IN-pairing and OUT-pairing protocols. Scale bar – y axis: 100 ms, x axis: 5 μm. D) Example recording (top) and profile of Ca^{2+} imaging after uncaging induction artefact correction (see below).

4.2.1.2 IN sequence results in a greater Ca^{2+} influx than OUT sequence

Previously, Branco et al. (2010) showed that the IN sequence preferentially activates NMDA receptors when compared to the OUT sequence. However, the stimuli used in the study were supra-linear which likely resulted in enhanced NMDA activation. Branco et al. (2010) and my own analysis show that even in case of mostly passive small-magnitude EPSPs in a layer 2/3 (Branco et al. (2010)) and layer 5 (Figure 4.4), somatic voltage responses for the IN sequence are larger than the OUT sequence. Accordingly, Ca^{2+} influx for the IN sequence was significantly larger than for OUT sequence (Figure 4.4 and Figure 4.5, N=7, $p < 0.05$) presumably due to enhanced activation of NMDA receptors.

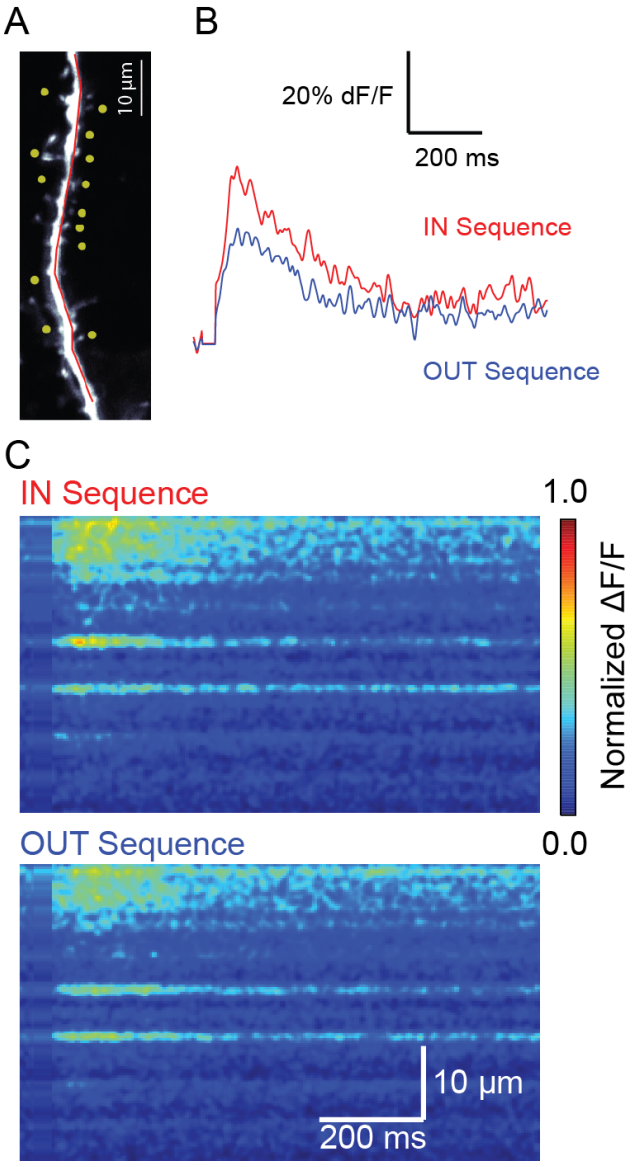

Figure 4.4 IN sequence results in greater Ca^{2+} influx than OUT sequence.

A) Basal dendrite of layer 5 pyramidal neuron. Uncaging points indicated in yellow, line-scan profile used for Ca^{2+} imaging in red. B) Averaged ΔF/F trace across spatial locations in the dendrite. C) Spatiotemporal profile of Ca^{2+} signals following IN and OUT input patterns.

4.2.1.3 IN- and OUT-sequence induction pairing result in supra-linear Ca^{2+} influx

I next investigated whether spatiotemporal induction patterns, IN-pairing and OUT-pairing, can be differentiated from one another in terms of their spatial profile of the Ca^{2+} influx. Because of action potential backpropagation, I expected an increase in recruitment of voltage-gated calcium-

permeable conductances (i.e. VGCCs and NMDA receptors) resulting in an enhancement of Ca^{2+} influx compared to a linear sum of Ca^{2+} profile from IN/OUT input pattern and backpropagating action potential. Consistently, I found that IN- and OUT-pairings are supra-linear in their Ca^{2+} recruitment as compared to the linear sum of IN/OUT input patterns and backpropagating action potentials (Figure 4.5E, N=7, paired t-test: 2.6, $p < 0.05$).

There was a significant difference between sequential stimulation, linear sum of bAP and pairing induction protocol (Friedmann $\chi^2 = 10.3$, $p < 0.01$). The pairing induction protocol resulted in a significantly greater Ca^{2+} increase than the linear sum of the bAP and sequence stimulation (N=6, post-hoc paired t-test: 2.6, $p < 0.05$). Compared to the OUT-pairing protocol, IN-pairing resulted in a significantly larger Ca^{2+} increase (N=7, post-hoc paired t-test: 4.2, $p < 0.01$). To control for the movement of slice preparation artefacts between interleaved trials, I looked at whether there was a difference between bAPs recorded with the same separation as was used in the interleaved IN/OUT-pairing protocol. No uniform enhancement was observed in the experiment with only bAPs (N=6, post-hoc paired t-test: 1.29, $p > 0.05$). To verify whether there is a spatial profile in the increased Ca^{2+} influx in the case of IN-pairing protocol over the OUT-pairing protocol I split the dendrite into three segments normalized by their spatial dimension – proximal, medial and distal. There was no significant difference between the individual segments of the dendrite in the degree of IN-pairing protocol Ca^{2+} increase over the OUT-pairing protocol (Friedmann $\chi^2 = 2.0$, $p > 0.05$). Whilst it is possible that a more complex spatial rule exists, the most parsimonious explanation is the uniformly greater Ca^{2+} influx during the IN-pairing protocol as compared to the OUT-pairing protocol. In further analysis of dendritic integration of different stimulation protocols, I discovered that the linear sum of bAP and sequential stimulation was significantly greater than sequential stimulation on its own (N=6, post-hoc paired t-test: 5.8, $p < 0.01$) and the Ca^{2+} influx to a train of bAPs were significantly greater than sequential stimulation on its own (N=6, post-hoc paired t-test: -2.85, $p < 0.05$).

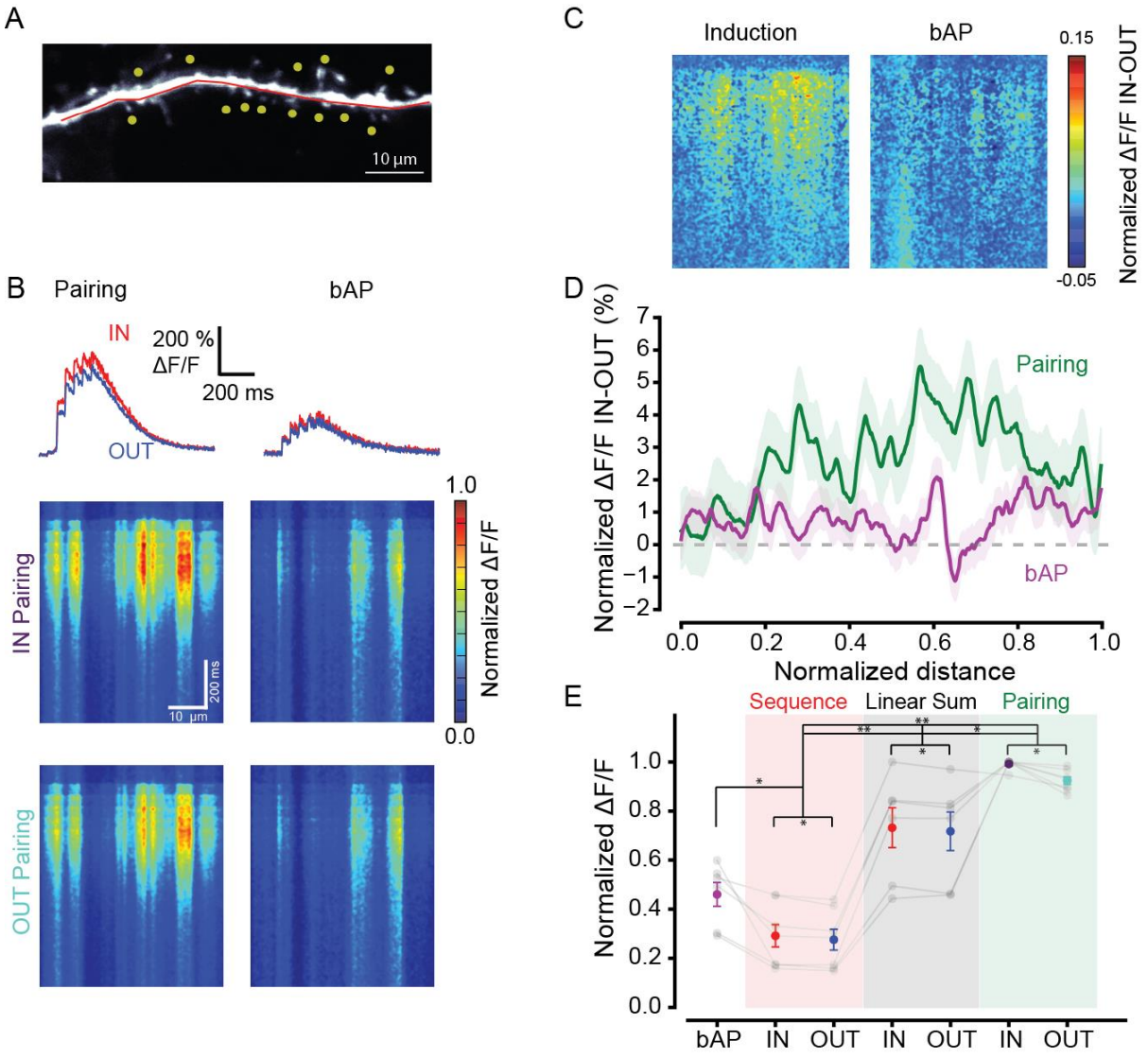

Figure 4.5 EPSP and AP pairing protocol results in a cooperative increase of Ca^{2+} influx into the dendrite

A) A sample dendrite with selected uncaging points and a line scan taken along the dendrite (red). B) (Left) A sample dendritic Ca2+ response to IN/OUT pairing protocol and bAPs alone. (Right) A sample spatial profile of the Ca2+ signal for induction protocol and bAPs only. C) Spatial profile of the difference between IN and OUT induction protocols (N=6) and for the bAPs condition only (control, N=6). Shaded regions indicate SEM. D) Average normalized ΔF/F trace difference between IN- and OUT-pairing protocols and between bAP controls. IN-pairing protocol shows a uniform increase in Ca^{2+} influx compared to OUT pairing protocol. E) Normalized ΔF/F

averages for different conditions (N=7 cells, N=6 for bAP condition). IN- and OUT-pairing protocols result in cooperative increase in Ca2+ influx compared to bAP and IN and OUT readout protocols (EPSP only). IN-pairing protocol results in a significant increase in Ca2+ influx compared to OUT-pairing protocol. Error bars indicate SEM.

4.2.2 NMDA receptors are required for the induction of spatiotemporal potentiation

Most traditional forms of pre- or post-synaptic plasticity in principal cells are dependent on NMDA receptors. As a result, I investigated whether whole-branch plasticity and spatiotemporal plasticity could be induced in the presence of NMDA blocker (D-AP5 bath, 50 µM). I did not detect any potentiation following IN- or OUT-pairing protocols (N=6, $p > 0.05$) and I also did not observe any significant spatiotemporal plasticity.

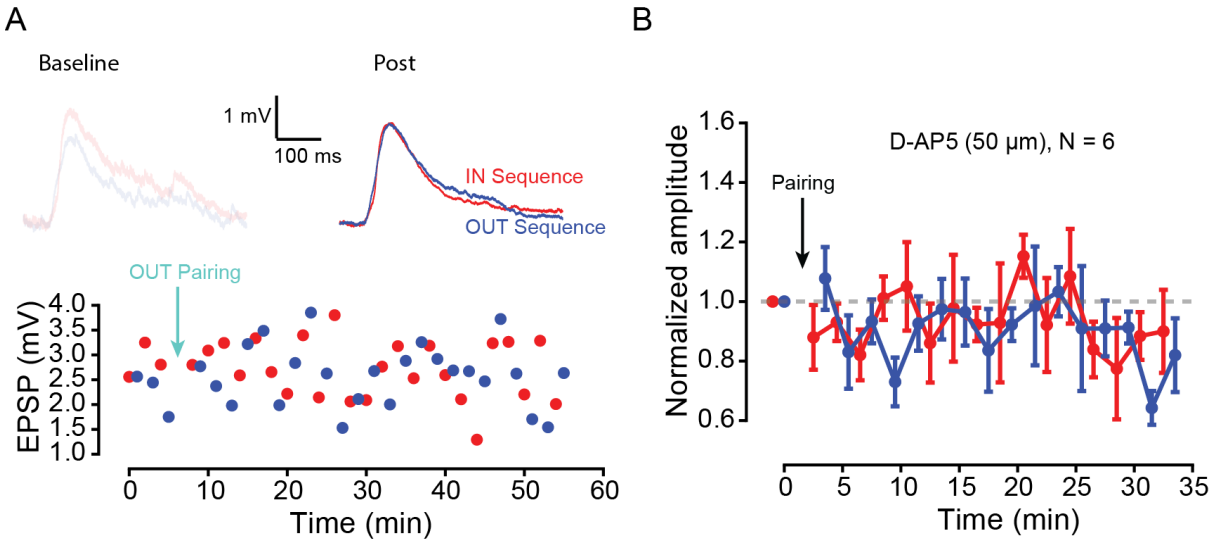

Figure 4.6 NMDA receptors are required for the induction of spatiotemporal plasticity.

A) (Top) Somatic responses to the IN and OUT input patterns in the presence of bath-applied D-AP5 (50 µM) for baseline (left) and after spatiotemporal pairing (right). (Bottom) Example of individual response amplitudes to interleaved IN and OUT input patterns. B) Long-term potentiation and sequence-dependent plasticity are blocked in the presence of D-AP5 (N=3, 50 µM).

4.3 DISCUSSION

In this chapter, I investigated the role of Ca^{2+} in the induction of spatiotemporal plasticity. I have discovered Ca^{2+} inflow differs depending on which type of spatiotemporal pairing protocol is utilized. Consistent with previous findings, IN-sequences paired with action potentials results in a higher Ca^{2+} elevation than similarly paired OUT-sequences. Interestingly, this inflow is uniform across the extent of the dendrite suggesting that a fairly simple plasticity rule may underlie the generation of the spatiotemporal plasticity described in previous chapter.

Ca^{2+} influx is required for the induction of long-term potentiation and depression in neurons (Hansel *et al.*, 1997; Cho *et al.*, 2001; Nevian & Sakmann, 2006). Consistent with previous reports, I verified that spatiotemporal plasticity is mediated by NMDA receptors, as is the case in traditional LTP induction protocols (Bliss & Collingridge, 1993; Sjöström *et al.*, 2008). In different areas of the brain, LTP can be expressed pre- or post-synaptically. One advantage of the uncaging method is that pre-synapse is bypassed and the locus of (post)-synaptic plasticity can be identified. Nevertheless it is interesting to speculate as to the potential role of the pre-synapse in spatiotemporal plasticity. As I mentioned previously, in situations where synaptic release is insufficient to activate fully receptors on the post-synaptic membrane, pre-synaptic modifications could, similarly, lead to the emergence of spatiotemporal plasticity. Research in optogenetics resulted in the generation of opsin variants that can faithfully drive cells to high frequency firing rates (Lin *et al.*, 2009) which were shown to be capable of reliable induction of long-term potentiation and long-term depression (Nabavi *et al.*, 2014). Sparse expression of such opsins in presynaptic cells of cortical and hippocampal circuits could be used to drive activation of presynaptic terminals to elicit plasticity. Such experimental context is not only more physiological than uncaging method but also allows the study of the possible role of pre-synapse in spatiotemporal plasticity.

Furthermore, my experiments were primarily performed by imaging calcium influx into the dendrite and not into spines. Spines are often viewed as structures which enable electrical and biochemical compartmentalization (London & Häusser, 2005; Harnett *et al.*, 2012). Single spines may be important sites of protein synthesis which importantly determine the magnitude of plasticity (Tanaka *et al.*, 2008). As a result, an important next step in the analysis of the role of Ca^{2+} in induction of spatiotemporal plasticity is to analyse the Ca^{2+} influx into individual spines. Several key parameters of spines are important in the context of spatiotemporal plasticity. First, the morphology of spine head and neck determine the degree of Ca^{2+} influx and diffusion (Alvarez & Sabatini, 2007; Chen & Sabatini, 2012). A second important parameter is the location of the spine on the dendritic tree. As I previously mentioned, an impedance gradient importantly affects the recruitment of active conductances. As a result, evaluating Ca^{2+} influx in different morphologies and spine locations could importantly modify the current expectation of largely uniform increase in Ca^{2+} entry into the dendrite.

Because my experiments visualized dendrites by injecting dye through the patch-clamp pipette, evaluation of structural changes during and after induction of plasticity were methodologically difficult. In cells with complex dendrites such as layer 5 pyramidal cells or Purkinje cells, dispersion of dyes into the dendrite following establishment of whole-cell configuration can take tens of minutes. Because whole-cell configuration was previously found susceptible to washout of plasticity, from methodological standpoint, it is important to induce plasticity as early as possible upon breaking the plasma membrane of the cell. Furthermore, analysis of structural plasticity is complicated due to the difficulty of separating increase in the size of the spine through plasticity induction from simple dye dispersion into the dendrite. The use of cells expressing GFP through viral transfection or transgenic lines could be used to evaluate the role of structural changes of spines, if any, in the induction of spatiotemporal plasticity.

A variety of mechanisms could potentially underlie observed spatiotemporal plasticity such as an increasing or decreasing gradient of synapse potentiation with the distance from the soma, or a complex spatial code of synapse potentiation or depression. The size of Ca^{2+} influx was previously linked with the sign and magnitude of plasticity (Koester & Sakmann, 1998). As a result, I hypothesized that the spatial Ca^{2+} profile would be predictive of the magnitude of observed individual synapse potentiations (or depressions). Consistent with previous reports, I observed a supra-linear increase in the Ca^{2+} influx following EPSP-bAP pairing as well as an increased Ca^{2+} entry following IN input pattern as compared to the OUT input pattern. I observed a greater uniform increase in the Ca^{2+} influx following IN-pairing protocol as opposed to the OUT-pairing protocol. Interestingly, I did not observe differences in the spatial profile of Ca^{2+} influx between IN-pairing and OUT-pairing protocols. Whilst these results seem to rule out the spatial rule of spatiotemporal plasticity induction explained in the introduction (Figure 4.2 – middle), a complex rule where the spatial Ca^{2+} profile is driven primarily by synaptic weights may still be valid.

Since I performed Ca^{2+} imaging across different dendrites, the averaged spatial profile may hide the complexity of synaptic weight distributions of individual dendrites. A future experiment to address this issue is to monitor individual synaptic weights and evaluate whether synaptic weight based rule compared to uniform rule can better predict observed spatiotemporal Ca^{2+} profile . The uniform model of conductance is the more parsimonious model of synaptic weight update. Previous work shows some support for the role of the dendrite as the primary locus of plasticity. Co-stimulation of nearby spines with suprathreshold and subthreshold protocols concurrently produces similar changes in synaptic strength (Harvey & Svoboda, 2007). Plasticity protocols across multiple dendrites are less likely to induce synaptic strength changes (Govindarajan *et al.*, 2011). The dendritic locus is consistent with the location of organelles involved in local protein translation at the dendritic branch. Local protein translation was previously shown to be required for the induction of plasticity (Sutton & Schuman, 2006) and it is hypothesized to play a key role in the setting of synaptic plasticity tags (Redondo & Morris, 2011). Nevertheless, it is important to

appreciate that baseline synaptic weights importantly determine the magnitude of plasticity observed (Abraham & Bear, 1996).

In this chapter, I empirically tested the Ca^{2+} profile in dendrite following the spatiotemporal plasticity induction protocol. Assuming that the Ca^{2+} profile corresponds to the magnitude of plasticity observed, a fairly simple rule emerges from my Ca^{2+} imaging data – differential uniform scaling of synaptic weights in the dendrite. The advantage of such simplicity is the potential of generality of such rule. Any neuron capable of scaling synaptic weights is able to make use of such a rule and thus learn to respond to a particular spatiotemporal sequence of synaptic inputs. In this reduced model, neurons determine their spatiotemporal preference by a simple dialing up or down of their synaptic weights. Such parsimonious rule is a useful baseline approximation that I employed in the next chapter in compartmental simulation of spatiotemporal plasticity.

Whilst such plasticity rule is enticing for its simplicity, it is currently controversial whether Ca^{2+} imaging can be used as a proxy for synaptic weight scaling. Glutamate uncaging does allow the probing of single synapses, however, the high phototoxicity of such a protocol reduces yield considerably for long experiments such as plasticity protocols. As a result, it is also difficult to test other features on which spatiotemporal plasticity may depend, such as the role of distance and velocity of synaptic activations. Compartmental modelling of morphologically realistic neuronal models was previously shown to be a useful approximation when an experimental approach was not feasible. In the next chapter, I describe the evaluation of uniform scaling rule in eliciting spatiotemporal preference in a compartmental model of layer 2/3 and layer 5 pyramidal neurons.

5 MODELLING OF SPATIOTEMPORAL PLASTICITY INDUCTION

5.1 INTRODUCTION

Many sensory pathways, across a diverse range of animal species such as locusts, primates and humans, have the remarkable ability to encode stimuli with precisely tuned action potentials (deCharms & Merzenich, 1996; Wehr & Laurent, 1996; Johansson & Birznieks, 2004). Structural plasticity changes were reported in the learning of arbitrary sensorimotor behaviours such as the rotarod task (Yang *et al.*, 2014). Spatiotemporal plasticity is a good candidate for refining circuits to better encode such behaviours. Nevertheless, it is still unknown how spatiotemporal patterns could potentially be stored on the level of dendrites. In this chapter, I will consider a theoretical framework for implementing plasticity rules that are dependent on temporal sequences.

The ability of neurons to learn to represent an arbitrary temporal pattern is currently an actively researched area. The Remote Supervision Method (ReSuMe) and Tempotron model are two methods that are currently at the forefront of the field. In the ReSuMe model (see Figure 5.1), inputs are strengthened when the target spike is observed, and depressed when the trained neuron spikes (Ponulak & Kasiński, 2010). If potentiation and depression are balanced, the actual spiking of the neuron converges to the target value even in the case of highly overlapped information (such as neural noise from overlapping patterns). Tempotron, a variant of the ReSuMe model (Florian, 2008), was demonstrated to be useful in learning to encode tasks requiring time-warp invariant processing such as in the case of speech stimuli (Gütig & Sompolinsky, 2009) or in tasks such as classification of retinal spike trains (Gütig *et al.*, 2013). Nevertheless, as I described in previous chapters Tempotron or ReSuMe models are not physiological representations of plastic changes in dendrites of neurons.

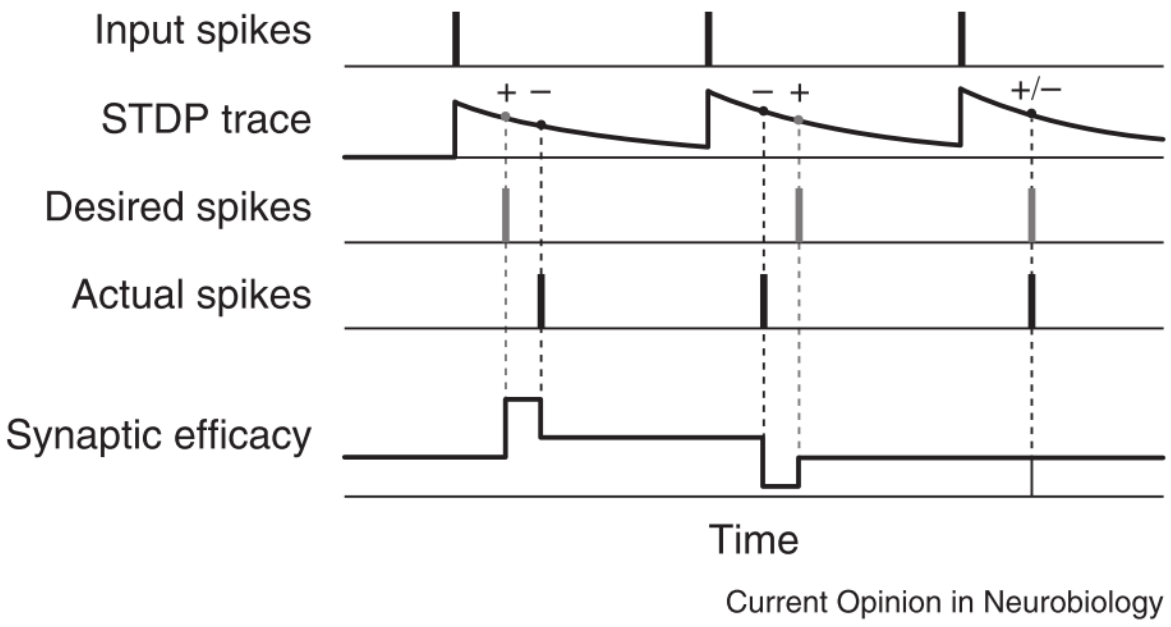

Figure 5.1 Illustration of the ReSuME model for an excitatory connection.

The input spikes (top row) give rise to an exponentially decaying STDP trace (second row) that determines the magnitudes of synaptic changes (bottom row). Desired spikes (gray, third row) potentiate the synaptic efficacy and actual spikes (black, forth row) depress it. The effects of coincident desired and actual spikes cancel such that the synaptic efficacy remains unchanged. Source: Gütig (2014).

An ReSuMe model expects depression in the pre-post pairing which is not commonly observed in cortical synapses (Feldman, 2000, 2009; Sjöström *et al.*, 2001). Neither of the models uses active dendrites as integrative units. Most importantly, both ReSuMe and Tempotron models are based on integrate-and-fire neurons in which the spatial component of the input is absent. Nevertheless, in Chapter 3 of this thesis, I described a novel variant of plasticity that is sensitive to the spatiotemporal activation of inputs that cannot be accounted for with current theoretical models. In Chapter 4, I found that individual spatiotemporal plasticity induction protocols are associated with different Ca^{2+} spatial profiles in the dendrite. In particular, the IN-induction protocol is associated with greater Ca^{2+} influx than the OUT-induction protocol. In this chapter, I will describe

the induction of spatiotemporal plasticity using simple rule derived from my Ca^{2+} imaging study. I will simulate induction of plasticity by uniform scaling of synapses on the dendrite. Consistent with Ca^{2+} data, I will assume greater scaling of synapses in the simulation of IN-potentiation compared to OUT-potentiation. I will then describe how such a parsimonious plasticity rule can account for the induction of spatio-temporal plasticity.

There is currently a gap in the theoretical literature on the potential plasticity mechanisms that would result in spatiotemporal pattern storage. In this chapter, I describe a potential theoretical mechanism that underpins the generation of plasticity rules that are dependent on temporal sequences. The model of plasticity I present in this chapter is constrained by the empirical data from Ca^{2+} imaging that I presented above (namely the greater uniform increase in Ca^{2+} influx following IN sequence compared to the OUT sequence).

5.1.1 Aims of the chapter

My aim in this chapter is to use theoretical simulations to describe possible candidates for a physiological mechanism underlying observed spatiotemporal plasticity. I constrained the plasticity rule by my experimental findings, namely a prediction of the magnitude of the plasticity changes derived from Chapter 5 and the distribution of anticipated weight changes using Ca^{2+} influx as a proxy presented in Chapter 6 of the thesis. Using computational models of morphological reconstructions of neurons in the NEURON environment (Hines & Carnevale, 1997), I attempted to describe the underlying factors that influence the induction of spatiotemporal plasticity.

5.2 RESULTS

5.2.1 Optimization of NEURON model parameters using a genetic algorithm

Compartmental models often contain many nonlinear and nonhomogeneous distributions of conductances across the dendritic tree. Defining parameter sets, even restricted to physiologically observable values, that faithfully replicate experimental data is not practicable manually. On the other hand, brute-force approaches, due to exponential increase in complexity with increased number of parameters, are also not feasible, except for a very restricted set of circumstances.

Thus to discover parameters of model that was capable of reproducing my experimental findings, I used a genetic algorithm optimization technique constrained within physiological ranges of parameters (as reported in previous studies - see Table 5.1) The natural parallelization character of genetic algorithms makes them well-suited for optimization of NEURON parameters (Keren *et al.*, 2005; Almog & Korngreen, 2014). Constraining parameter sets using pharmacological or numerical peeling procedures allowed the construction of detailed ionic mechanism of dendritic spikes in neurons displaying large number of heterogeneous conductance gradients (Almog & Korngreen, 2014). Genetic algorithms use mechanisms borrowed from Darwinian evolution such as point mutations and cross-over to breed better models from random starting populations. Whilst the original algorithm presented in Keren et al. (2005) did not breed the new generation based on the fitness score of each individual in the population, I observed that such approach converges to a minimum faster to both NEURON models (not shown) and a randomly generated linear function with 16 parameters (Figure 5.2B). An example cost function is shown which was used to optimize the ratio of peak voltages of preferred and non-preferred spatiotemporal sequences (see Figure 5.2C). The optimal ratio was selected based on the average ratio obtained in experimental data presented in chapter 3.

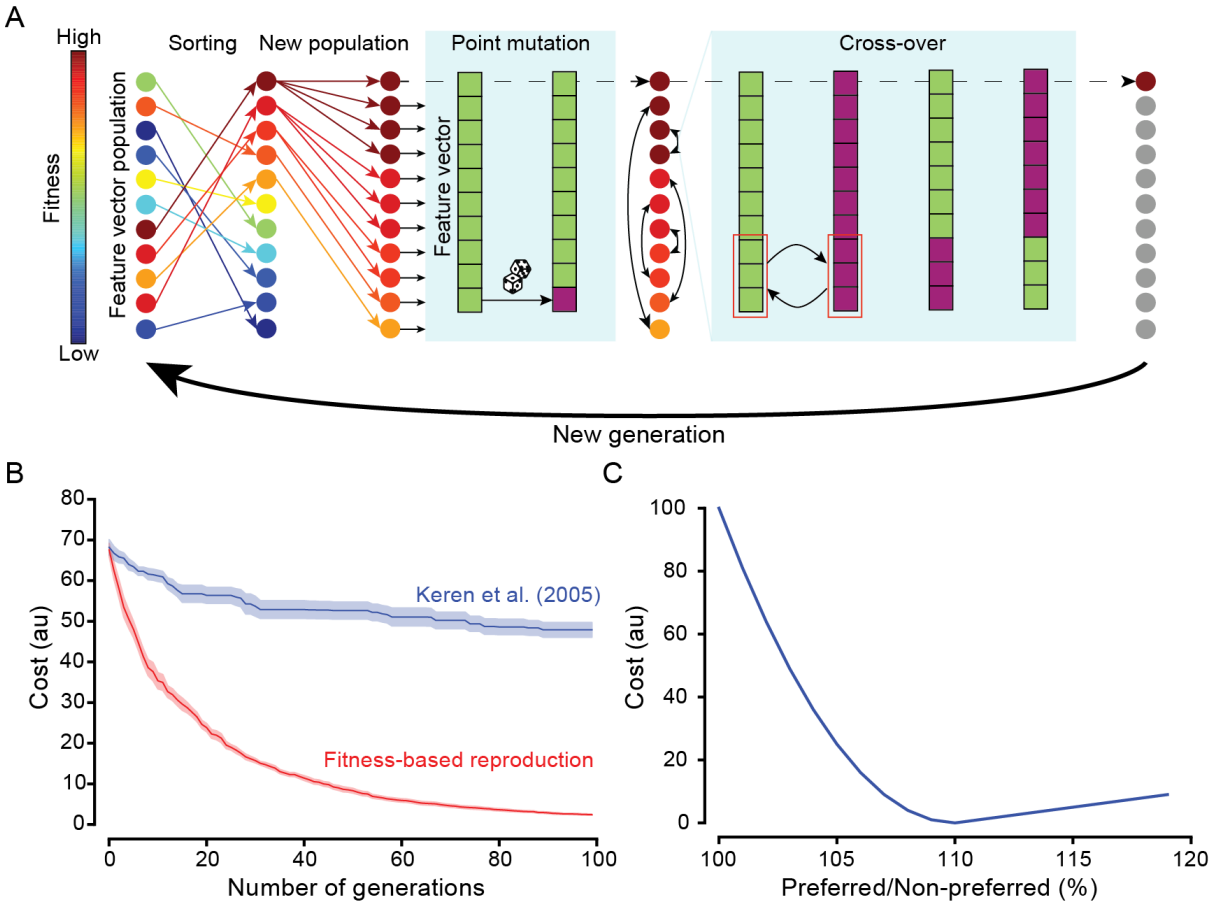

Figure 5.2 Genetic algorithm overview of performance and cost functions.

A) Schematic of a single generation of the genetic algorithm optimization. Generated feature vectors are initially sorted based on their fitness score. Children are produced based on the normalized fitness of each of the parents. Children are then subjected to a point mutation process with defined probability (usually 0.1) and a cross-over where random features are exchanged (with a probability 0.2). The most successful individual is moved to next generation unchanged to prevent drift. B) Comparison of fitness-based reproduction performance with the original Keren et al. (2005) in optimization of 16-variable linear function with random multipliers. C) An example of asymmetric cost function used in optimizations to penalize potentiation of non-preferred pattern.

5.2.2 Uniform scaling of synaptic weights is sufficient for the induction of spatiotemporal plasticity in a model of Layer 2/3 neuron

In the simulations presented in this chapter, I used the Layer 2/3 compartmental cell model in which spatiotemporal sensitivity was initially demonstrated (Branco *et al.*, 2010). The development of spatiotemporal pattern preference was tested in a simple passive model containing AMPA and NMDA conductances. Consistently, the peak difference between the IN and OUT patterns of activation was dependent on the velocity of the input and NMDAR activation as previously reported. The genetic optimization was run with a set of constraints that were drawn from experimental data and from previous literature (see Table 5.1).

In the generation of first population, AMPA and NMDA baseline conductance values were selected from a random uniform distribution with an upper bound equal to that employed in the previous study (Branco *et al.*, 2010). Plasticity was simulated by multiplying the baseline conductance values by a multiplier that was uniform for all synapses on the dendrite. The uniform constraint was taken from the Ca^{2+} imaging data described in chapter 4. The conductance multiplier for both AMPA and NMDA was allowed to vary based on the previously published literature on the subject (Benke *et al.*, 1998; Watt *et al.*, 2004). In practice, the optimization never reached the upper-bound of conductance values or multipliers. In the analysis below, I describe a further constraint on the conductance values based on the physiologically observed AMPA/NMDA ratios in the literature. The model was further constrained to with a 2 ms of inter-spine activation time that corresponded to experimental data. Furthermore, the number of synapses was allowed to vary within the range I used in the experiments. Finally, the locations of synapses on the dendrite, as well as the synapse spread, were allowed to vary freely. For all constraints and parameters employed in the model, see Table 5.1.

Table 5.1 Optimization results and constraints used in NEURON simulations

Parameter	Unit	L2/3 Pyramidal Cell				L5 Pyramidal Cell	
Figure		Figure 5.3	Figure 5.4	Video 1	Video 2	Figure 5.7	Figure 5.8
Passive Parameters							
R_a	Ωcm	150	150	150	150	120.48	120.48
R_m	Ωcm^2	10000	10000	10000	10000	25812	25812
C_m	$\mu F/cm^2$	1	1	1	1	0.6	0.6
$E_{passive}$	mV	-75	-75	-75	-75	-75	-75
Optimized values							
g_{AMPA}	$pS/\mu m^2$	350	217	203	298	229	638
g_{NMDA}	$pS/\mu m^2$	1491	3459	2964	5752	8947	9314
Number of synapses	unitless	18	16	20	20	15	19
Synapse spread	$(\mu m, \mu m)$	(31,72)	(26,79)	(0,31)	(3,27)	(42,99)	(37,85)
Inter-spine interval	ms	2	2	2	2	2	2
OUT scaling AMPA	unitless	1.1	1.21	2.42	2.24	2.6	1.74
IN scaling AMPA	unitless	1.32	2.02	2.52	2.8	2.12	2.3
OUT scaling NMDA	unitless	2.04	1	2.42	1	1.22	1
IN scaling NMDA	unitless	2.16	1	2.52	1	1.4	1
Constraints range							
g_{AMPA}	$(min, max)\ pS/\mu m^2$	(0,1500)	(0,1500)	(0,1500)	(0,1500)	(0,1500)	(0,1500)
g_{NMDA}	$(min, max)\ pS/\mu m^2$	(0,24000)	(0,24000)	(0,24000)	(0,24000)	(0,24000)	(0,24000)
Number of synapses	(min, max)	(8,20)	(8,20)	(8,20)	(8,20)	(8,20)	(8,20)
Synapse spread	$(min, max)\ \mu m$	(0,99.02)	(0,99.02)	(0,99.02)	(0,99.02)	(0,113.6)	(0,113.6)
Inter-spine interval	ms	2	2	2	2	2	2
OUT scaling range	(min, max)	(1,3)	(1,3)	(1,3)	(1,3)	(1,3)	(1,3)
IN scaling range	(min, max)	(1,3)	(1,3)	(1,3)	(1,3)	(1,3)	(1,3)

The cost of the model was derived based on the distance of ratio of peak voltages of preferred and non-preferred spatiotemporal sequences following potentiation (uniform scaling of conductances) from the ratio observed in experimental data (see Methods). Following the genetic optimization run, I observed that uniform scaling of conductances can result in both IN-preference and OUT-preference (Figure 5.3).

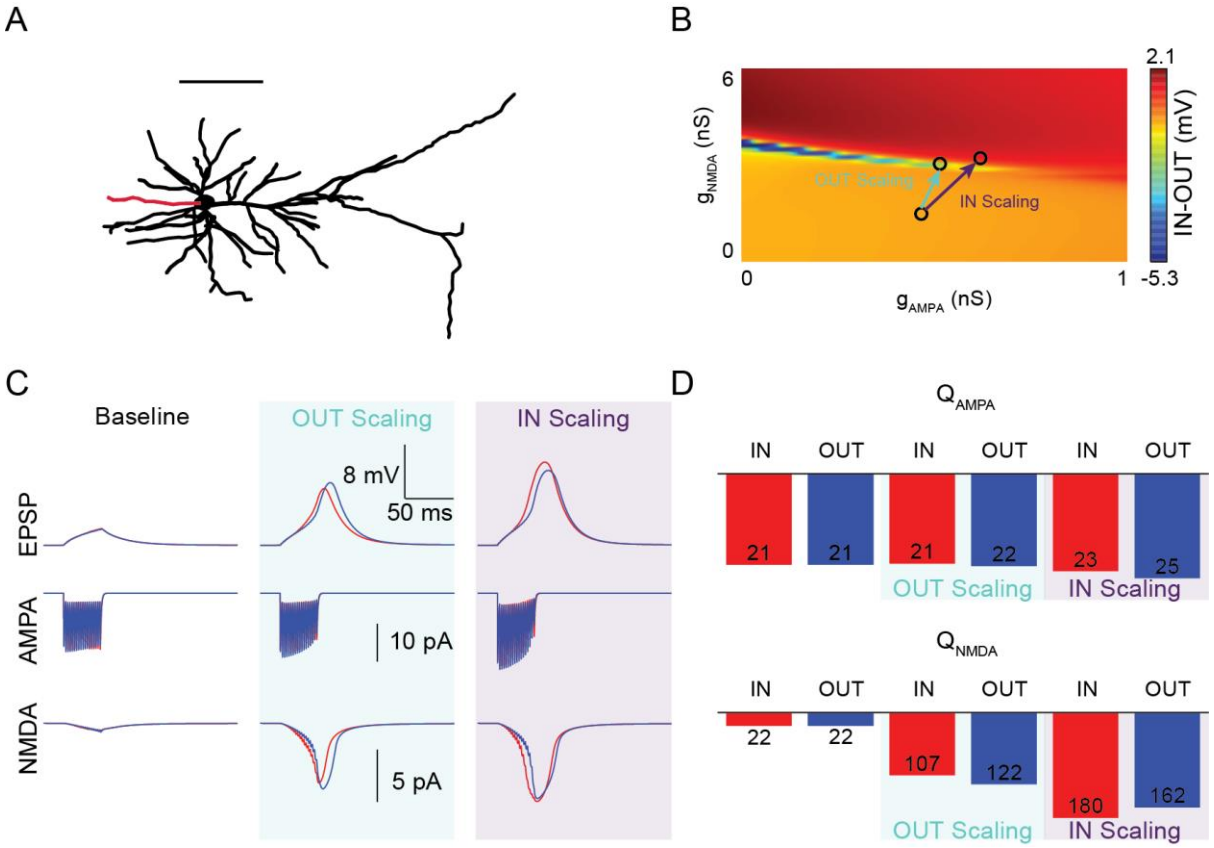

Figure 5.3 Uniform increase in AMPA and NMDA conductances results in the emergence of spatiotemporal input preference

A) A Neurolucida reconstruction of a layer 2/3 pyramidal neuron adapted from Branco et al. (2010). The selected dendrite for genetic optimization protocol is marked in red. Scale bar: 100 μm. B) A profile of differences of maximal amplitude of simulated EPSPs of played IN and OUT patterns at different AMPA and NMDA conductance values. The arrows display the vectors defining the direction of AMPA and NMDA scaling. C) Simulated EPSP and AMPA and NMDA current profiles corresponding to baseline values and following OUT and IN uniform scaling of AMPA values. AMPA and NMDA conductance values are shown by the circles in B). D) Integral of AMPA and NMDA currents under baseline, OUT and IN uniform scaling conditions.

For the progressive development of spatiotemporal preference across linear increase of AMPA and NMDA conductance values see Video 5.1. In summary, for a given set of parameters, IN-preference requires enhanced conductance increase compared to the OUT-preference (Figure

5.3B,D). This result is consistent with the observed amplification of Ca^{2+} influx following IN-pairing compared with OUT-pairing (see Chapter 4).

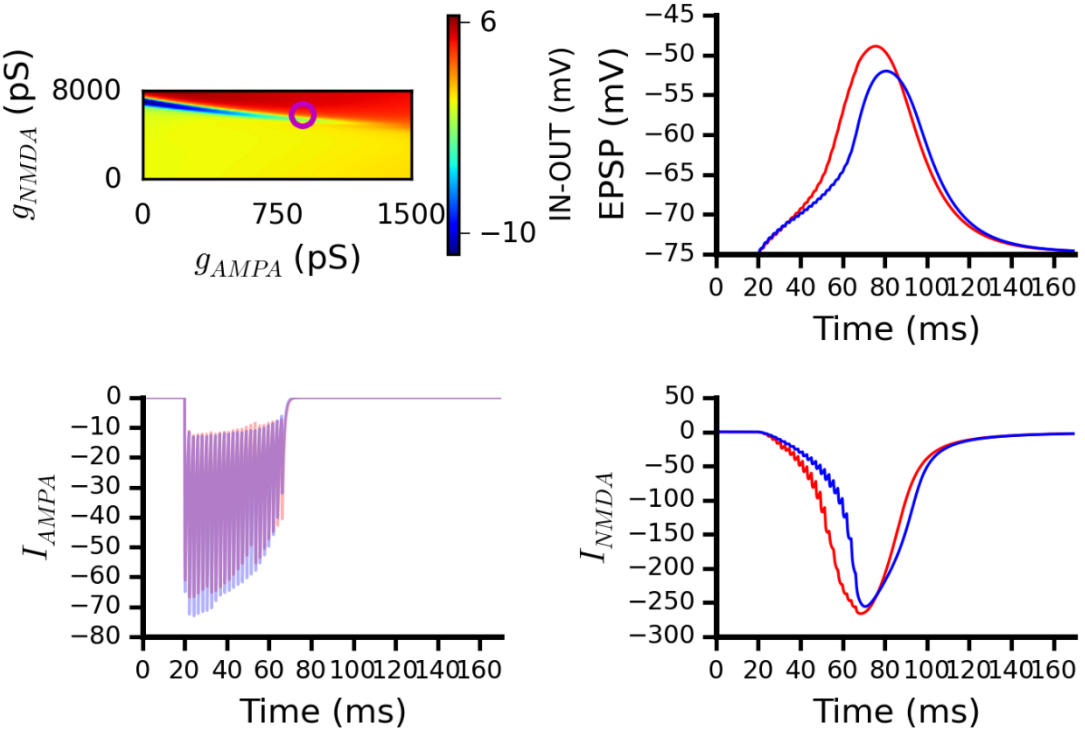

Video 5.1 Uniform increase in AMPA and NMDA conductance results in the emergence of spatiotemporal input preference.

(Top left) A profile of the differences between IN and OUT simulated EPSPs. Black circle represents the example trace shown in the remaining figure panels. (Top right) Example EPSPs for simulated IN and OUT sequences. (Bottom left) A mean profile of AMPA conductances for IN and OUT simulated sequences. (Bottom right) A mean profile of NMDA conductances for IN and OUT simulated sequences. Web Source: YouTube - http://tinyurl.com/VivaVideo51

5.2.3 Uniform enhancement of AMPA conductances only is sufficient for the induction of spatiotemporal plasticity

While an increases in both AMPA (Shi *et al.*, 2001; Malinow & Malenka, 2002; Kessels & Malinow, 2009) and NMDA (Watt *et al.*, 2004) receptors were reported following plasticity induction protocols, the NMDAR component of plasticity was markedly slower to develop than the AMPA component. My recordings, which showed strong changes in spatiotemporal preference post-induction, were usually only ~30 minutes in duration. At such time-scale, it is likely that the NMDAR component is not significantly enhanced. Therefore, I performed a more conservative simulation test by uniformly scaling only AMPA conductance in the optimization run (Figure 5.4). Following convergence, I observed that uniform AMPA-only scaling is sufficient to induce spatiotemporal preference.

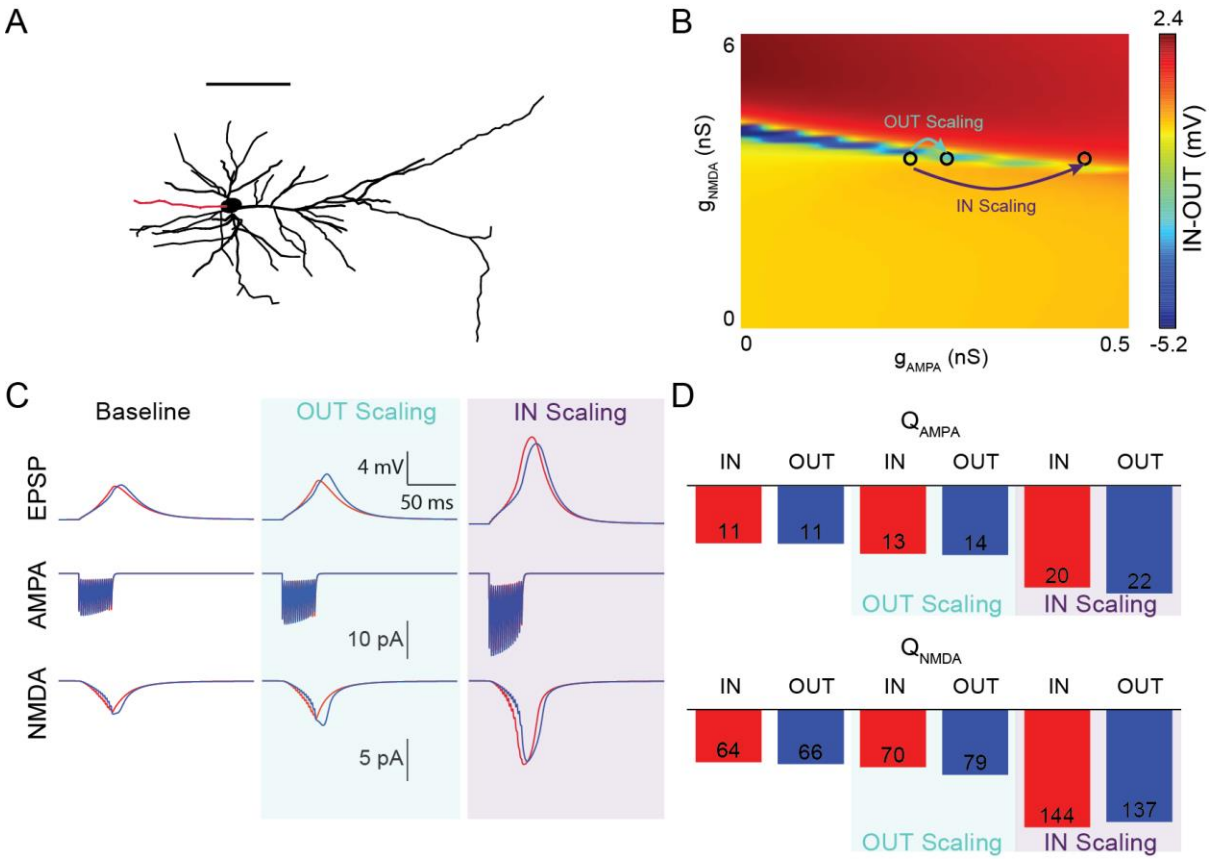

Figure 5.4 Uniform increase in AMPA conductance results in the emergence of spatiotemporal input preference

A) A Neurolucida reconstruction of a layer 2/3 pyramidal neuron adapted from Branco et al. (2010). The selected dendrite for genetic optimization protocol is marked in red. Scale bar: 100 μm. B) A profile of differences of maximal amplitude of simulated EPSPs of played IN and OUT patterns at different AMPA and NMDA conductance values. The arrows display the vectors defining the direction of AMPA scaling. C) Simulated EPSP and AMPA and NMDA current profiles corresponding to baseline values and following OUT and IN uniform scaling of AMPA values. AMPA and NMDA conductance values are shown by the circles in B). D) Integral of AMPA and NMDA currents under baseline, OUT and IN uniform scaling conditions.

For the progressive development of spatiotemporal preference across linear AMPA conductance scaling values see Video 5.2 below. Consistent with previous results, the generation of IN-preference required greater uniform scaling of synaptic conductances compared to the OUT-preference. In summary, my simulations demonstrate that uniform scaling of AMPA conductance is sufficient to elicit spatiotemporal preference in a passive compartmental model of morphologically realistic neuron.

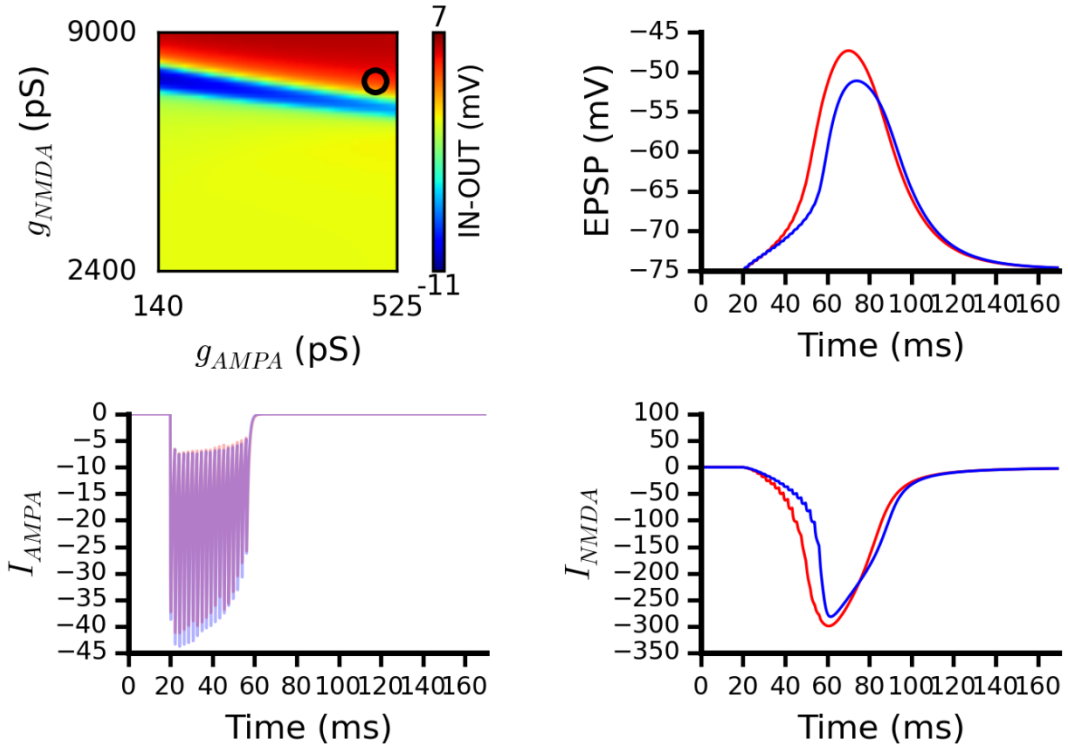

Video 5.2 Uniform increase in AMPA conductance results in the emergence of spatiotemporal input preference.

(Top left) A profile of the differences between IN and OUT simulated EPSPs. Black circle represents the example trace shown in the remaining figure panels. (Top right) Example EPSPs for simulated IN and OUT sequences. (Bottom left) A mean profile of AMPA conductances for IN and OUT simulated sequences. (Bottom right) A mean profile of NMDA conductances for IN and OUT simulated sequences. Web Source: YouTube - http://tinyurl.com/VivaVideo52

5.2.4 Properties of the IN and OUT pattern enhancement

5.2.4.1 Description of the modelling approach

The results of uniform scaling that I have obtained could have been the result of over-fitting of the genetic algorithm. To verify that the parameters obtained were in the physiological range, I performed an exhaustive evaluation of the difference between peak voltages of IN and OUT

spatiotemporal sequences across a range of parameters that the genetic algorithm was optimizing for (see Table 5.2).

Table 5.2 Range of parameters used in brute force search in Layer 2/3 model of neuron

Parameter	Unit	Range	Values
g_{AMPA}	$(min, max)\ pS/\mu m^2$	(0,1500)	100
g_{NMDA}	$(min, max)\ pS/\mu m^2$	(0,24000)	100
Number of synapses	(min, max)	(8,18)	6
Synapse spread	$(min, max)\ \mu m$	(49.5-99)	3
Velocity	$(min, max)\ \mu m/ms$	(1,13)	7
Mean distance	μm	(24.7-74.3)	3

Based on the previous results (Branco *et al.*, 2010) as well as theoretical work by Rall (1964), IN pattern is expected to result in a higher EPSP peak amplitude than the OUT pattern. I was thus interested in the stimulation parameters that generate OUT-preference. I defined a metric OUT_{AREA} which corresponds to the proportion of the space of conductance values where peak voltages of OUT pattern predominate over peak voltages of IN pattern (see Figure 5.5 for a visual schematic of OUT_{AREA}).

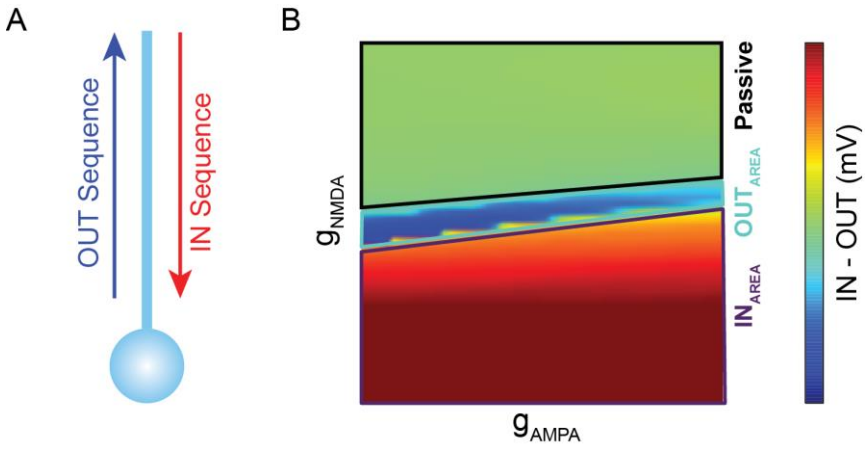

Figure 5.5 Schematic of spatiotemporal modes of integration at different synaptic conductance values.

A) Schematic of the spatiotemporal stimulation protocol showing centrifugal IN-sequence and centripetal OUT-sequence. B) Profile of spatiotemporal integration pattern for different values of g_{AMPA} and g_{NMDA} values. OUT_{AREA} is defined as a region of simulated EPSP values where OUT pattern is preferred, the converse holds for the IN_{AREA} region.

5.2.4.2 Spatiotemporal preference generation is most likely for physiological AMPA/NMDA ratios

To calculate OUT_{AREA} within physiological parameters, I defined conductance bounds by the empirically observed range of AMPA/NMDA ratios in the principal cells (Feldmeyer *et al.*, 2002; Myme *et al.*, 2003; Watt & Desai, 2010; Kohl *et al.*, 2011; Bittner *et al.*, 2012) that resulted in a physiological single synapse EPSP amplitude (0.1-0.5 mV) (see Figure 5.6C). I then explored combinations of AMPA and NMDA conductance values for which the likelihood of induction of an OUT-preference is the highest. I explored the two conditions by varying the number of synapses stimulated between 8 and 16 synapses. I then generated IN and OUT EPSP peak voltage difference plot (Figure 5.5B) for different inter-spine intervals. To evaluate which conductance combinations are likely to result in OUT-preference, I calculated standard deviation of difference values for which IN and OUT peak voltage difference is negative (i.e. OUT peak voltage predominates over IN peak voltage). The region of synaptic conductance values where the induction of spatiotemporal preference is most likely is expected to correspond to the region of highest standard deviation values (within the range of parameters listed in Table 5.2). The region of highest values of standard deviations corresponds well with the region of physiological AMPA/NMDA ratios (Figure 5.6E). Therefore physiological synaptic conductance values are well suited for the generation of spatiotemporal preference in a passive model of dendrite in morphologically realistic reconstruction of a layer 2/3 neuron.

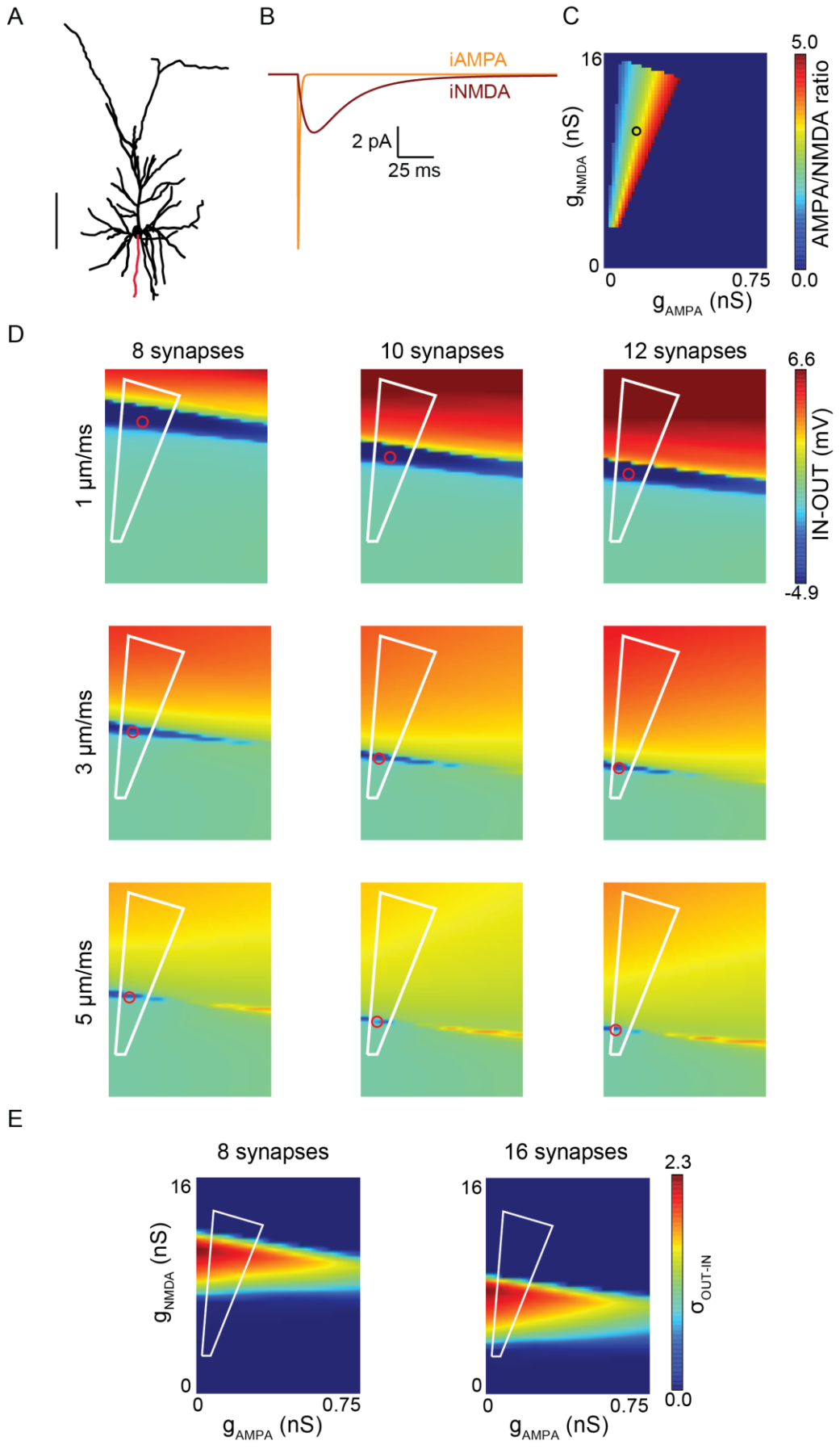
A
B
iAMPA
iNMDA
2 pA
25 ms
C
16
0
0
0.75
g_{NMDA} (nS)
g_{AMPA} (nS)
5.0
0.0
AMPA/NMDA ratio
D
8 synapses
10 synapses
12 synapses
1 µm/ms
3 µm/ms
5 µm/ms
6.6
-4.9
IN-OUT (mV)
E
8 synapses
16 synapses
2.3
0.0
σ_{OUT-IN}

Figure 5.6 Physiological AMPA/NMDA ratios correspond to the region where OUT potentiation induction is favoured.

A) A Neurolucida reconstruction of a layer 2/3 pyramidal neuron adapted from Branco et al. (2010). The selected dendrite for genetic optimization protocol is marked in red. Scale bar: 100 μm. B) Example simulation of a one synapse AMPA and NMDA current profile. The AMPA/NMDA ratio is calculated as a proportion of the peak amplitudes. C) AMPA/NMDA ratio profile for different AMPA and NMDA conductance values. The boundaries of the accepted AMPA/NMDA ratios correspond to AMPA/NMDA ratios in the range of 1-5 that elicit EPSPs in the range of 0.1-0.5 mV. The black circle corresponds to selected AMPA and NMDA conductance values presented in B). D) Example AMPA and NMDA conductance profile grid of IN-OUT peak EPSP values for different velocities and synapse numbers. White polygon corresponds to selected AMPA/NMDA ratios in B). Red circle represents the center of mass of the OUT_{AREA}. E) Profile of standard deviation values of simulation runs where OUT peak voltage predominates over IN peak voltage across different AMPA and NMDA conductance values with (Left) 8 synapses or (Right) 16 synapses stimulated.

5.2.4.3 Number of synapses stimulated and velocity of stimulation modulate the synaptic conductance required for generating spatiotemporal preference

I was then interested in exploring the role of individual parameters (listed in Table 5.2) in eliciting spatiotemporal preference in dendrites. I first evaluated the role of number of synapses in the induction of spatiotemporal preference. Increasing the number of synapses from 8 to 16 shifted the region where spatiotemporal preference was most likely induced to lower values of AMPA and NMDA conductances per synapse. Thus increasing effective synaptic conductance in dendrite shifts the region where IN and OUT preference varies the most. To analyse this relationship further, I localized OUT_{AREA} by calculating the center of mass in conductance space where the

OUT sequence predominates over the IN sequence (red circle, Figure 5.6D). Interestingly, increasing the number of synapses correspondingly decreases the NMDA conductance (but not AMPA conductance) values for the center of mass of the OUT_{AREA} (Figure 5.6E and Figure 5.7). This is consistent with previous reports which demonstrated the importance of NMDA receptors in mediating spatiotemporal preference (Branco *et al.*, 2010).

To further analyse the role of overall effective dendritic conductance, I varied the velocity of stimulation of synapses in my model. I found that low velocity values shift the center of the OUT_{AREA} to higher NMDA values (Figure 5.7A,B). Thus increasing the overall effective synaptic conductance (such as by varying the number of synapses or velocity) decreases the amount of synaptic conductance (especially NMDA) needed for the generation of an OUT-preference.

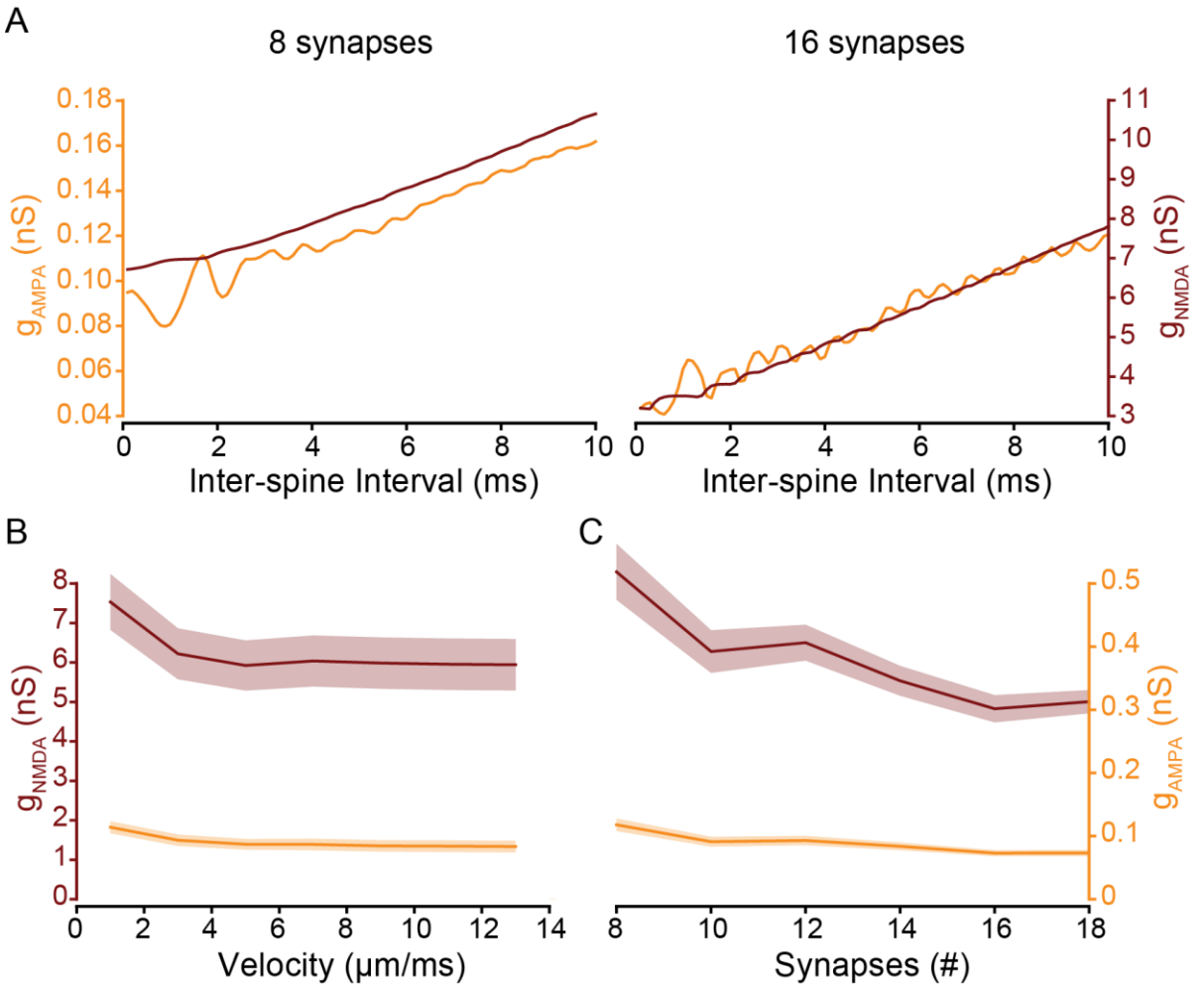

Figure 5.7 Effective conductance per unit of time determines the size and position of OUT_{AREA}.

A) Center of mass of the OUT_{AREA} in AMPA and NMDA conductance values per synapse as a function of inter-spine interval. With higher inter-spine intervals (lower velocity) more NMDA and AMPA conductance is required. Increasing the effective dendritic conductance decreases the individual synaptic conductances required for generation of an OUT-preference. B) and C) Center of mass of the OUT_{AREA} in AMPA and NMDA conductance values per synapse as a function of B) velocity and C) number of synapses across different stimulation parameter values described in Table 5.2. The error bars are SEM.

For a gradual visualization of the changes of the location of OUT_{AREA} in the synaptic conductance space with changes in velocity of stimulation, I generated videos for conditions where 8 (Video 5.3) or 16 synapses (Video 5.4) are stimulated.

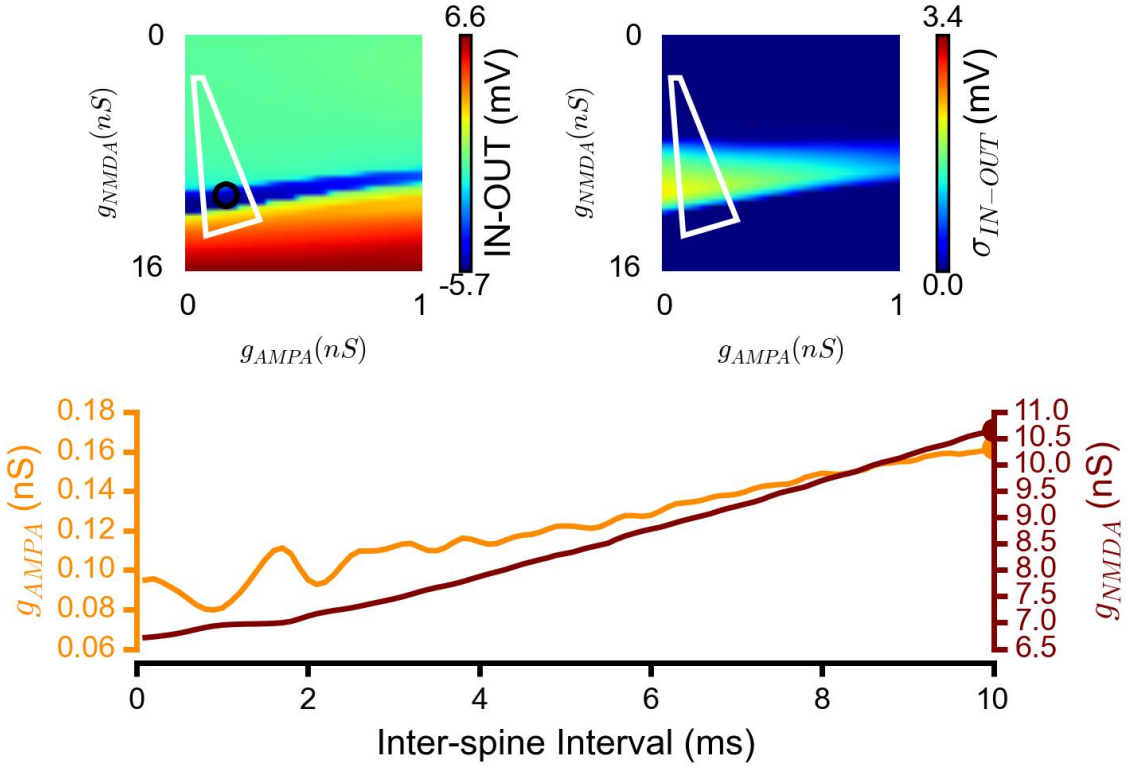

Video 5.3 Magnitude of synaptic conductance to generate OUT-preference depends on the effective dendritic conductance (8 synapses).

(Top left) A profile of the differences between IN and OUT EPSP amplitudes plotted at different AMPA and NMDA conductance values. The range of accepted AMPA/NMDA ratios is defined by the white polygon. The black circle shows the centre of mass of area that corresponds to OUT-sequence preference. (Top right) Standard deviation profile of IN and OUT differences plotted at different AMPA and NMDA conductance values. The range of accepted AMPA/NMDA ratios is defined by the white polygon. (Bottom) AMPA (dark orange) and NMDA (maroon) conductance values corresponding to the centre of mass of OUT_{AREA} plotted against the inter-spine interval of stimulation. Web Source: YouTube - http://tinyurl.com/VivaVideo53

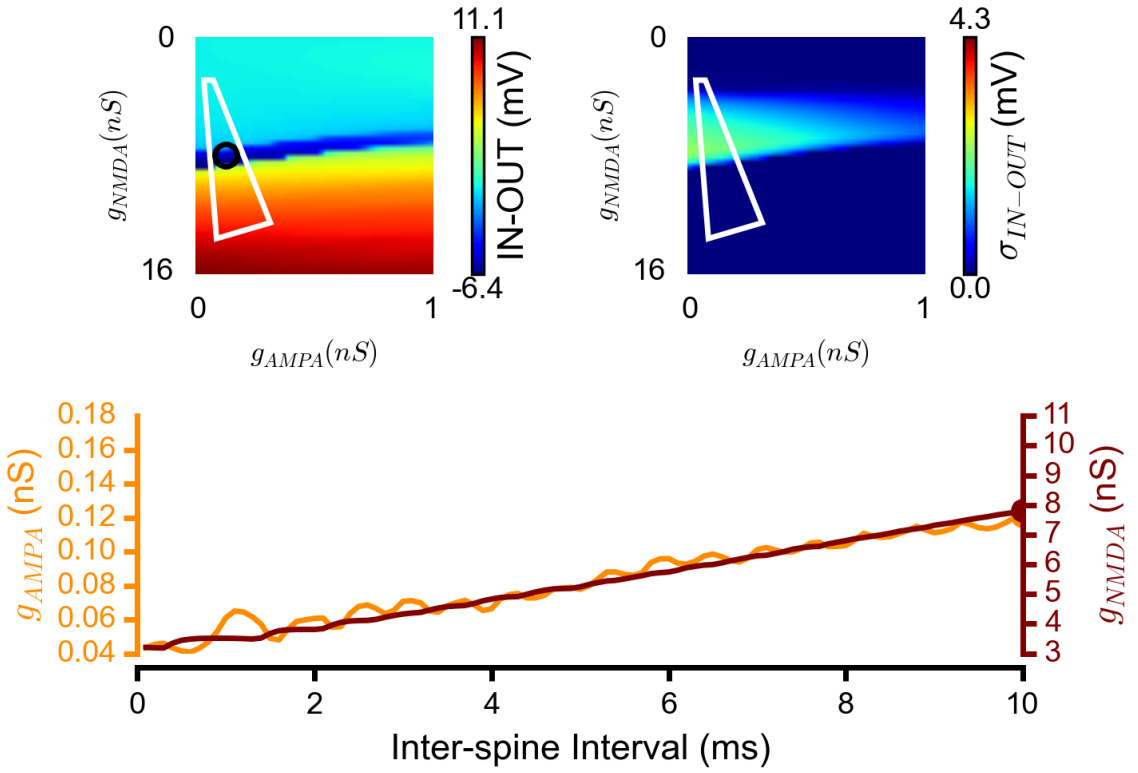

Video 5.4 Magnitude of synaptic conductance to generate OUT-preference depends on the effective dendritic conductance (16 synapses).

(Top left) A profile of the differences between IN and OUT EPSP amplitudes plotted at different AMPA and NMDA conductance values. The range of accepted AMPA/NMDA ratios is defined by the white polygon. The black circle shows the centre of mass of area that corresponds to OUT-sequence preference. (Top right) Standard deviation profile of IN and OUT differences plotted at different AMPA and NMDA conductance values. The range of accepted AMPA/NMDA ratios is defined by the white polygon. (Bottom) AMPA (dark orange) and NMDA (maroon) conductance values corresponding to the centre of mass of OUT_{AREA} plotted against the inter-spine interval of stimulation. Web Source: YouTube - http://tinyurl.com/VivaVideo54

In conclusion, my analysis shows that passive dendrite sensitivity to different spatiotemporal sequences is modulated the overall level of effective synaptic conductance.

5.2.4.4 Distance of synapses from the soma and clustering modulate the synaptic conductance required for generating spatiotemporal preference

As I discussed in the introduction, the distance of synaptic input has a major influence on its readout in the soma. As a result, I tested three synapse distributions and their role in generating spatiotemporal preference - inputs localized to the proximal half of the dendrite (P), to the distal part of the dendrite (D) and inputs distributed across the whole dendrite (W). In agreement with my experimental results, OUT_{AREA} is present in all clustering modalities within physiological AMPA/NMDA ratios. Surprisingly, I discovered that OUT-preference is less prominent than the IN-preference at distal compared to proximal synapses (Figure 5.8). Consistent with previous findings, increasing velocity and the number of synapses increases the likelihood of IN-preference in the dendrite.

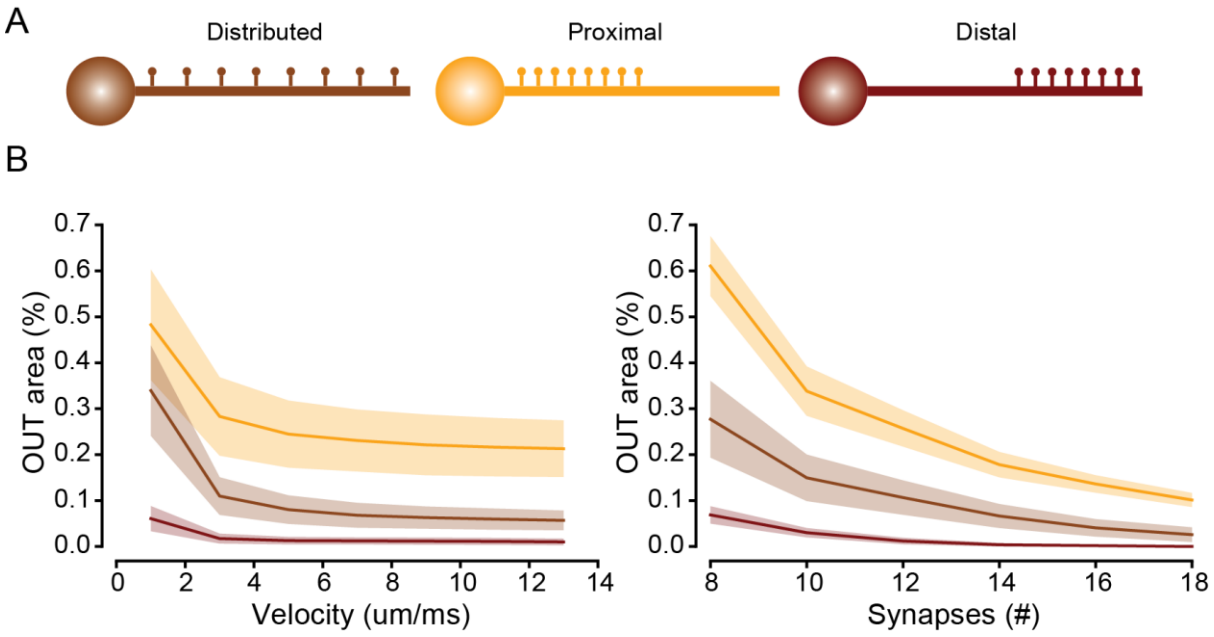

Figure 5.8 The likelihood of OUT pattern predomination is influenced by the distance from soma.

A) Colour-code schematic of synapse distributions in the dendrite tested using the Branco et al. (2010) layer 2/3 model neuron. B) OUT_{AREA} plotted against different synapse distributions across the parameters studied and against velocity (left) and number of synapses on the dendrite (right). The error bars are SEM.

5.2.5 Uniform scaling of synaptic conductances is sufficient for induction of spatiotemporal plasticity in a model of layer 5 pyramidal neuron

Finally, I was interested in whether the likelihood of induction of OUT-potentiation using only uniform scaling is preserved in a physiological model of layer 5 neuron. For this reason, I used the layer 5 pyramidal cell morphological reconstruction from the work done by Almog & Korngreen (2014). The Almog & Korngreen (2014) has several advantages. The model was shown to faithfully predict a wide range of physiological activity including dendritic spikes and voltage-activated channel kinetics and distribution. The passive parameters were also optimized using the numerical

peeling procedure and thus are expected to be more physiological. In the experiments presented in this chapter, I used a passive version of the model and included synaptic conductances as described in the methods for the layer 2/3 model. I used the same constraints for the optimization run as described in the layer 2/3 model (listed in Table 5.1.) Following optimization run, I showed that uniform scaling of AMPA and NMDA conductances can result in both IN and OUT-preferences. Consistent with previous results from the layer 2/3 model, IN-preference requires greater conductance scaling than OUT-preference (Figure 5.9). Furthermore, the NMDA channel scaling is the major driver of the type of spatiotemporal preference in the dendrite (Figure 5.9B).

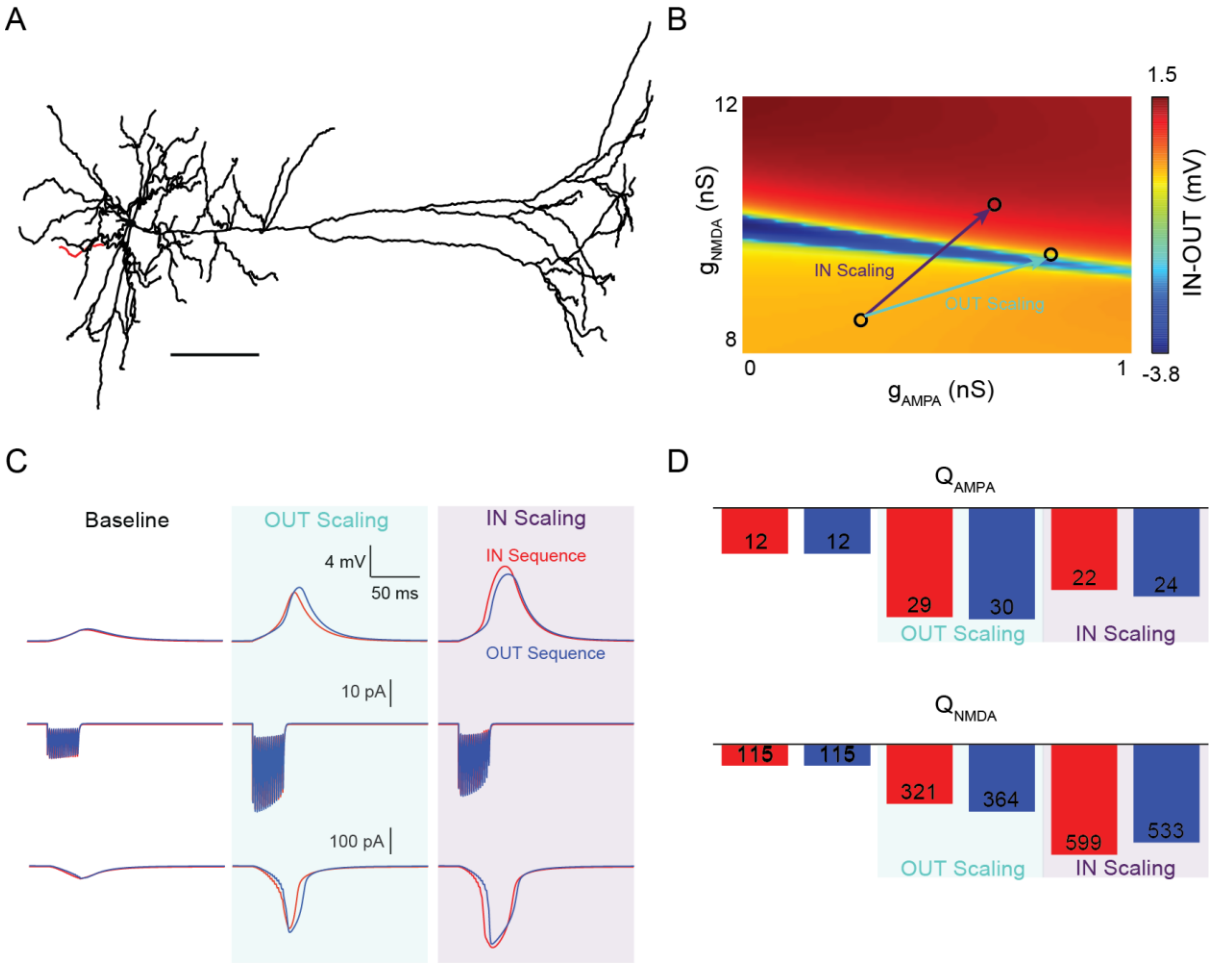

Figure 5.9 Uniform increase in AMPA and NMDA conductance in Layer 5 model results in the emergence of spatiotemporal input preference.

A) A Neurolucida reconstruction of a layer 5 pyramidal neuron adapted from Almog and Korngreen (2014). The selected dendrite for genetic optimization protocol is marked in red. Scale bar: 200 μm. B) A profile of differences of maximal amplitude of simulated EPSPs of played IN and OUT patterns at different AMPA and NMDA conductance values. The arrows display the vectors defining the direction of AMPA and NMDA scaling. C) Simulated EPSP and AMPA and NMDA current profiles corresponding to baseline values and following OUT and IN uniform scaling of AMPA values. AMPA and NMDA conductance values are shown by the circles in B). D) Integral of AMPA and NMDA currents under baseline, OUT and IN uniform scaling conditions.

Verifying that the model of layer 5 neuron corresponds to the findings from layer 2/3 neuron, I then proceeded to evaluate the role of AMPA only uniform scaling across the dendrite. In this optimization run, the NMDA conductance was not scaled between baseline and simulated plasticity conditions. I confirmed that the AMPA-only scaling is sufficient to elicit both types of spatiotemporal preference (Figure 5.10). IN-preference required greater AMPA scaling than OUT-preference, consistent with results from the layer 2/3 model.

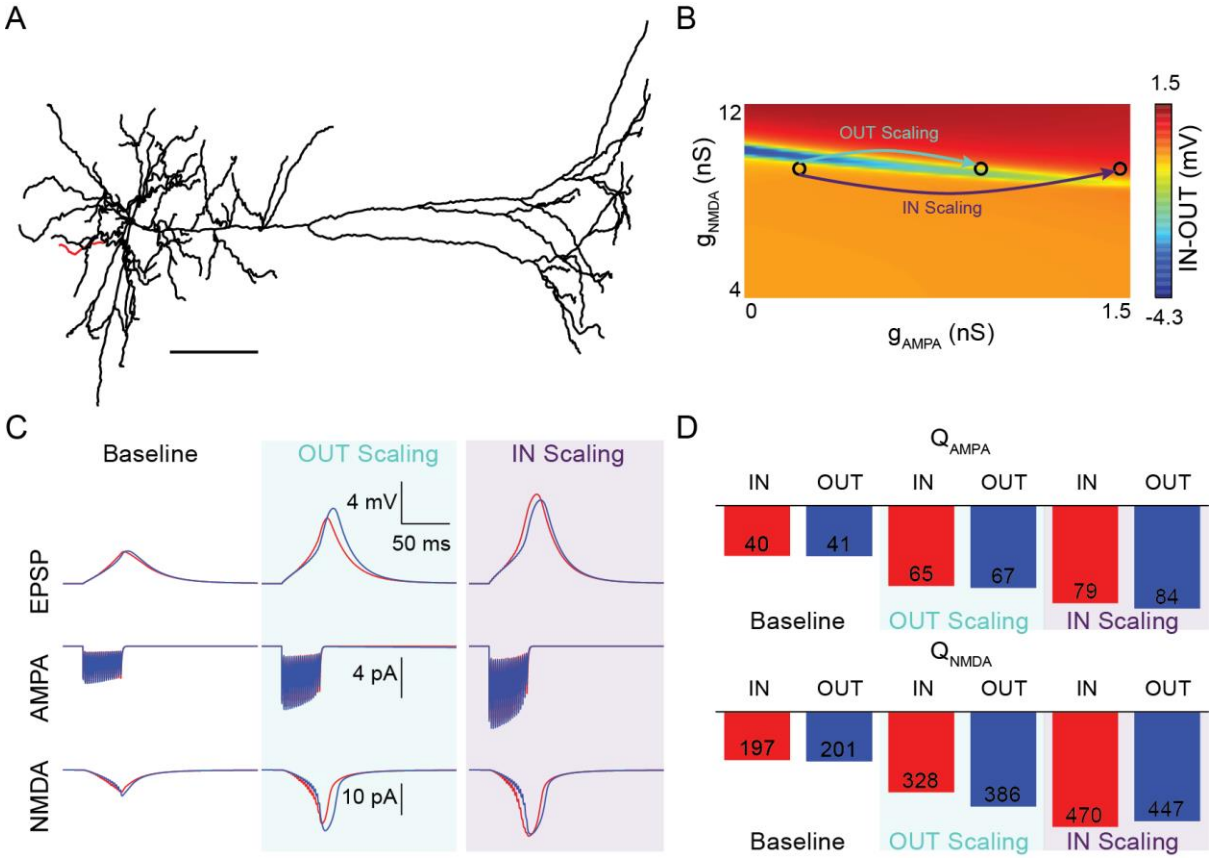

Figure 5.10 Uniform increase in AMPA conductance in Layer 5 model results in the emergence of spatiotemporal input preference.

A) A Neurolucida reconstruction of a layer 5 pyramidal neuron adapted from Almog and Korngreen (2014). The selected dendrite for genetic optimization protocol is marked in red. Scale bar: 200 μm. B) A profile of differences of maximal amplitude of simulated EPSPs of played IN and OUT patterns at different AMPA and NMDA conductance values. The arrows display the vectors defining the direction of AMPA scaling. C) Simulated EPSP and AMPA and NMDA current profiles corresponding to baseline values and following OUT and IN uniform scaling of AMPA values. AMPA and NMDA conductance values are shown by the circles in B). D) Integral of AMPA and NMDA currents under baseline, OUT and IN uniform scaling conditions.

5.3 DISCUSSION

In this chapter, I demonstrated that uniform scaling is sufficient to induce IN- and OUT-preference in layer 2/3 and layer 5 compartmental models of dendrites. To discover parameters that induce spatiotemporal preference, I employed a genetic algorithm model. Consistent with previous findings, the genetic algorithm was useful in optimizing NEURON parameters. A large number of free parameters in a typical compartmental model results in a multi-dimensional solution set that is generally too large for a brute-force approach. The inherent parallelized nature of the genetic algorithm and ease of constraining of models enables a time-efficient and physiological exploration of the simulation parameters. Additionally, I discovered that creating new generation based on the normalized fitness results in a faster optimization of parameters.

The results of simulations confirm that simple uniform scaling of synaptic conductances can underpin different types of spatiotemporal preference in the dendrite. Even a minimal condition, when only AMPA conductance was scaled uniformly, was sufficient for eliciting preference for different types of temporal sequences. My work is therefore consistent with a wide modalities of synaptic conductance changes that were reported in the literature (Benke *et al.*, 1998; Watt *et al.*, 2004). Crucially, such plasticity induction is possible within a constrained set of synaptic conductances which correspond to physiologically observed AMPA/NMDA ratios. Finally, this result was not dependent on any active-conductances (apart from NMDA receptors) and could be fully reproduced in a passive model of neuron. For a long time, passive neuron was known to produce spatiotemporal preference for the IN direction, famously described by Wilfrid Rall (1964). Such spatiotemporal preference, however, was dependent on dendrites with long electrotonic length that is not present in basal dendrites. NMDA conductance is a natural mechanism by which this passive propensity could become boosted. The finding that effective synaptic conductance (passive and active) determines a sign of plasticity is a potential addition to the theory of spatiotemporal preference in dendrites.

This minimal model, presented in this thesis, raises a tantalizing prospect that spatiotemporal plasticity that I described in my model could be present in other neuronal cell types across the brain. The possible generality of the rule is supported by previous work describing the presence of sensitivity to spatiotemporal sequences in a wide range of neurons (Branco *et al.*, 2010), as well as the simplicity of the mechanism (uniform scaling of synaptic conductances).

A more physiological model incorporating active conductances is an important next step to the work presented in this thesis. My finding that the type of spatiotemporal preference depends on the amount of recruited effective synaptic conductance raises interesting questions for future research. For example, previous reports indicated that A-type potassium channels are acting as a gate for eliciting plasticity in dendrites of CA1 pyramidal neurons (Losonczy *et al.*, 2008). The A-type K^+ channel recruitment was inversely related to the likelihood of dendritic spike propagation to the soma. My model predicts that the degree of blocking A-type K^+ outward currents should be associated with different types of spatiotemporal preference elicited in the dendrite. In apical dendrites of layer 5 neurons, I_h currents were previously found to normalize temporal summation in the dendrite (Williams & Stuart, 2000*b*). Since I_h is activated at hyperpolarizing potentials and closed at depolarizing potentials, I_h gating results in a net outward current during synaptic stimulation (Magee, 1999). As a result, I_h could importantly modulate the overall synaptic conductance in apical dendrites of layer 5 neurons and thus the type of spatiotemporal preference for the dendrite. Further exploration of the importance of effective overall synaptic conductance is necessary both in theoretical work utilizing active models of dendrites and in empirical verification of modelling results.

Surprisingly, in distal regions, the size of the conductance space that exhibits OUT-preference (OUT_{AREA}) was lower than in the proximal regions of the dendrite. It is known that temporal integration window of dendrites differs based on their distance from the soma (Branco & Häusser, 2011) with more distal dendrites having longer integration windows. However, in my empirical

work the type of spatiotemporal preference was not dependent on the distance of synapses from the soma. My current data can partly account for the discrepancy. My model shows that all dendritic locations (proximal or distal) contained regions in which both types of spatiotemporal preference could be elicited. Distal regions exhibited smaller regions in which OUT-preference was seen. Currents such as I_A and I_h could modulate the effective synaptic conductance and thus the likelihood of OUT-preference in distal dendrites. Whilst I_h does not show the same gradient increase in basal dendrites as it does in apical dendrites (Berger *et al.*, 2001; Almog & Korngreen, 2014), the I_A gradient in basal dendrites is, to my knowledge, unknown, possibly because of the methodological difficulty of obtaining outside-out patches from thin basal dendrites. Another possible candidate are the G-protein inactivated K^+ channels which were previously shown to be important in modulating dendritic integration in CA3 pyramidal neurons (Makara & Magee, 2013).

A further improvement of the model would be to model the ongoing synaptic activity to simulate *in vivo*-like conditions (Paré *et al.*, 1998; Destexhe *et al.*, 2003). A high-conductance state is expected to increase the overall level of effective conductance and thus decrease the NMDA component required to elicit OUT-preference in dendrites. Furthermore, cortical neurons are significantly modulated by cortical states exhibiting significant depolarized UP states and hyperpolarized DOWN states (Steriade *et al.*, 1993; Sanchez-Vives & McCormick, 2000). Based on my model findings, such variable conductance state is expected to importantly modulate the type of preferred spatiotemporal preference of dendrites. This further enhances the computational complexity of the information that can be potentially represented by cortical neurons. Transitions between brain states in cortex can be induced in brain slices by chemical or electrical stimulation (Rigas & Castro-Alamancos, 2007). Such experimental model could be used in conjunction with uncaging, as described in this thesis, to empirically verify the relationship between conductance states and the type of preferred spatiotemporal sequence.

In this chapter, I present a model of neuron employing realistic morphology and physiological synaptic conductances capable of generating different spatiotemporal preferences in dendrites. I provide mechanistic insight into the main driver of the type of spatiotemporal preference elicited – the effective overall synaptic conductance, and I describe the parameters that importantly influence it. The main finding of my theoretical model is the potential physiological mechanism by which neurons can modify their synaptic weights to favour certain type of spatiotemporal sequence of inputs. My findings contribute to the body of theoretical literature on how neurons can be modified to represent precise spike timings.

6 GENERAL DISCUSSION AND OUTLOOK

In my work, I have demonstrated the capacity of pyramidal neurons to preferentially potentiate their response to distinct spatiotemporal input patterns. My results contribute to the growing body of the plasticity toolkit available to neurons in the cortex.

6.1 SUMMARY OF THE FINDINGS

In chapter 3, I experimentally demonstrated the existence of spatiotemporal potentiation. I tested two different spatiotemporal patterns that were previously found to result in different amplitude EPSP events – a distal-to-proximal stimulation or IN sequence and proximal-to-distal stimulation or OUT sequence (Branco *et al.*, 2010). Pairing a given sequence with a train of action potentials resulted in a potentiation of that sequence as compared to the non-paired sequence. Such potentiation was shown to be dependent on the magnitude of plasticity and was not influenced by factors such as distance or clustering. In Chapter 4, I described the NMDAR dependence of the potentiation. I further evaluated the magnitude of Ca^{2+} influx during induction pairing. Whilst both IN- and OUT-pairing protocols were found to be supralinearly increased during pairing, IN-sequence pairing exhibited a significantly larger Ca^{2+} influx than the OUT-sequence pairing protocol that was uniformly increased along the dendrite. My experimental findings from Chapter 3 and Chapter 4 were then used to constrain the simulation of models in NEURON environment. In Chapter 5, I described that uniform scaling of AMPA and NMDA, or AMPA only, conductances can lead to specific potentiation of both IN and OUT spatiotemporal patterns. I further discovered that the overall level of the synaptic conductance on the level of the dendrite determines the spatiotemporal preference. Increasing velocity and the number of synapses decreases the AMPA and NMDA levels required to induce OUT-preference. My passive model of the neuron was in agreement with the data from Ca^{2+} imaging and with my electrophysiological evaluation.

6.2 THE ROLE OF SPATIOTEMPORAL PLASTICITY IN NEURONAL PROCESSING

The expected role of the spatiotemporal plasticity is to enhance the computational capacity of individual neurons. The functional importance of storing temporal sequences of inputs was described previously in theoretical literature (Gütig & Sompolinsky, 2006; Florian, 2012; Gütig, 2014). Models based on temporal learning were found to be efficient at computational tasks such as time-warp invariant processing (in speech recognition) or in classifying trains of complex visual spikes (Gütig & Sompolinsky, 2009; Gütig *et al.*, 2013). Previous empirical literature showed that the pattern of presynaptic input can influence the sign of plasticity (Kwag & Paulsen, 2009). Furthermore, cortical neurons were found to be sensitive to purely temporal patterns of the presynaptic input in the induction of depression (Rodríguez-Moreno *et al.*, 2013). Following the finding of differential potentiation of IN and OUT sequences in my experimental results, the key further question is the capacity of pattern storage of a single dendrite. In the tempotron model, Gütig and Sompolinsky (2006) showed that the capacity to reach error-free classification is equal to the number of synapses multiplied by 2-3x (see Figure 6.1).

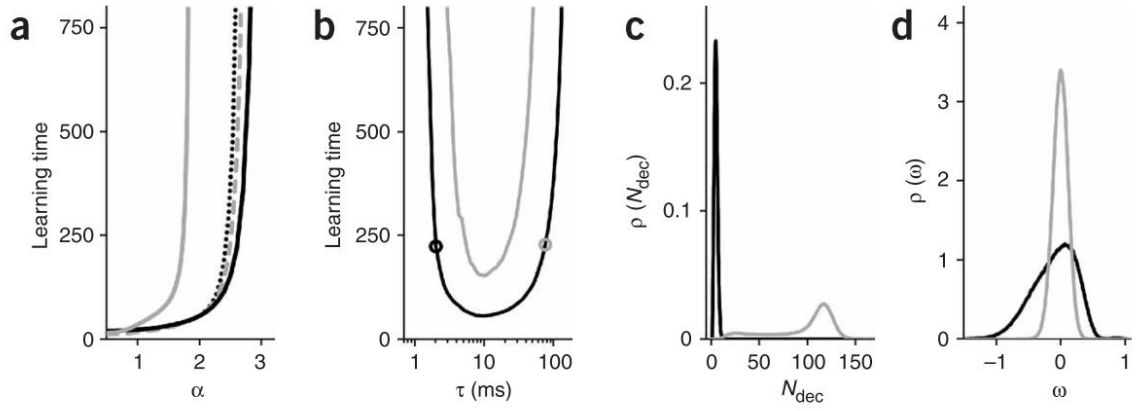

Figure 6.1 Tempotron performance

A) Learning time – defined as the mean number of pattern presentation cycles required for error-free classification-versus load α. The load is defined as the ratio of the number of patterns over

the number of afferents. Results for random latency patterns with $N = 500$ afferents (black solid line) were obtained with a synaptic integration time of $\tau = 10\ ms$. For $N = 1000$ afferents (gray dashed line) and $N = 1500$ afferents (black dotted line), τ was set to 4 ms and 3 ms respectively. These values of τ are close to the respective optimal τ. For comparison, the learning times for $N = 1000$ and $N = 1500$ were scaled to match the learning time for $N = 500$ at $\alpha = 2$. The gray solid line depicts learning times for perceptron-like input patterns with $N = 500$ afferents. B) – D) In B) learning time for $N = 500$ afferents versus PSP time constant for τ for $\alpha = 2$ (black line) and $\alpha = 2.5$ (gray line). Open circles mark $\tau = 2\ ms$ (black) and $\tau = 75\ ms$ (gray) used in C)-D). In C), distributions of effective number of contributing synapses N_{dec} after learning ($\alpha = 2$) for $\tau = 2$ (black) and $\tau = 75\ ms$ (gray). In D) distributions of learned synaptic efficacies ω (in units of the spike threshold V_{thr}) for parameters as in C) (same colors). Data are averaged over 1,000 realizations. Source: Gütig and Sompolinsky (2006).

As I previously discussed, tempotron is not a physiologically valid representation of neuron. Several questions need to be answered for the computational capacity of a realistic neuron to be evaluated. For example, does the spatiotemporal potentiation rule extend to other types of stimulation patterns apart from IN and OUT sequences I used? Discovering whether dendrites can be preferentially potentiated to an arbitrary sequence of inputs is a natural next step. In chapter 5, I showed how modulating effective levels of synaptic conductances can lead to a gradual change in the spatiotemporal preference between IN and OUT sequences. In principle, such a mechanism could lead to spatiotemporal pattern preference with an arbitrary degree of directionality and thus storage of multiple patterns on a single dendrite. This can be verified by an adjustment of my theoretical model in which optimization would be performed for multiple sequences within the physiological conductance parameters as I described above. Such adjustment could provide an important theoretical insight into the number of patterns that a single dendrite can store.

There were other simplifying assumptions in my model that could correspond to an underestimate of the potential storage capacity of dendrites. Firstly, in my simulations of spatiotemporal plasticity, synapses were of equal weight. Neurons exhibit varied distribution of spine morphologies (Hering & Sheng, 2001; Bourne & Harris, 2011) and the relationship between spine morphology and synapse weight has been established previously (Matsuzaki *et al.*, 2004). The possibility of unequal weights on dendrites allows for another free parameter for optimization of my theoretical model.

Secondly, the type of conductance used in my NEURON model is another simplification. Although, the 10-state kinetic model of NMDA receptors used in this study is currently state-of-art, it is known that NMDA receptors show significant variability of subtypes and their expression during development (Cull-Candy *et al.*, 2001; Cull-Candy & Leszkiewicz, 2004). For example, NR2A containing NMDA receptors have 6-fold slower weighted deactivation time-constant as seen in NR2B containing NMDA-receptors (Vicini *et al.*, 1998; Cull-Candy *et al.*, 2001). The expression of different NMDA subunits during development importantly determines the types of plasticity that can be induced. For example, NR2C/D receptor which is expressed during young juvenile stage is required for the induction of t-LTD on layer 4 to layer 2/3 synapses but not on layer 2/3-layer 2/3 connections (Banerjee *et al.*, 2009).

Thirdly, a change in intrinsic excitability of the dendrite has been described for a variety of cell-types (Aizenman & Linden, 2000; Zhang & Linden, 2003; Fan *et al.*, 2005). As I have shown in Chapter 5, changing the overall level of available synaptic conductance modulates the preferred type of spatiotemporal pattern. Such modulation may be important for normalization of the distance-dependence preference for specific patterns.

Finally, I assumed that the input is clustered on a single dendrite in both my experiments and my theoretical simulations. However, spatiotemporal preference is conserved when uncaging stimulation is applied in a distributed manner (Branco *et al.*, 2010). The distributed stimulation using uncaging is methodologically difficult as dendrites are generally not aligned in a single plane

of focus, which significantly reduces experimental yield. One possible alternative is to use dissociated cultures, which are guaranteed to have dendrites in a single plane of focus. Alternatively, three-dimensional acousto-optic two-photon scanning or piezoelectric stepping of objective could be used to stimulate synapses in 3D (Göbel *et al.*, 2007; Kirkby *et al.*, 2010). Whilst the speed of stimulation in 3D is usually lower than using the traditional two-photon setup, the potential advantages in increasing yield are considerable. The likelihood of inducing spatiotemporal plasticity for distributed input remains a key open question.

The important advantage of such simplified model of spatiotemporal plasticity is its potential applicability across cell-types. My simulations on layer 2/3 and layer 5 cells suggest that both cell types are capable of generating preference for both spatiotemporal integration modes. Previous data from the lab suggest that spatiotemporal preference for the IN sequence is conserved across cell types of the brain (Branco *et al.*, 2010). Based on the previous experimental results from the lab as well as my modelling results, it is tantalizing to hypothesise the generality of the spatiotemporal plasticity across neuronal types.

In their landmark study, Poirazi and Mel (2001) described the role of active dendrites and neuronal morphology in enhancing memory storage. Both non-linear activation functions of dendrites and high number of small subunits were associated with an increase in storage capacity of neurons. In an elegant two layer representation of CA1 pyramidal cell, Poirazi and colleagues (2003) demonstrated that such simplified abstraction can account for substantial proportion of spike variance. Later studies modified this two-layer representation for layer 5 dendrites by adding a "third layer" corresponding to the Ca^{2+} initiation zone in the apical dendrite (Larkum *et al.*, 2009). In the hierarchical parallel processing representation, dendrites are also represented as sites of local output that are allowed to interact with one another (Branco & Häusser, 2010). The discovery of spatiotemporal plasticity adds another consideration of the history of synaptic stimulation patterns of a dendrite. My theoretical model shows that the overall effective synaptic conductance of a

dendrite provides a good starting point for evaluating the particular spatiotemporal preference of the dendrite. Nevertheless, more complex rules than uniform synaptic scaling are likely to occur such as synapse-specific changes in the magnitude of conductance increase. As hinted above, a more comprehensive evaluation of pattern storage capacity is needed to evaluate the theoretical increase in informational capacity that the neuron can store.

6.3 SPATIOTEMPORAL PLASTICITY IN NEURAL CIRCUITS

The key question following the discovery of spatiotemporal plasticity is its role in refinement of neural circuits and whether such plasticity can be observed *in vivo*. In the last couple of years, we witnessed a remarkable progress in our capacity to perform *in vivo* imaging experiments with a single spine resolution (Chen *et al.*, 2011*b*, 2012), *in vivo* imaging in freely moving animals (Piyawattanametha *et al.*, 2009). Previous work showed that repeated presentation of the same stimulus produces reverberation of cortical waves in the visual cortex (Han *et al.*, 2008). Nevertheless, due to poor resolution of the voltage-sensitive dye method used, the authors could not possibly evaluate the changes at a single cell-level. However, spatial light modulator systems have been demonstrated to be capable of optical readout and activation of tens of neurons (Packer *et al.*, 2015). Is it possible to use such multi-cell stimulation methods to reproduce reverberation in cortical circuits? Are circuits that can faithfully reproduce previous patterns of spatiotemporal activation also more likely to have dendrites that favour certain spatiotemporal sequences of inputs? Or even more importantly, do stimuli with defined spatiotemporal sequences such as repeating visual patterns or multi-whisker piezo-stimulation protocols (Jacob *et al.*, 2012) result in a higher likelihood of spatiotemporal pattern generation in the dendrites of cortical neurons? For the first time, available methods allow probing of neural circuits with such fine spatiotemporal resolution *in vivo*. Concurrently, the development of new opsin structures allows for fast activation enhancing our ability to recruit plasticity processes in the cell. Previous work using the ultra-fast opsin oChIEF was shown to allow for reversible switching between LTP and LTD and concurrent

expression or depression of behaviour (Nabavi *et al.*, 2014). Such opsins could be used to reversibly switch between different spatiotemporal modes of integration *in vivo*.

Finally, brain state can be a powerful modulator of spatiotemporal pattern preference in neurons. UP and DOWN states, which powerfully modulate conductance levels in dendrites, are expected to strongly affect preferred temporal sequences to which dendrites are sensitive. Neuromodulation exerts powerful influence over a range of parameters on which spatiotemporal plasticity depends. Acetylcholine receptor activation via carbachol was shown to mediate branch specific plasticity and down-regulation of A-type K^+ channels in CA1 pyramidal cells. Dopamine agonists can potentiate or depress NMDA function depending on the type of dopamine receptor recruited (Seamans *et al.*, 2001; Seamans & Yang, 2004). α2A adrenergic receptor stimulation was shown to be associated with downregulation of HCN channels in prefrontal cortex (Wang *et al.*, 2007*a*). Furthermore, the type of neuromodulatory tone often importantly affects target cells. For example, phasic and tonic adrenaline release affects the performance of monkeys on visual discrimination tasks (Usher *et al.*, 1999). Given such varied effects on intrinsic properties of dendrites, synaptic conductances and behaviour, it is difficult to form an expectation of the effect of neuromodulation on spatiotemporal plasticity. Nevertheless, an interesting test of the role of neuromodulation would be to evaluate the induction of spatiotemporal plasticity under conditions of different neuromodulation tone such as by phasic and tonic activation of dopamine or noradrenaline afferents through electrical or optogenetic stimulation. Thus neuromodulation remains an important unexplored frontier in the study of plasticity in general and spatiotemporal plasticity in particular.

Finally, the role of spatiotemporal plasticity in the modulation of behaviour is even more uncertain. Previous reports, however, do provide an intriguing possibility of evaluation of the plasticity model in behavioural tasks. The Rotarod assay is a complex sensorimotor task that evaluates the ability of mice to remain, without falling, on a rod with a progressively increasing speed of rotation (Figure

6.2A). Such task is associated with an increase in spine formation (Figure 6.2) in motor cortex (Yang *et al.*, 2009) which was shown to be branch specific and sleep-dependent (Yang *et al.*, 2014).

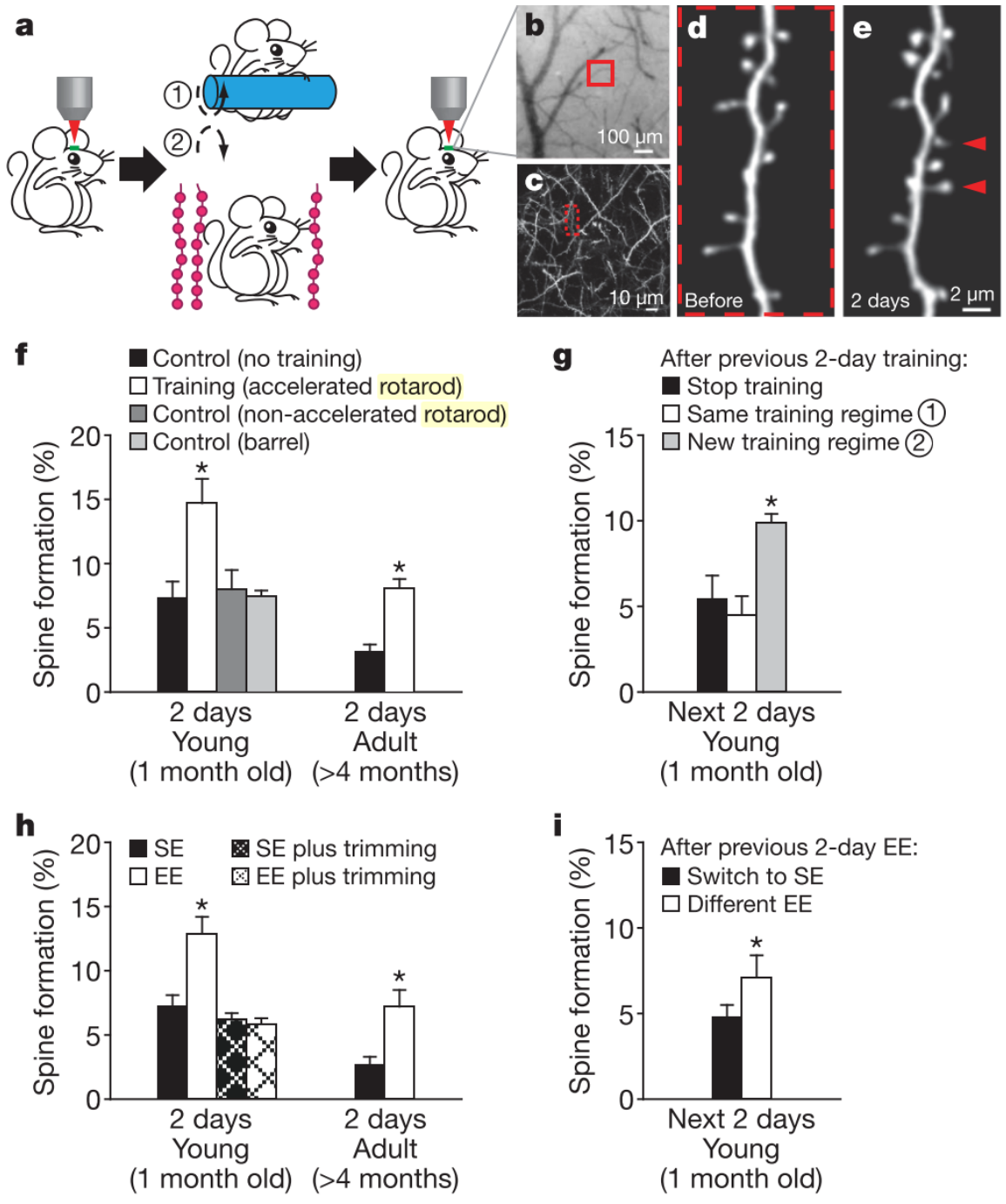

Figure 6.2 Motor learning and novel sensory experience promote rapid dendritic spine formation

A) Transcranial two-photon imaging of spines before and after rotarod training or sensory enrichment. B) CCD camera view of the vasculature of motor cortex. C) Two-photon image of apical dendrites from the boxed region in B). A higher magnification view of a dendritic segment in C) is shown in D). D), E) Repeated imaging of a dendritic branch before D) and after rotarod training E). Arrowheads indicate new spines formed over 2 days. F) The percentage of new spines formed within 2 days in the motor cortex was significantly higher in young or adult mice after training as compared with controls with no training or running on a non-accelerated rotarod. No increase in spine formation was found in the barrel cortex after training. G) After previous 2-day training, only a new training regime (reverse running) caused a significant increase in spine formation. H) Environmental enrichment (EE) increased spine formation over 2 days in the barrel cortex in both young and adult animals. No significant increase in spine formation was found under EE when the whiskers were trimmed. I) After previous 2-day EE, animals switched to a different EE showed a higher rate of spine formation than those returned to SE. Data are presented as mean ± s.d. *$p<0.005$. Source: (Yang *et al.*, 2009)

6.4 OUTLOOK FOR SPATIOTEMPORAL PLASTICITY

The dendritic locus, as well as complex spatial and temporal learning aspects, make it an ideal candidate for testing spatiotemporal plasticity in a behavioural context. It is particularly interesting whether branch specific structural plasticity is also associated with a specific spatiotemporal profile of Ca^{2+} influx into the dendrite.

In conclusion, my thesis builds on the important finding that dendrites are capable of distinct processing of spatiotemporal input (Branco *et al.*, 2010). I discovered that dendrites are capable of storing distinct spatiotemporal patterns, and, through a theoretical model, proposed a candidate

mechanism mediating the changes. Spatiotemporal plasticity is an important finding with consequences for the fields of plasticity, dendritic integration and computational neuroscience. The functional importance of plasticity of temporal sequences is yet to be elucidated but is likely important for learning of diverse sensorimotor tasks and feature binding in sensation

7 BIBLIOGRAPHY

Abbott LF & Blum KI (1996). Functional Significance of Long-Term Potentiation for Sequence Learning and Prediction. *Cereb Cortex* **6,** 406–416.

Abbott LF, Farhi E & Gutmann S (1991). The path integral for dendritic trees. *Biol Cybern* **66,** 49–60.

Abraham WC & Bear MF (1996). Metaplasticity: The plasticity of synaptic plasticity. *Trends Neurosci* **19,** 126–130.

Aizenman CD, Akerman CJ, Jensen KR & Cline HT (2003). Visually driven regulation of intrinsic neuronal excitability improves stimulus detection in vivo. *Neuron* **39,** 831–842.

Aizenman CD & Linden DJ (2000). Rapid, synaptically driven increases in the intrinsic excitability of cerebellar deep nuclear neurons. *Nat Neurosci* **3,** 109–111.

Almog M & Korngreen A (2014). A quantitative description of dendritic conductances and its application to dendritic excitation in layer 5 pyramidal neurons. *J Neurosci* **34,** 182–196.

Alvarez V a & Sabatini BL (2007). Anatomical and physiological plasticity of dendritic spines. *Annu Rev Neurosci* **30,** 79–97.

Amitai Y, Friedman A, Connors BW & Gutnick MJ (1993). Regenerative activity in apical dendrites of pyramidal cells in neocortex. *Cereb Cortex* **3,** 26–38.

Andrasfalvy BK & Magee JC (2001). Distance-dependent increase in AMPA receptor number in the dendrites of adult hippocampal CA1 pyramidal neurons. *J Neurosci* **21,** 9151–9159.

Antic SD, Zhou W-L, Moore AR, Short SM & Ikonomu KD (2010). The decade of the dendritic NMDA spike. *J Neurosci Res* **88,** 2991–3001.

Araya R, Vogels TP & Yuste R (2014). Activity-dependent dendritic spine neck changes are correlated with synaptic strength. *Proc Natl Acad Sci U S A,* 2895–2904.

Banerjee A, Meredith RM, Rodríguez-Moreno A, Mierau SB, Auberson YP & Paulsen O (2009). Double dissociation of spike timing-dependent potentiation and depression by subunit-preferring NMDA receptor antagonists in mouse barrel cortex. *Cereb Cortex* **19,** 2959–2969.

Banke TG, Bowie D, Lee H, Huganir RL, Schousboe A & Traynelis SF (2000). Control of GluR1 AMPA receptor function by cAMP-dependent protein kinase. *J Neurosci* **20,** 89–102.

Barria a, Muller D, Derkach V, Griffith LC & Soderling TR (1997). Regulatory phosphorylation of AMPA-type glutamate receptors by CaM-KII during long-term potentiation. *Science* **276,** 2042–2045.

Barria A & Malinow R (2005). NMDA receptor subunit composition controls synaptic plasticity by regulating binding to CaMKII. *Neuron* **48,** 289–301.

Bekkers JM (2000). Distribution and activation of voltage-gated potassium channels in cell-attached and outside-out patches from large layer 5 cortical pyramidal neurons of the rat. *J Physiol* **525 Pt 3,** 611–620.

Bell CC, Han VZ, Sugawara Y & Grant K (1997). Synaptic plasticity in a cerebellum-like structure depends on temporal order. *Nature* **387,** 278–281.

Bender V a, Bender KJ, Brasier DJ & Feldman DE (2006). Two coincidence detectors for spike timing-dependent plasticity in somatosensory cortex. *J Neurosci* **26,** 4166–4177.

Benke TA, Lüthi A, Isaac JT & Collingridge GL (1998). Modulation of AMPA receptor unitary conductance by synaptic activity. *Nature* **393,** 793–797.

Berger T, Larkum ME & Lüscher HR (2001). High I(h) channel density in the distal apical dendrite of layer V pyramidal cells increases bidirectional attenuation of EPSPs. *J Neurophysiol* **85,** 855–868.

Berger T, Senn W & Lüscher H-R (2003). Hyperpolarization-activated current Ih disconnects somatic and dendritic spike initiation zones in layer V pyramidal neurons. *J Neurophysiol* **90,** 2428–2437.

Berlucchi G & Buchtel H A (2009). Neuronal plasticity: historical roots and evolution of meaning. *Exp brain Res* **192,** 307–319.

Berridge MJ (2006). Calcium microdomains: Organization and function. *Cell Calcium* **40,** 405–412.

Bi GQ & Poo MM (1998). Synaptic modifications in cultured hippocampal neurons: dependence on spike timing, synaptic strength, and postsynaptic cell type. *J Neurosci* **18,** 10464–10472.

Bienenstock EL, Cooper LN & Munro PW (1982). Theory for the development of neuron selectivity: orientation specificity and binocular interaction in visual cortex. *J Neurosci* **2,** 32–48.

Birtoli B & Ulrich D (2004). Firing mode-dependent synaptic plasticity in rat neocortical pyramidal neurons. *J Neurosci* **24,** 4935–4940.

Bischofberger J & Jonas P (1997). Action potential propagation into the presynaptic dendrites of rat mitral cells. *J Physiol* **504 (Pt 2,** 359–365.

Bittner KC, Andrasfalvy BK & Magee JC (2012). Ion channel gradients in the apical tuft region of CA1 pyramidal neurons. *PLoS One* **7,** e46652.

Bliss T & Collingridge G (1993). A synaptic model of memory: long-term potentiation in the hippocampus. *Nature* **361,** 31–39.

Bliss T V & Lomo T (1973). Long-lasting potentiation of synaptic transmission in the dentate area of the anaesthetized rabbit following stimulation of the perforant path. *J Physiol* **232,** 331–356.

Bourne JN & Harris KM (2011). Nanoscale analysis of structural synaptic plasticity. *Curr Opin Neurobiol*1–11.

Bramham CR (2008). Local protein synthesis, actin dynamics, and LTP consolidation. *Curr Opin Neurobiol* **18,** 524–531.

Branco T, Clark BA & Häusser M (2010). Dendritic Discrimination of Temporal Input Sequences in Cortical Neurons. *Science* **329,** 1671–1675.

Branco T & Häusser M (2009). The selfish spike: local and global resets of dendritic excitability. *Neuron* **61,** 815–817.

Branco T & Häusser M (2010). The single dendritic branch as a fundamental functional unit in the nervous system. *Curr Opin Neurobiol* **20,** 494–502.

Branco T & Häusser M (2011). Synaptic Integration Gradients in Single Cortical Pyramidal Cell Dendrites. *Neuron* **69,** 885–892.

Bredt DS & Nicoll RA (2003). AMPA receptor trafficking at excitatory synapses. *Neuron* **40,** 361–379.

Brown HF, DiFrancesco D & Noble SJ (1979). How does adrenaline accelerate the heart? *Nature* **280,** 235–236.

Buonomano D V & Merzenich MM (1998). Cortical plasticity: from synapses to maps. *Annu Rev Neurosci* **21,** 149–186.

Cais O, Sedlacek M, Horak M, Dittert I & Vyklicky L (2008). Temperature dependence of NR1/NR2B NMDA receptor channels. *Neuroscience* **151,** 428–438.

Cajal SRY (1894). The Croonian Lecture: La Fine Structure des Centres Nerveux. *Proc R Soc London* **55,** 444–468.

Caporale N & Dan Y (2008). Spike timing-dependent plasticity: a Hebbian learning rule. *Annu Rev Neurosci* **31,** 25–46.

Cash S & Yuste R (1999). Linear summation of excitatory inputs by CA1 pyramidal neurons. *Neuron* **22,** 383–394.

Cassenaer S & Laurent G (2012). Conditional modulation of spike-timing-dependent plasticity for olfactory learning. *Nature* **482,** 47–52.

Castro JB & Urban NN (2009). Subthreshold glutamate release from mitral cell dendrites. *J Neurosci* **29,** 7023–7030.

Celikel T, Szostak V A & Feldman DE (2004). Modulation of spike timing by sensory deprivation during induction of cortical map plasticity. *Nat Neurosci* **7,** 534–541.

Chen X, Leischner U, Rochefort NL, Nelken I & Konnerth A (2011). Functional mapping of single spines in cortical neurons in vivo. *Nature* **475,** 501–505.

Chen X, Leischner U, Varga Z, Jia H, Deca D, Rochefort NL & Konnerth A (2012). LOTOS-based two-photon calcium imaging of dendritic spines in vivo. *Nat Protoc* **7,** 1818–1829.

Chen Y & Sabatini BL (2012). Signaling in dendritic spines and spine microdomains. *Curr Opin Neurobiol* **22,** 389–396.

Cho K, Aggleton JP, Brown MW & Bashir ZI (2001). An experimental test of the role of postsynaptic calcium levels in determining synaptic strength using perirhinal cortex of rat. *J Physiol* **532,** 459–466.

Choquet D & Triller A (2013). The Dynamic Synapse. *Neuron* **80,** 691–703.

Cichon J & Gan W-B (2015). Branch-specific dendritic Ca^{2+} spikes cause persistent synaptic plasticity. *Nature* **520,** 180–185.

Cingolani LA & Goda Y (2008). Actin in action: the interplay between the actin cytoskeleton and synaptic efficacy. *Nat Rev Neurosci* **9,** 344–356.

Clopath C & Gerstner W (2010). Voltage and Spike Timing Interact in STDP - A Unified Model. *Front Synaptic Neurosci* **2,** 25.

Coetzee W A., Amarillo Y, Chiu J, Chow A, Lau D, McCormack T, Moreno H, Nadal MS, Ozaita A, Pountney D, Saganich M, Vega-Saenz De Miera E & Rudy B (1999). Molecular diversity of K^+ channels. *Ann N Y Acad Sci* **868,** 233–285.

Colgan L A & Yasuda R (2014). Plasticity of dendritic spines: subcompartmentalization of signaling. *Annu Rev Physiol* **76,** 365–385.

Collingridge GL, Kehl SJ & McLennan H (1983). Excitatory amino acids in synaptic transmission in the Schaffer collateral-commissural pathway of the rat hippocampus. *J Physiol* **334,** 33–46.

Cormier RJ, Greenwood AC & Connor JA (2013). Bidirectional Synaptic Plasticity Correlated With the Magnitude of Dendritic Calcium Transients Above a Threshold Bidirectional Synaptic Plasticity Correlated With the Magnitude of Dendritic Calcium Transients Above a Threshold. 399–406.

Cudmore RH & Turrigiano GG (2004). Long-term potentiation of intrinsic excitability in LV visual cortical neurons. *J Neurophysiol* **92,** 341–348.

Cull-Candy S, Brickley S & Farrant M (2001). NMDA receptor subunits: diversity, development and disease. *Curr Opin Neurobiol* **11,** 327–335.

Cull-Candy S, Kelly L & Farrant M (2006). Regulation of Ca2+-permeable AMPA receptors: synaptic plasticity and beyond. *Curr Opin Neurobiol* **16,** 288–297.

Cull-Candy SG & Leszkiewicz DN (2004). Role of distinct NMDA receptor subtypes at central synapses. *Sci STKE* **2004,** re16.

Dacey DM, Peterson BB, Robinson FR & Gamlin PD (2003). Fireworks in the Primate Retina: In Vitro Photodynamics Reveals Diverse LGN-Projecting Ganglion Cell Types. *Neuron* **37,** 15–27.

deCharms RC & Merzenich MM (1996). Primary cortical representation of sounds by the coordination of action-potential timing. *Nature* **381,** 610–613.

DeFelipe J (2006). Brain plasticity and mental processes: Cajal again. *Nat Rev Neurosci* **7,** 811–817.

DeFelipe J et al. (2013). New insights into the classification and nomenclature of cortical GABAergic interneurons. *Nat Rev Neurosci* **14,** 202–216.

Derkach V (2011). Zooming in on AMPA receptor regulation by CaMKII. *Nat Neurosci* **14,** 674–675.

Destexhe A, Rudolph M & Paré D (2003). The high-conductance state of neocortical neurons in vivo. *Nat Rev Neurosci* **4,** 739–751.

Dillon C & Goda Y (2005*a*). The actin cytoskeleton: integrating form and function at the synapse. *Annu Rev Neurosci* **28,** 25–55.

Dillon C & Goda Y (2005*b*). The actin cytoskeleton: integrating form and function at the synapse. *Annu Rev Neurosci* **28,** 25–55.

Druckmann S, Feng L, Lee B, Yook C, Zhao T, Magee JC & Kim J (2014). Structured Synaptic Connectivity between Hippocampal Regions. *Neuron* **81,** 629–640.

Dudek SM & Bear MF (1992). Homosynaptic long-term depression in area CA1 of hippocampus and effects of N-methyl-D-aspartate receptor blockade. *Proc Natl Acad Sci U S A* **89,** 4363–4367.

Ehlers MD, Heine M, Groc L, Lee M-C & Choquet D (2007). Diffusional Trapping of GluR1 AMPA Receptors by Input-Specific Synaptic Activity. *Neuron* **54,** 447–460.

Emri Z, Antal K, Gulyás A. I, Megías M & Freund TF (2001). Electrotonic profile and passive propagation of synaptic potentials in three subpopulations of hippocampal CA1 interneurons. *Neuroscience* **104,** 1013–1026.

Engert F & Bonhoeffer T (1999). Dendritic spine changes associated with hippocampal long-term synaptic plasticity. *Nature* **399,** 66–70.

Fan Y, Fricker D, Brager DH, Chen X, Lu H-C, Chitwood R A & Johnston D (2005). Activity-dependent decrease of excitability in rat hippocampal neurons through increases in I(h). *Nat Neurosci* **8,** 1542–1551.

Farrant M & Nusser Z (2005). Variations on an inhibitory theme: phasic and tonic activation of GABA(A) receptors. *Nat Rev Neurosci* **6,** 215–229.

Feldman D (2009). Synaptic mechanisms for plasticity in neocortex. *Annu Rev Neurosci*33–55.

Feldman DE (2000). Timing-based LTP and LTD at vertical inputs to layer II/III pyramidal cells in rat barrel cortex. *Neuron* **27,** 45–56.

Feldman DE (2012). The spike-timing dependence of plasticity. *Neuron* **75,** 556–571.

Feldmeyer D, Lübke J, Silver RA & Sakmann B (2002). Synaptic connections between layer 4 spiny neurone-layer 2/3 pyramidal cell pairs in juvenile rat barrel cortex: physiology and anatomy of interlaminar signalling within a cortical column. *J Physiol* **538,** 803–822.

Fino E, Araya R, Peterka DS, Salierno M, Etchenique R & Yuste R (2009). RuBi-Glutamate : two-photon and visible-light photoactivation of neurons and dendritic spines. **3,** 1–9.

Fino E, Deniau J-M & Venance L (2008). Cell-specific spike-timing-dependent plasticity in GABAergic and cholinergic interneurons in corticostriatal rat brain slices. *J Physiol* **586,** 265–282.

Fino E, Glowinski J & Venance L (2005). Bidirectional activity-dependent plasticity at corticostriatal synapses. *J Neurosci* **25,** 11279–11287.

Florian R V (2012). The chronotron: a neuron that learns to fire temporally precise spike patterns. *PLoS One* **7,** e40233.

Florian V (2008). Tempotron-Like Learning with ReSuMe. In *Artificial Neural Networks - ICANN 2008 (Part II)*, ed. Kůrková V, Neruda R & Koutník J, pp. 368–375. Springer, Prague, Czech Republic.

Frégnac Y, Shulz D, Thorpe S & Bienenstock E (1988). A cellular analogue of visual cortical plasticity. *Nature* **333,** 367–370.

Frey U & Morris RG (1997). Synaptic tagging and long-term potentiation. *Nature* **385,** 533–536.

Frey U & Morris RGM (1998). Synaptic tagging: implications for late maintenance of hippocampal long-term potentiation. *Trends Neurosci* **21,** 181–188.

Frick A, Magee J & Johnston D (2004). LTP is accompanied by an enhanced local excitability of pyramidal neuron dendrites. *Nat Neurosci* **7,** 126–135.

Froemke R, Merzenich M & Schreiner C (2007). A synaptic memory trace for cortical receptive field plasticity. *Nature* **450,** 425–429.

Froemke RC, Carcea I, Barker AJ, Yuan K, Seybold B A, Martins ARO, Zaika N, Bernstein H, Wachs M, Levis P A, Polley DB, Merzenich MM & Schreiner CE (2012). Long-term modification of cortical synapses improves sensory perception. *Nat Neurosci*; DOI: 10.1038/nn.3274.

Froemke RC, Letzkus JJ, Kampa BM, Hang GB & Stuart GJ (2010). Dendritic synapse location and neocortical spike-timing-dependent plasticity. *Front Synaptic Neurosci* **2,** 29.

Froemke RC, Poo M & Dan Y (2005). Spike-timing-dependent synaptic plasticity depends on dendritic location. *Nature* **434,** 221–225.

Fu M, Yu X, Lu J & Zuo Y (2012). Repetitive motor learning induces coordinated formation of clustered dendritic spines in vivo. *Nature* **1,** 2–6.

Gall D, Prestori F, Sola E, D'Errico A, Roussel C, Forti L, Rossi P & D'Angelo E (2005). Intracellular calcium regulation by burst discharge determines bidirectional long-term synaptic plasticity at the cerebellum input stage. *J Neurosci* **25,** 4813–4822.

Gambino F & Holtmaat A (2012). Spike-timing-dependent potentiation of sensory surround in the somatosensory cortex is facilitated by deprivation-mediated disinhibition. *Neuron* **75,** 490–502.

Gambino F, Pagès S, Kehayas V, Baptista D, Tatti R, Carleton A & Holtmaat A (2014). Sensory-evoked LTP driven by dendritic plateau potentials in vivo. *Nature*; DOI: 10.1038/nature13664.

Ganguly K, Kiss L & Poo M (2000). Enhancement of presynaptic neuronal excitability by correlated presynaptic and postsynaptic spiking. *Nat Neurosci* **3,** 1018–1026.

Gazina E V, Richards KL, Mokhtar MBC, Thomas E a, Reid C a & Petrou S (2010). Differential expression of exon 5 splice variants of sodium channel alpha subunit mRNAs in the developing mouse brain. *Neuroscience* **166,** 195–200.

Gee S, Ellwood I, Patel T, Luongo F, Deisseroth K & Sohal VS (2012). Synaptic Activity Unmasks Dopamine D2 Receptor Modulation of a Specific Class of Layer V Pyramidal Neurons in Prefrontal Cortex. *J Neurosci* **32,** 4959–4971.

Gentet LJ & Williams SR (2007). Dopamine gates action potential backpropagation in midbrain dopaminergic neurons. *J Neurosci* **27,** 1892–1901.

Gerstner W (2010). From hebb rules to spike-timing-dependent plasticity: a personal account. *Front Synaptic Neurosci* **2,** 151.

Gerstner W, Kempter R, van Hemmen JL & Wagner H (1996). A neuronal learning rule for sub-millisecond temporal coding. *Nature* **383,** 76–81.

Gidon A & Segev I (2012). Principles governing the operation of synaptic inhibition in dendrites.

Neuron **75,** 330–341.

Göbel W, Kampa BM & Helmchen F (2007). Imaging cellular network dynamics in three dimensions using fast 3D laser scanning. *Nat Methods* **4,** 73–79.

Golding NL, Kath WL & Spruston N (2001). Dichotomy of action-potential backpropagation in CA1 pyramidal neuron dendrites. *J Neurophysiol* **86,** 2998–3010.

Golding NL, Mickus TJ, Katz Y, Kath WL & Spruston N (2005). Factors mediating powerful voltage attenuation along CA1 pyramidal neuron dendrites. *J Physiol* **568,** 69–82.

Golding NL, Staff NP & Spruston N (2002). Dendritic spikes as a mechanism for cooperative long-term potentiation. *Nature* **418,** 326–331.

Gollisch T & Meister M (2008). Rapid neural coding in the retina with relative spike latencies. *Science* **319,** 1108–1111.

Gordon U, Polsky A & Schiller J (2006). Plasticity compartments in basal dendrites of neocortical pyramidal neurons. *J Neurosci* **26,** 12717–12726.

Govindarajan A, Israely I, Huang S-Y & Tonegawa S (2011). The Dendritic Branch Is the Preferred Integrative Unit for Protein Synthesis-Dependent LTP. *Neuron* **69,** 132–146.

Govindarajan A, Kelleher RJ & Tonegawa S (2006). A clustered plasticity model of long-term memory engrams. *Nat Rev Neurosci* **7,** 575–583.

Granger AJ, Shi Y, Lu W, Cerpas M & Nicoll R a (2013). LTP requires a reserve pool of glutamate receptors independent of subunit type. *Nature* **493,** 495–500.

Graves AR, Moore SJ, Bloss EB, Mensh BD, Kath WL & Spruston N (2012). Hippocampal pyramidal neurons comprise two distinct cell types that are countermodulated by metabotropic receptors. *Neuron* **76,** 776–789.

Grimes WN, Zhang J, Graydon CW, Kachar B & Diamond JS (2010). Retinal Parallel Processors: More than 100 Independent Microcircuits Operate within a Single Interneuron. *Neuron* **65,** 873–885.

Grunditz A, Holbro N, Tian L, Zuo Y & Oertner TG (2008). Spine neck plasticity controls postsynaptic calcium signals through electrical compartmentalization. *J Neurosci* **28,** 13457–13466.

Gulledge AT & Stuart GJ (2003). Action potential initiation and propagation in layer 5 pyramidal neurons of the rat prefrontal cortex: absence of dopamine modulation. *J Neurosci* **23,** 11363–11372.

Gütig R (2014). To spike, or when to spike? *Curr Opin Neurobiol* **25,** 134–139.

Gütig R, Gollisch T, Sompolinsky H & Meister M (2013). Computing complex visual features with retinal spike times. *PLoS One* **8,** e53063.

Gütig R & Sompolinsky H (2006). The tempotron: a neuron that learns spike timing-based decisions. *Nat Neurosci* **9,** 420–428.

Gütig R & Sompolinsky H (2009). Time-warp-invariant neuronal processing. *PLoS Biol* **7,** e1000141.

Haas JS, Nowotny T & Abarbanel HDI (2006). Spike-timing-dependent plasticity of inhibitory synapses in the entorhinal cortex. *J Neurophysiol* **96,** 3305–3313.

Han F, Caporale N & Dan Y (2008). Reverberation of Recent Visual Experience in Spontaneous Cortical Waves. *Neuron* **60,** 321–327.

Hansel C, Artola a. & Singer W (1996). Different threshold levels of postsynaptic $[Ca^{2+}]$(i) have to be reached to induce LTP and LTD in neocortical pyramidal cells. *J Physiol Paris* **90,** 317–319.

Hansel C, Artola a. & Singer W (1997). Relation between dendritic Ca^{2+} levels and the polarity of synaptic long-term modifications in rat visual cortex neurons. *Eur J Neurosci* **9,** 2309–2322.

Hao J, Wang X, Dan Y, Poo M & Zhang X (2009). An arithmetic rule for spatial summation of excitatory and inhibitory inputs in pyramidal neurons. *Proc Natl Acad Sci U S A* **106,** 21906–21911.

Harauzov A, Spolidoro M, DiCristo G, De Pasquale R, Cancedda L, Pizzorusso T, Viegi A, Berardi N & Maffei L (2010). Reducing intracortical inhibition in the adult visual cortex promotes ocular dominance plasticity. *J Neurosci* **30,** 361–371.

Harnett MT, Makara JK, Spruston N, Kath WL & Magee JC (2012). Synaptic amplification by dendritic spines enhances input cooperativity. *Nature*3–9.

Harvey CD & Svoboda K (2007). Locally dynamic synaptic learning rules in pyramidal neuron dendrites. *Nature* **450,** 1195–1200.

Harvey CD, Yasuda R, Zhong H & Svoboda K (2008). The spread of Ras activity triggered by activation of a single dendritic spine. *Science* **321,** 136–140.

Häusser M (2001). Synaptic function: Dendritic democracy. *Curr Biol* **11,** 10–12.

Häusser M & Mel B (2003). Dendrites: bug or feature? *Curr Opin Neurobiol* **13,** 372–383.

Häusser M, Spruston N & Stuart GJ (2000). Diversity and dynamics of dendritic signaling. *Science* **290,** 739–744.

Häusser M, Stuart G, Racca C & Sakmann B (1995). Axonal initiation and active dendritic propagation of action potentials in substantia nigra neurons. *Neuron* **15,** 637–647.

Hayashi Y, Shi SH, Esteban JA, Piccini A, Poncer JC & Malinow R (2000). Driving AMPA receptors into synapses by LTP and CaMKII: requirement for GluR1 and PDZ domain interaction. *Science (80-)* **287,** 2262.

Hebb DO (1949). *The Organization of Behavior*. John Wiley & Sons, Inc., New York.

Hell JW (2014). CaMKII: Claiming Center Stage in Postsynaptic Function and Organization. *Neuron* **81,** 249–265.

Hering H & Sheng M (2001). Dendritic spines: structure, dynamics and regulation. *Nat Rev Neurosci* **2,** 880–888.

Higley MJ & Sabatini BL (2008). Calcium signaling in dendrites and spines: practical and functional considerations. *Neuron* **59,** 902–913.

Hines ML & Carnevale NT (1997). The NEURON simulation environment. *Neural Comput* **9,** 1179–1209.

Hirase H, Nikolenko V, Goldberg JH & Yuste R (2002). Multiphoton stimulation of neurons. *J Neurobiol* **51,** 237–247.

Hodgkin AL & Huxley AF (1952). A quantitative description of membrane current and its application to conduction and excitation in nerve. *J Physiol* **117,** 500–544.

Hodgkin AL & Rushton WAH (1946). The electrical constants of a crustacean nerve fibre. *Proc R Soc Med* **134,** 444–479.

Hofer SB, Mrsic-Flogel TD, Bonhoeffer T & Hübener M (2009). Experience leaves a lasting structural trace in cortical circuits. *Nature* **457,** 313–317.

Hoffman DA, Magee JC, Colbert CM & Johnston D (1997). K^+ channel regulation of signal propagation in dendrites of hippocampal pyramidal neurons. *Nature* **387,** 869–875.

Holmgren CD & Zilberter Y (2001). Coincident spiking activity induces long-term changes in inhibition of neocortical pyramidal cells. *J Neurosci* **21,** 8270–8277.

Holthoff K, Kovalchuk Y, Yuste R & Konnerth A (2004). Single-shock LTD by local dendritic spikes in pyramidal neurons of mouse visual cortex. *J Physiol* **560,** 27–36.

Holtmaat A & Svoboda K (2009). Experience-dependent structural synaptic plasticity in the mammalian brain. *Nat Rev Neurosci* **10,** 647–658.

Holtmaat AJGD, Trachtenberg JT, Wilbrecht L, Shepherd GM, Zhang X, Knott GW & Svoboda K (2005). Transient and persistent dendritic spines in the neocortex in vivo. *Neuron* **45,** 279–291.

Ismailov I, Kalikulov D, Inoue T & Friedlander MJ (2004). The kinetic profile of intracellular calcium predicts long-term potentiation and long-term depression. *J Neurosci* **24,** 9847–9861.

Itami C & Kimura F (2012). Developmental switch in spike timing-dependent plasticity at layers 4-2/3 in the rodent barrel cortex. *J Neurosci* **32,** 15000–15011.

Jack JJB, Noble D & Tsien RW (1975). *Electric current flow in excitable cells*. Clarendon Press, Oxford.

Jackson AC & Nicoll R A (2011). The expanding social network of ionotropic glutamate receptors: TARPs and other transmembrane auxiliary subunits. *Neuron* **70,** 178–199.

Jacob V, Brasier DJ, Erchova I, Feldman D & Shulz DE (2007). Spike timing-dependent synaptic depression in the in vivo barrel cortex of the rat. *J Neurosci* **27,** 1271–1284.

Jacob V, Petreanu L, Wright N, Svoboda K & Fox K (2012). Regular Spiking and Intrinsic Bursting Pyramidal Cells Show Orthogonal Forms of Experience-Dependent Plasticity in Layer V of Barrel Cortex. *Neuron* **73,** 391–404.

James W (1890). *Principles of psychology, 2 vols.* Macmillan Publishers Limited., London.

Jia H, Rochefort NL, Chen X & Konnerth A (2010). Dendritic organization of sensory input to cortical neurons in vivo. *Nature* **464,** 1307–1312.

Johansson RS & Birznieks I (2004). First spikes in ensembles of human tactile afferents code complex spatial fingertip events. *Nat Neurosci* **7,** 170–177.

Kampa BM, Clements J, Jonas P & Stuart GJ (2004). Kinetics of Mg2+ unblock of NMDA receptors: implications for spike-timing dependent synaptic plasticity. *J Physiol* **556,** 337–345.

Kampa BM, Letzkus JJ & Stuart GJ (2006). Requirement of dendritic calcium spikes for induction of spike-timing-dependent synaptic plasticity. *J Physiol* **574,** 283–290.

Kampa BM & Stuart GJ (2006). Calcium spikes in basal dendrites of layer 5 pyramidal neurons during action potential bursts. *J Neurosci* **26,** 7424–7432.

Kandel ER & Tauc L (1964). Mechanism of Prolonged Heterosynaptic Facilitation. *Nature* **202,** 145–147.

Kaneda M, Farrant M & Cull-Candy SG (1995). Whole-cell and single-channel currents activated by GABA and glycine in granule cells of the rat cerebellum. *J Physiol* **485,** 419–435.

Kang H & Schuman EM (1996). A Requirement for Local Protein Synthesis in Neurotrophin-Induced Hippocampal Synaptic Plasticity. *Science (80-)* **273,** 1402–1406.

Kasai H, Fukuda M, Watanabe S, Hayashi-Takagi A & Noguchi J (2010). Structural dynamics of dendritic spines in memory and cognition. *Trends Neurosci* **33,** 121–129.

Kastellakis G, Cai DJ, Mednick SC, Silva AJ & Poirazi P (2015). Progress in Neurobiology Synaptic clustering within dendrites : An emerging theory of memory formation. *Prog Neurobiol*1–17.

Kelso SR, Ganong AH & Brown TH (1986). Hebbian synapses in hippocampus. *Proc Natl Acad Sci U S A* **83,** 5326–5330.

Keren N, Peled N & Korngreen A (2005). Constraining compartmental models using multiple voltage recordings and genetic algorithms. *J Neurophysiol* **94,** 3730–3742.

Kessels HW & Malinow R (2009). Synaptic AMPA Receptor Plasticity and Behavior. *Neuron* **61,** 340–350.

Kirkby P A, Srinivas Nadella KMN & Silver RA (2010). A compact Acousto-Optic Lens for 2D and 3D femtosecond based 2-photon microscopy. *Opt Express* **18,** 13721–13745.

Kirkwood A & Bear MF (1994). Homosynaptic long-term depression in the visual cortex. *J Neurosci* **14,** 3404–3412.

Klausberger T & Somogyi P (2008). Neuronal diversity and temporal dynamics: the unity of hippocampal circuit operations. *Science* **321,** 53–57.

Kleindienst T, Winnubst J, Roth-Alpermann C, Bonhoeffer T & Lohmann C (2011). Activity-Dependent Clustering of Functional Synaptic Inputs on Developing Hippocampal Dendrites. *Neuron* **72,** 1012–1024.

Koch C, Poggio T & Torre V (1983). Nonlinear interactions in a dendritic tree: localization, timing, and role in information processing. *Proc Natl Acad Sci U S A* **80,** 2799–2802.

Kodangattil JN, Dacher M, Authement ME & Nugent FS (2013). Spike timing-dependent plasticity at GABAergic synapses in the Ventral tegmental area. *J Physiol* **00,** 1–12.

Koester HJ & Sakmann B (1998). Calcium dynamics in single spines during coincident pre- and postsynaptic activity depend on relative timing of back-propagating action potentials and subthreshold excitatory postsynaptic potentials. *Proc Natl Acad Sci U S A* **95,** 9596–9601.

Kohl MM, Shipton O A, Deacon RM, Rawlins JNP, Deisseroth K & Paulsen O (2011). Hemisphere-specific optogenetic stimulation reveals left-right asymmetry of hippocampal plasticity. *Nat Neurosci* **14,** 1413–1415.

Kopec CD, Li B, Wei W, Boehm J & Malinow R (2006). Glutamate receptor exocytosis and spine enlargement during chemically induced long-term potentiation. *J Neurosci* **26,** 2000–2009.

Korngreen A & Sakmann B (2000). Voltage-gated K^+ channels in layer 5 neocortical pyramidal neurones from young rats: subtypes and gradients. *J Physiol* **525 Pt 3,** 621–639.

Kristensen AS, Jenkins M a, Banke TG, Schousboe A, Makino Y, Johnson RC, Huganir R & Traynelis SF (2011). Mechanism of Ca^{2+}/calmodulin-dependent kinase II regulation of AMPA receptor gating. *Nat Neurosci*; DOI: 10.1038/nn.2804.

Kuczewski N, Porcher C, Ferrand N, Fiorentino H, Pellegrino C, Kolarow R, Lessmann V, Medina I & Gaiarsa J-L (2008). Backpropagating action potentials trigger dendritic release of BDNF during spontaneous network activity. *J Neurosci* **28,** 7013–7023.

Kuczewski N, Porcher C, Lessmann V, Medina I & Gaiarsa JL (2009). Activity-dependent dendritic release of BDNF and biological consequences. *Mol Neurobiol* **39,** 37–49.

Kullmann DM (2010). Neurological channelopathies. *Annu Rev Neurosci* **33,** 151–172.

Kwag J & Paulsen O (2009). The timing of external input controls the sign of plasticity at local synapses. *Nat Neurosci* **12,** 1219–1221.

Kwon H-B & Sabatini BL (2011). Glutamate induces de novo growth of functional spines in developing cortex. *Nature* **474,** 100–104.

Larkum ME, Kaiser KM & Sakmann B (1999*a*). Calcium electrogenesis in distal apical dendrites of layer 5 pyramidal cells at a critical frequency of back-propagating action potentials. *Proc Natl Acad Sci U S A* **96,** 14600–14604.

Larkum ME & Nevian T (2008). Synaptic clustering by dendritic signalling mechanisms. *Curr Opin Neurobiol* **18,** 321–331.

Larkum ME, Nevian T, Sandler M, Polsky A & Schiller J (2009). Synaptic Integration in Tuft Dendrites of Layer 5 Pyramidal Neurons: A New Unifying Principle. *Science (80-)* **325,** 756–760.

Larkum ME, Zhu JJ & Sakmann B (1999*b*). A new cellular mechanism for coupling inputs arriving at

different cortical layers. *Nature* **398,** 338–341.

Larkum ME, Zhu JJ & Sakmann B (2001). Dendritic mechanisms underlying the coupling of the dendritic with the axonal action potential initiation zone of adult rat layer 5 pyramidal neurons. *J Physiol* **533,** 447–466.

Lau CG & Zukin RS (2007). NMDA receptor trafficking in synaptic plasticity and neuropsychiatric disorders. *Nat Rev Neurosci* **8,** 413–426.

Lavzin M, Rapoport S, Polsky A, Garion L & Schiller J (2012). Nonlinear dendritic processing determines angular tuning of barrel cortex neurons in vivo. *Nature*5–9.

Lee HK, Barbarosie M, Kameyama K, Bear MF & Huganir RL (2000). Regulation of distinct AMPA receptor phosphorylation sites during bidirectional synaptic plasticity. *Nature* **405,** 955–959.

Lee S-JR, Escobedo-Lozoya Y, Szatmari EM & Yasuda R (2009). Activation of CaMKII in single dendritic spines during long-term potentiation. *Nature* **458,** 299–304.

Lester R a & Jahr CE (1992). NMDA channel behavior depends on agonist affinity. *J Neurosci* **12,** 635–643.

Letzkus JJ, Kampa BM & Stuart GJ (2006). Learning rules for spike timing-dependent plasticity depend on dendritic synapse location. *J Neurosci* **26,** 10420–10429.

Lev-Ram V, Miyakawa H, Lasser-Ross N & Ross WN (1992). Calcium transients in cerebellar Purkinje neurons evoked by intracellular stimulation. *J Neurophysiol* **68,** 1167–1177.

Lin JY, Lin MZ, Steinbach P & Tsien RY (2009). Characterization of engineered channelrhodopsin variants with improved properties and kinetics. *Biophys J* **96,** 1803–1814.

Lisman J (1989). A mechanism for the Hebb and the anti-Hebb processes underlying learning and memory. *Proc Natl Acad Sci U S A* **86,** 9574–9578.

Lisman J, Schulman H & Cline H (2002). The molecular basis of CaMKII function in synaptic and behavioural memory. *Nat Rev Neurosci* **3,** 175–190.

Lisman J & Spruston N (2005). Postsynaptic depolarization requirements for LTP and LTD: a critique of spike timing-dependent plasticity. *Nat Neurosci* **8,** 839–841.

Lisman J & Spruston N (2010). Questions about STDP as a General Model of Synaptic Plasticity. *Front Synaptic Neurosci* **2,** 140.

Lisman J, Yasuda R & Raghavachari S (2012). Mechanisms of CaMKII action in long-term potentiation. *Nat Rev Neurosci* **13,** 169–182.

Llinás R, Nicholson C, Freeman JA & Hillman DE (1968). Dendritic spikes and their inhibition in alligator Purkinje cells. *Science* **160,** 1132–1135.

Llinás R & Sugimori M (1980). Electrophysiological properties of in vitro Purkinje cell dendrites in mammalian cerebellar slices. *J Physiol* **305,** 197–213.

London M & Häusser M (2005). Dendritic computation. *Annu Rev Neurosci* **28,** 503–532.

London M & Segev I (2001). Synaptic scaling in vitro and in vivo. *Nat Neurosci* **4,** 853–855.

Losonczy A & Magee JC (2006). Integrative properties of radial oblique dendrites in hippocampal CA1 pyramidal neurons. *Neuron* **50,** 291–307.

Losonczy A, Makara JK & Magee JC (2008). Compartmentalized dendritic plasticity and input feature storage in neurons. *Nature* **452,** 436–441.

Ludwig M & Pittman QJ (2003). Talking back: Dendritic neurotransmitter release. *Trends Neurosci* **26,** 255–261.

Lüscher C & Slesinger P A (2010). Emerging roles for G protein-gated inwardly rectifying potassium

(GIRK) channels in health and disease. *Nat Rev Neurosci* **11,** 301–315.

Lynch G, Larson J, Kelso S, Barrionuevo G & Schottler F (1983). Intracellular injections of EGTA block induction of hippocampal long-term potentiation. *Nature* **305,** 719–721.

Magee JC (1998). Dendritic hyperpolarization-activated currents modify the integrative properties of hippocampal CA1 pyramidal neurons. *J Neurosci* **18,** 7613–7624.

Magee JC (1999). Dendritic lh normalizes temporal summation in hippocampal CA1 neurons. *Nat Neurosci* **2,** 508–514.

Magee JC & Cook EP (2000). Somatic EPSP amplitude is independent of synapse location in hippocampal pyramidal neurons. *Nat Neurosci* **3,** 895–903.

Magee JC & Johnston D (1995). Characterization of single voltage-gated Na+ and Ca2+ channels in apical dendrites of rat CA1 pyramidal neurons. *J Physiol* **487 (Pt 1,** 67–90.

Magee JC & Johnston D (1997). A synaptically controlled, associative signal for Hebbian plasticity in hippocampal neurons. *Science* **275,** 209–213.

Maier W, Corrie JET, Papageorgiou G, Laube B & Grewer C (2005). Comparative analysis of inhibitory effects of caged ligands for the NMDA receptor. *J Neurosci Methods* **142,** 1–9.

Mainen ZF & Sejnowski TJ (1996). Influence of dendritic structure on firing pattern in model neocortical neurons. *Nature* **382,** 363–366.

Majewska A, Tashiro A & Yuste R (2000). Regulation of spine calcium dynamics by rapid spine motility. *J Neurosci* **20,** 8262–8268.

Major G, Larkum ME & Schiller J (2013). Active Properties of Neocortical Pyramidal Neuron Dendrites. *Annu Rev Neurosci* **36,** 1–24.

Major G, Polsky A, Denk W, Schiller J & Tank DW (2008). Spatiotemporally graded NMDA spike/plateau potentials in basal dendrites of neocortical pyramidal neurons. *J Neurophysiol* **99,** 2584–2601.

Makara JK, Losonczy A, Wen Q & Magee JC (2009). Experience-dependent compartmentalized dendritic plasticity in rat hippocampal CA1 pyramidal neurons. *Nat Neurosci* **12,** 1485–1487.

Makara JK & Magee JC (2013). Variable Dendritic Integration in Hippocampal CA3 Pyramidal Neurons. *Neuron* **80,** 1438–1450.

Makino H & Malinow R (2009). AMPA receptor incorporation into synapses during LTP: the role of lateral movement and exocytosis. *Neuron* **64,** 381–390.

Makino H & Malinow R (2011). Compartmentalized versus Global Synaptic Plasticity on Dendrites Controlled by Experience. *Neuron* **72,** 1001–1011.

Malenka RC & Bear MF (2004). LTP and LTD: An embarrassment of riches. *Neuron* **44,** 5–21.

Malenka RC, Kauer JA, Zucker RS, Nicoll RA & Kauer A (1988). Postsynaptic Calcium Is Sufficient for Potentiation of Hippocampal Synaptic Transmission Postsynaptic Calcium Is Sufficient for Potentiation of Hippocampal Synaptic Transmission. *Science (80-)* **242,** 81–84.

Malinow R & Malenka RC (2002). AMPA receptor trafficking and synaptic plasticity. *Annu Rev Neurosci* **25,** 103–126.

Markram H, Gerstner W & Sjöström PJ (2011). A history of spike-timing-dependent plasticity. *Front Synaptic Neurosci* **3,** 4.

Markram H, Gerstner W & Sjöström PJ (2012). Spike-timing-dependent plasticity: a comprehensive overview. *Front Synaptic Neurosci* **4,** 2.

Markram H, Helm PJ & Sakmann B (1995). Dendritic calcium transients evoked by single back-propagating action potentials in rat neocortical pyramidal neurons. *J Physiol* **485 (Pt 1,** 1–20.

Markram H, Lübke J, Frotscher M & Sakmann B (1997). Regulation of synaptic efficacy by coincidence of postsynaptic APs and EPSPs. *Science* **275,** 213–215.

Matsuzaki M, Honkura N, Ellis-Davies GCR & Kasai H (2004). Structural basis of long-term potentiation in single dendritic spines. *Nature* **429,** 761–766.

Matus A (2000). Actin-Based Plasticity in Dendritic Spines. *Science (80-)* **290,** 754–758.

McBride TJ, Rodriguez-Contreras A, Trinh A, Bailey R & Debello WM (2008). Learning drives differential clustering of axodendritic contacts in the barn owl auditory system. *J Neurosci* **28,** 6960–6973.

McCormick DA (2008). Membrane Potential and Action Potential. In *Fundamental Neuroscience (3rd edition)*, 3rd edn., ed. Squire LR, Bloom FE & Spitzer NC, pp. 111–132. Academic Press.

McCulloch WS & Pitts W (1943). A logical calculus of the ideas immanent in nervous activity. *Bull Math Biophys* **5,** 115–133.

Meister M, Lagnado L & Baylor D A (1995). Concerted signaling by retinal ganglion cells. *Science* **270,** 1207–1210.

Mel BW (1994). Information processing in dendritic trees. *Neural Comput* **6,** 1031–1085.

Meliza CD & Dan Y (2006). Receptive-field modification in rat visual cortex induced by paired visual stimulation and single-cell spiking. *Neuron* **49,** 183–189.

Migliore M & Shepherd GM (2002). Emerging rules for the distributions of active dendritic conductances. *Nat Rev Neurosci* **3,** 362–370.

Milstein AD & Nicoll R A (2008). Regulation of AMPA receptor gating and pharmacology by TARP auxiliary subunits. *Trends Pharmacol Sci* **29,** 333–339.

Min R & Nevian T (2012). Astrocyte signaling controls spike timing–dependent depression at neocortical synapses. *Nat Neurosci*; DOI: 10.1038/nn.3075.

Mower AF, Kwok S, Yu H, Majewska AK, Okamoto K-I, Hayashi Y & Sur M (2011). Experience-dependent regulation of CaMKII activity within single visual cortex synapses in vivo. *Proc Natl Acad Sci* **108,** 21241–21246.

Mulkey RM & Malenka RC (1992). Mechanisms underlying induction of homosynaptic long-term depression in area CA1 of the hippocampus. *Neuron* **9,** 967–975.

Müller C, Beck H, Coulter D & Remy S (2012). Inhibitory Control of Linear and Supralinear Dendritic Excitation in CA1 Pyramidal Neurons. *Neuron* **75,** 851–864.

Müller-Dahlhaus F, Ziemann U & Classen J (2010). Plasticity resembling spike-timing dependent synaptic plasticity: the evidence in human cortex. *Front Synaptic Neurosci* **2,** 34.

Myme CIO, Sugino K, Turrigiano GG & Nelson SB (2003). The NMDA-to-AMPA ratio at synapses onto layer 2/3 pyramidal neurons is conserved across prefrontal and visual cortices. *J Neurophysiol* **90,** 771–779.

Nabavi S, Fox R, Proulx CD, Lin JY, Tsien RY & Malinow R (2014). Engineering a memory with LTD and LTP. *Nature*; DOI: 10.1038/nature13294.

Neveu D & Zucker RS (1996). Postsynaptic levels of [Ca^{2+}]i needed to trigger LTD and LTP. *Neuron* **16,** 619–629.

Nevian T, Larkum ME, Polsky A & Schiller J (2007). Properties of basal dendrites of layer 5 pyramidal neurons: a direct patch-clamp recording study. *Nat Neurosci* **10,** 206–214.

Nevian T & Sakmann B (2004). Single spine Ca^{2+} signals evoked by coincident EPSPs and backpropagating action potentials in spiny stellate cells of layer 4 in the juvenile rat somatosensory barrel cortex. *J Neurosci* **24,** 1689–1699.

Nevian T & Sakmann B (2006). Spine Ca^{2+} signaling in spike-timing-dependent plasticity. *J Neurosci* **26,** 11001–11013.

Nicoll R a, Tomita S & Bredt DS (2006). Auxiliary subunits assist AMPA-type glutamate receptors. *Science* **311,** 1253–1256.

Nishimura Y, Perlmutter SI, Eaton RW & Fetz EE (2013). Spike-Timing-Dependent Plasticity in Primate Corticospinal Connections Induced during Free Behavior. *Neuron* **80,** 1301–1309.

Noguchi J, Matsuzaki M, Ellis-Davies GCR & Kasai H (2005). Spine-neck geometry determines NMDA receptor-dependent Ca^{2+} signaling in dendrites. *Neuron* **46,** 609–622.

Packer AM, Russell LE, Dalgleish HWP & Häusser M (2015). Simultaneous all-optical manipulation and recording of neural circuit activity with cellular resolution in vivo. *Nat Methods* **12,** 140–146.

Palmer LM, Shai AS, Reeve JE, Anderson HL, Paulsen O & Larkum ME (2014). NMDA spikes enhance action potential generation during sensory input. *Nat Neuroscience,* 1–10.

Paré D, Shink E, Gaudreau H, Destexhe A & Lang EJ (1998). Impact of spontaneous synaptic activity on the resting properties of cat neocortical pyramidal neurons In vivo. *J Neurophysiol* **79,** 1450–1460.

Park M, Penick EC, Edwards JG, Kauer J a & Ehlers MD (2004). Recycling endosomes supply AMPA receptors for LTP. *Science* **305,** 1972–1975.

Paulsen O & Sejnowski TJ (2000). Natural patterns of activity and long-term synaptic plasticity. *Curr Opin Neurobiol* **10,** 172–179.

Pawlak V, Greenberg DS, Sprekeler H, Gerstner W & Kerr JN (2013). Changing the responses of cortical neurons from sub- to suprathreshold using single spikes in vivo. *Elife* **2,** e00012.

Pawlak V & Kerr JND (2008). Dopamine receptor activation is required for corticostriatal spike-timing-dependent plasticity. *J Neurosci* **28,** 2435–2446.

Piyawattanametha W, Cocker ED, Burns LD, Barretto RP, Jung JC, Ra H, Solgaard O & Schnitzer MJ (2009). In vivo brain imaging using a portable 2.9 g two-photon microscope based on a microelectromechanical systems scanning mirror. *Opt Lett* **34,** 2309–2311.

Poirazi P, Brannon T & Mel BW (2003). Pyramidal neuron as two-layer neural network. *Neuron* **37,** 989–999.

Poirazi P & Mel BW (2001). Impact of active dendrites and structural plasticity on the memory capacity of neural tissue. *Neuron* **29,** 779–796.

Polsky A, Mel BW & Schiller J (2004). Computational subunits in thin dendrites of pyramidal cells. *Nat Neurosci* **7,** 621–627.

Ponulak F & Kasiński A (2010). Supervised learning in spiking neural networks with ReSuMe: sequence learning, classification, and spike shifting. *Neural Comput* **22,** 467–510.

Rall W (1964). Theoretical significance of dendritic trees for neuronal input-output relations. In *Neural theory and modeling*, ed. Reiss RF, pp. 73–97. Stanford University Press, Stanford.

Rall W (1967). Distinguishing theoretical synaptic potentials computed for different soma-dendritic distributions of synaptic input. *J Neurophysiol* **30,** 1138–1168.

Rall W (2011). Core Conductor Theory and Cable Properties of Neurons. In *Comprehensive Physiology*, ed. Terjung R, pp. 39–97. John Wiley & Sons, Inc., Hoboken, NJ, USA.

Rall W & Rinzel J (1973). Branch input resistance and steady attenuation for input to one branch of a dendritic neuron model. *Biophys J* **13,** 648–687.

Redondo RL & Morris RGM (2011). Making memories last: the synaptic tagging and capture

hypothesis. *Nat Rev Neurosci* **12,** 17–30.

Remme MWH, Lengyel M & Gutkin BS (2010). Democracy-independence trade-off in oscillating dendrites and its implications for grid cells. *Neuron* **66,** 429–437.

Remy S, Csicsvari J & Beck H (2009). Activity-dependent control of neuronal output by local and global dendritic spike attenuation. *Neuron* **61,** 906–916.

Remy S & Spruston N (2007). Dendritic spikes induce single-burst long-term potentiation. *Proc Natl Acad Sci U S A* **104,** 17192–17197.

Rigas P & Castro-Alamancos M a (2007). Thalamocortical Up states: differential effects of intrinsic and extrinsic cortical inputs on persistent activity. *J Neurosci* **27,** 4261–4272.

Rinzel J & Rall W (1974). Transient response in a dendritic neuron model for current injected at one branch. *Biophys J* **14,** 759–790.

Roberts TF, Tschida K A, Klein ME & Mooney R (2010). Rapid spine stabilization and synaptic enhancement at the onset of behavioural learning. *Nature* **463,** 948–952.

Rochefort NL & Konnerth A (2012). Dendritic spines: from structure to in vivo function. *EMBO Rep* **13,** 699–708.

Rodríguez-Moreno A, Banerjee A & Paulsen O (2010). Presynaptic NMDA Receptors and Spike Timing-Dependent Depression at Cortical Synapses. *Front Synaptic Neurosci* **2,** 18.

Rodríguez-Moreno A, González-Rueda A, Banerjee A, Upton AL, Craig MT & Paulsen O (2013). Presynaptic Self-Depression at Developing Neocortical Synapses. *Neuron* **77,** 35–42.

Rodríguez-Moreno A & Paulsen O (2008). Spike timing-dependent long-term depression requires presynaptic NMDA receptors. *Nat Neurosci* **11,** 744–745.

Rosenkranz JA & Johnston D (2006). Dopaminergic regulation of neuronal excitability through modulation of Ih in layer V entorhinal cortex. *J Neurosci* **26,** 3229–3244.

van Rossum MC, Bi GQ & Turrigiano GG (2000). Stable Hebbian learning from spike timing-dependent plasticity. *J Neurosci* **20,** 8812–8821.

Roth A & Häusser M (2001). Compartmental models of rat cerebellar Purkinje cells based on simultaneous somatic and dendritic patch-clamp recordings. *J Physiol* **535,** 445–472.

Safo P & Regehr WG (2008). Timing dependence of the induction of cerebellar LTD. *Neuropharmacology* **54,** 213–218.

Sale A, Maya Vetencourt JF, Medini P, Cenni MC, Baroncelli L, De Pasquale R & Maffei L (2007). Environmental enrichment in adulthood promotes amblyopia recovery through a reduction of intracortical inhibition. *Nat Neurosci* **10,** 679–681.

Sanchez-Vives M V & McCormick D a (2000). Cellular and network mechanisms of rhythmic recurrent activity in neocortex. *Nat Neurosci* **3,** 1027–1034.

Schaefer AT, Larkum ME, Sakmann B & Roth A (2003). Coincidence detection in pyramidal neurons is tuned by their dendritic branching pattern. *J Neurophysiol* **89,** 3143–3154.

Schiller J, Major G, Koester HJ & Schiller Y (2000). NMDA spikes in basal dendrites of cortical pyramidal neurons. *Nature* **404,** 285–289.

Schiller J & Schiller Y (2001). NMDA receptor-mediated dendritic spikes and coincident signal amplification. *Curr Opin Neurobiol* **11,** 343–348.

Schuett S, Bonhoeffer T & Hübener M (2001). Pairing-induced changes of orientation maps in cat visual cortex. *Neuron* **32,** 325–337.

Sdrulla AD & Linden DJ (2007). Double dissociation between long-term depression and dendritic spine morphology in cerebellar Purkinje cells. *Nat Neurosci* **10,** 546–548.

Seamans JK, Durstewitz D, Christie BR, Stevens CF & Sejnowski TJ (2001). Dopamine D1/D5 receptor modulation of excitatory synaptic inputs to layer V prefrontal cortex neurons. *Proc Natl Acad Sci U S A* **98,** 301–306. Available at: http://www.pubmedcentral.nih.gov/articlerender.fcgi?artid=14585&tool=pmcentrez&rendertype=abstract.

Seamans JK & Yang CR (2004). The principal features and mechanisms of dopamine modulation in the prefrontal cortex. *Prog Neurobiol* **74,** 1–58.

Segal M (2005). Dendritic spines and long-term plasticity. *Nat Rev Neurosci* **6,** 277–284.

Segev I & Rall W (1998). Excitable dendrites and spines: earlier theoretical insights elucidate recent direct observations. *Trends Neurosci* **21,** 453–460.

Seung HS (2003). Learning in spiking neural networks by reinforcement of stochastic synaptic transmission. *Neuron* **40,** 1063–1073.

Shatz C (1992). The Developing Brain. *Sci Am* **267,** 60–67.

Shepherd GM (2008*a*). Electrotonic Properties of Axons and Dendrites. In *Fundamental Neuroscience (3rd edition)*, 3rd. edn., ed. Squire LR, Bloom FE & Spitzer NC, pp. 87–109. Academic Press.

Shepherd GM (2008*b*). Complex information processing in dendrites. In *Fundamental Neuroscience (3rd edition)*, 3rd edn., ed. Squire L, Berg D, Bloom Fl, Du Lac S, Ghosh A & Spitzer N, pp. 248–269. Academic Press.

Shepherd JD & Huganir RL (2007). The cell biology of synaptic plasticity: AMPA receptor trafficking. *Annu Rev Cell Dev Biol* **23,** 613–643.

Shi S-H, Hayashi Y, Esteban J A. & Malinow R (2001). Subunit-Specific Rules Governing AMPA Receptor Trafficking to Synapses in Hippocampal Pyramidal Neurons. *Cell* **105,** 331–343.

Shi SH, Hayashi Y, Petralia RS, Zaman SH, Wenthold RJ, Svoboda K & Malinow R (1999). Rapid spine delivery and redistribution of AMPA receptors after synaptic NMDA receptor activation. *Science* **284,** 1811–1816.

Silva DGE, Jino M & De Abreu BT (2010). Machine learning methods and asymmetric cost function to estimate execution effort of software testing. *ICST 2010 - 3rd Int Conf Softw Testing, Verif Valid*275–284.

Sjöström PJ & Häusser M (2006). A cooperative switch determines the sign of synaptic plasticity in distal dendrites of neocortical pyramidal neurons. *Neuron* **51,** 227–238.

Sjöström PJ, Rancz EA, Roth A & Häusser M (2008). Dendritic excitability and synaptic plasticity. *Physiol Rev* **88,** 769–840.

Sjöström PJ, Turrigiano GG & Nelson SB (2001). Rate, timing, and cooperativity jointly determine cortical synaptic plasticity. *Neuron* **32,** 1149–1164.

Sjöström PJ, Turrigiano GG & Nelson SB (2003). Neocortical LTD via coincident activation of presynaptic NMDA and cannabinoid receptors. *Neuron* **39,** 641–654.

Smith SL, Smith IT, Branco T & Häusser M (2013). Dendritic spikes enhance stimulus selectivity in cortical neurons in vivo. *Nature* **503,** 115–120.

Song S & Abbott LF (2001). Cortical Development and Remapping through Spike Timing-Dependent Plasticity. *Neuron* **32,** 339–350.

Song S, Miller KD & Abbott LF (2000). Competitive Hebbian learning through spike-timing-dependent synaptic plasticity. *Nat Neurosci* **3,** 919–926.

Sourdet V & Debanne D (1999). The role of dendritic filtering in associative long-term synaptic plasticity. *Learn Mem* **6,** 422–447.

Sourdet V, Russier M, Daoudal G, Ankri N & Debanne D (2003). Long-term enhancement of neuronal excitability and temporal fidelity mediated by metabotropic glutamate receptor subtype 5. *J Neurosci* **23,** 10238–10248.

Spruston N (2008). Pyramidal neurons: dendritic structure and synaptic integration. *Nat Rev Neurosci* **9,** 206–221.

Spruston N, Häusser M & Stuart GJ (2012). Information Processing in Dendrites and Spines. In *Fundamental Neuroscience*, 4th edn., ed. Squire LR, Berg D, Bloom FE, du Lac S, Ghosh A & Spitzer NC, pp. 231–260. Academic Press.

Spruston N, Jaffe DB & Johnston D (1994). Dendritic attenuation of synaptic potentials and currents: the role of passive membrane properties. *Trends Neurosci* **17,** 161–166.

Spruston N, Schiller Y, Stuart G & Sakmann B (1995). Activity-dependent action potential invasion and calcium influx into hippocampal CA1 dendrites. *Science* **268,** 297–300.

Steriade M, McCormick DA & Sejnowski TJ (1993). Thalamocortical oscillations in the sleeping and aroused brain. *Science* **262,** 679–685.

Stuart G & Häusser M (1994). Initiation and spread of sodium action potentials in cerebellar Purkinje cells. *Neuron* **13,** 703–712.

Stuart G & Spruston N (1998). Determinants of voltage attenuation in neocortical pyramidal neuron dendrites. *J Neurosci* **18,** 3501–3510.

Stuart G, Spruston N, Sakmann B & Häusser M (1997). Action potential initiation and backpropagation in neurons of the mammalian CNS. *Trends Neurosci* **20,** 125–131.

Stuart GJ, Dodt HU & Sakmann B (1993). Patch-clamp recordings from the soma and dendrites of neurons in brain slices using infrared video microscopy. *Pflugers Arch* **423,** 511–518.

Stuart GJ & Häusser M (2001). Dendritic coincidence detection of EPSPs and action potentials. *Nat Neurosci* **4,** 63–71.

Stuart GJ & Sakmann B (1994). Active propagation of somatic action potentials into neocortical pyramidal cell dendrites. *Nature* **367,** 69–72.

Su H, Sochivko D, Becker A, Chen J, Jiang Y, Yaari Y & Beck H (2002). Upregulation of a T-type Ca^{2+} channel causes a long-lasting modification of neuronal firing mode after status epilepticus. *J Neurosci* **22,** 3645–3655.

Sutton MA & Schuman EM (2006). Dendritic Protein Synthesis, Synaptic Plasticity, and Memory. *Cell* **127,** 49–58.

Takigawa T & Alzheimer C (1999). G protein-activated inwardly rectifying K^+ (GIRK) currents in dendrites of rat neocortical pyramidal cells. *J Physiol* **517,** 385–390.

Tanaka J-I, Horiike Y, Matsuzaki M, Miyazaki T, Ellis-Davies GCR & Kasai H (2008). Protein synthesis and neurotrophin-dependent structural plasticity of single dendritic spines. *Science* **319,** 1683–1687.

Tanaka K, Khiroug L, Santamaria F, Doi T, Ogasawara H, Ellis-Davies GCR, Kawato M & Augustine GJ (2007). Ca^{2+} Requirements for Cerebellar Long-Term Synaptic Depression: Role for a Postsynaptic Leaky Integrator. *Neuron* **54,** 787–800.

Tanzi E (1893). I fatti e le induzioni dell'odierna istologia del sistema nervoso. *Riv Sper Fren Med Leg* **19,** 419–472.

Thomson W (1854). On the Theory of the Electric Telegraph. *Proc R Soc London* **7,** 382–399.

Thorpe S, Delorme A & Van Rullen R (2001). Spike-based strategies for rapid processing. *Neural Networks* **14,** 715–725.

Tønnesen J, Katona G, Rózsa B & Nägerl UV (2014). Spine neck plasticity regulates compartmentalization of synapses. *Nat Neurosci* **17,** 678–685.

Trachtenberg JT, Chen BE, Knott GW, Feng G, Sanes JR, Welker E & Svoboda K (2002). Long-term in vivo imaging of experience-dependent synaptic plasticity in adult cortex. *Nature* **420,** 788–794.

Tsubokawa H & Ross WN (1996). IPSPs modulate spike backpropagation and associated $[Ca^{2+}]i$ changes in the dendrites of hippocampal CA1 pyramidal neurons. *J Neurophysiol* **76,** 2896–2906.

Turrigiano G (2011). Too Many Cooks? Intrinsic and Synaptic Homeostatic Mechanisms in Cortical Circuit Refinement. *Annu Rev Neurosci*; DOI: 10.1146/annurev-neuro-060909-153238.

Turrigiano GG, Leslie KR, Desai NS, Rutherford LC & Nelson SB (1998). Activity-dependent scaling of quantal amplitude in neocortical neurons. *Nature* **391,** 892–896.

Turrigiano GG & Nelson SB (2004). Homeostatic plasticity in the developing nervous system. *Nat Rev Neurosci* **5,** 97–107.

Tzounopoulos T, Kim Y, Oertel D & Trussell LO (2004). Cell-specific, spike timing-dependent plasticities in the dorsal cochlear nucleus. *Nat Neurosci* **7,** 719–725.

Usher M, Cohen JD, Servan-Schreiber D, Rajkowski J & Aston-Jones G (1999). The role of locus coeruleus in the regulation of cognitive performance. *Science* **283,** 549–554.

Usowicz MM, Sugimori M, Cherksey B & Llinas R (1992). P-type calcium channels in the somata and dendrites of adult cerebellar Purkinje cells. *Neuron* **9,** 1185–1199.

VanRullen R, Guyonneau R & Thorpe SJ (2005). Spike times make sense. *Trends Neurosci* **28,** 1–4.

Varga Z, Jia H, Sakmann B & Konnerth A (2011). Dendritic coding of multiple sensory inputs in single cortical neurons in vivo. *Proc Natl Acad Sci*; DOI: 10.1073/pnas.1112355108.

Vargas-Caballero M & Robinson HPC (2003). A slow fraction of Mg^{2+} unblock of NMDA receptors limits their contribution to spike generation in cortical pyramidal neurons. *J Neurophysiol* **89,** 2778–2783.

Vetter P, Roth A & Häusser M (2001). Propagation of action potentials in dendrites depends on dendritic morphology. *J Neurophysiol* **85,** 926–937.

Vicini S, Wang JF, Li JH, Zhu WJ, Wang YH, Luo JH, Wolfe BB & Grayson DR (1998). Functional and pharmacological differences between recombinant N-methyl-D-aspartate receptors. *J Neurophysiol* **79,** 555–566.

Wang M, Ramos BP, Paspalas CD, Shu Y, Simen A, Duque A, Vijayraghavan S, Brennan A, Dudley A, Nou E, Mazer JA, McCormick DA & Arnsten AFT (2007*a*). Alpha2A-adrenoceptors strengthen working memory networks by inhibiting cAMP-HCN channel signaling in prefrontal cortex. *Cell* **129,** 397–410.

Wang X, Yang Y & Zhou Q (2007*b*). Independent Expression of Synaptic and Morphological Plasticity Associated with Long-Term Depression. *J Neurosci* **27,** 12419–12429.

Waters J, Larkum M, Sakmann B & Helmchen F (2003). Supralinear Ca^{2+} influx into dendritic tufts of layer 2/3 neocortical pyramidal neurons in vitro and in vivo. *J Neurosci* **23,** 8558–8567.

Watt AJ & Desai NS (2010). Homeostatic Plasticity and STDP: Keeping a Neuron's Cool in a Fluctuating World. *Front Synaptic Neurosci* **2,** 5.

Watt AJ, Sjöström PJ, Häusser M, Nelson SB & Turrigiano GG (2004). A proportional but slower NMDA potentiation follows AMPA potentiation in LTP. *Nat Neurosci* **7,** 518–524.

Wehr M & Laurent G (1996). Odour encoding by temporal sequences of firing in oscillating neural assemblies. *Nature* **384,** 162–166.

Wilbrecht L, Holtmaat A, Wright N, Fox K & Svoboda K (2010). Structural plasticity underlies experience-dependent functional plasticity of cortical circuits. *J Neurosci* **30,** 4927–4932.

Williams SR & Stuart GJ (2000*a*). Action potential backpropagation and somato-dendritic distribution of ion channels in thalamocortical neurons. *J Neurosci* **20,** 1307–1317.

Williams SR & Stuart GJ (2000*b*). Site independence of EPSP time course is mediated by dendritic I(h) in neocortical pyramidal neurons. *J Neurophysiol* **83,** 3177–3182.

Williams SR & Stuart GJ (2002). Dependence of EPSP efficacy on synapse location in neocortical pyramidal neurons. *Science* **295,** 1907–1910.

Wittenberg GM & Wang SS-H (2006). Malleability of spike-timing-dependent plasticity at the CA3-CA1 synapse. *J Neurosci* **26,** 6610–6617.

Woodin M a., Ganguly K & Poo MM (2003). Coincident pre- and postsynaptic activity modifies GABAergic synapses by postsynaptic changes in Cl- transporter activity. *Neuron* **39,** 807–820.

Xu T, Yu X, Perlik AJ, Tobin WF, Zweig J a, Tennant K, Jones T & Zuo Y (2009). Rapid formation and selective stabilization of synapses for enduring motor memories. *Nature* **462,** 915–919.

Yadav A, Gao YZ, Rodriguez A, Dickstein DL, Wearne SL, Luebke JI, Hof PR & Weaver CM (2012). Morphologic evidence for spatially clustered spines in apical dendrites of monkey neocortical pyramidal cells. *J Comp Neurol* **520,** 2888–2902.

Yang G, Lai CSW, Cichon J, Ma L, Li W & Gan W-B (2014). Sleep promotes branch-specific formation of dendritic spines after learning. *Science* **344,** 1173–1178.

Yang G, Pan F & Gan W-B (2009). Stably maintained dendritic spines are associated with lifelong memories. *Nature* **462,** 920–924.

Yasuda R, Nimchinsky E A, Scheuss V, Pologruto T A, Oertner TG, Sabatini BL & Svoboda K (2004). Imaging calcium concentration dynamics in small neuronal compartments. *Sci STKE* **2004,** pl5.

Yuste R (2011). Dendritic Spines and Distributed Circuits. *Neuron* **71,** 772–781.

Yuste R (2013). Electrical Compartmentalization in Dendritic Spines. *Annu Rev Neurosci*; DOI: 10.1146/annurev-neuro-062111-150455.

Zhang LI, Tao HW, Holt CE, Harris W A & Poo M (1998). A critical window for cooperation and competition among developing retinotectal synapses. *Nature* **395,** 37–44.

Zhang W & Linden DJ (2003). The other side of the engram: experience-driven changes in neuronal intrinsic excitability. *Nat Rev Neurosci* **4,** 885–900.

Zilberter M, Holmgren C, Shemer I, Silberberg G, Grillner S, Harkany T & Zilberter Y (2009). Input specificity and dependence of spike timing-dependent plasticity on preceding postsynaptic activity at unitary connections between neocortical layer 2/3 pyramidal cells. *Cereb Cortex* **19,** 2308–2320.

Zito K, Scheuss V, Knott G, Hill T & Svoboda K (2009). Rapid functional maturation of nascent dendritic spines. *Neuron* **61,** 247–258.